

**RISK-BASED SEISMIC PERFORMANCE ASSESSMENT OF
PRESSURIZED PIPING SYSTEMS CONSIDERING
RATCHETING**

By
RAVI KIRAN AKELLA
ENGG01201504016

Bhabha Atomic Research Centre, Mumbai

*A thesis submitted to the
Board of Studies in Engineering Sciences*

*In partial fulfillment of requirements
for the Degree of*

DOCTOR OF PHILOSOPHY

of

HOMI BHABHA NATIONAL INSTITUTE



August, 2020

Homi Bhabha National Institute¹

Recommendations of the Viva Voce Committee

As members of the Viva Voce Committee, we certify that we have read the dissertation prepared by Mr. Ravi Kiran Akella entitled "Risk-based Seismic Performance Assessment of Pressurized Piping Systems considering Ratcheting" and recommend that it may be accepted as fulfilling the thesis requirement for the award of Degree of Doctor of Philosophy.

Chairman - Prof. B. K. Dutta



Date: 18/2/2020

Guide / Convener – Prof. G. R. Reddy



Date: 18/2/2020

Examiner - Prof. Yogesh M. Desai



Date: 18/2/2020

Member 1- Prof. J. Chattopadhyay



Date: 18/2/2020

Member 2- Prof. T. A. Dwarakanath



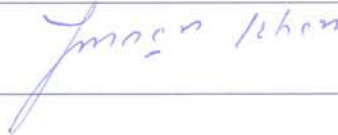
Date: 18/2/2020

Member 3- Prof. R. Balasubramaniam



Date: 18/2/2020

Member 4- Dr. Imran Ali Khan



Date: 18/2/2020

Final approval and acceptance of this thesis is contingent upon the candidate's submission of the final copies of the thesis to HBNI.

I/We hereby certify that I/we have read this thesis prepared under my/our direction and recommend that it may be accepted as fulfilling the thesis requirement.

Date: 18.2.2020

Place: Mumbai



(Prof. G. R. Reddy)

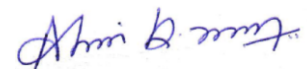
Guide

¹ This page is to be included only for final submission after successful completion of viva voce.

STATEMENT BY AUTHOR

This dissertation has been submitted in partial fulfillment of requirements for an advanced degree at Homi Bhabha National Institute (HBNI) and is deposited in the Library to be made available to borrowers under rules of the HBNI.

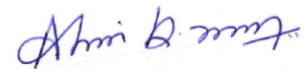
Brief quotations from this dissertation are allowable without special permission, provided that accurate acknowledgement of source is made. Requests for permission for extended quotation from or reproduction of this manuscript in whole or in part may be granted by the Competent Authority of HBNI when in his or her judgment the proposed use of the material is in the interests of scholarship. In all other instances, however, permission must be obtained from the author.



Ravi Kiran Akella

DECLARATION

I, hereby declare that the investigation presented in the thesis has been carried out by me.
The work is original and has not been submitted earlier as a whole or in part for a degree /
diploma at this or any other Institution / University.



Ravi Kiran Akella

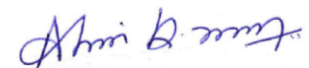
List of Publications arising from the thesis

Journal: 06

1. “Risk-based Seismic Performance Assessment of Pressurized Piping Systems considering Ratcheting”, A. Ravi Kiran, G. R. Reddy and M. K. Agrawal, *ASME Journal of Pressure Vessel Technology*, 2020, 142, pp. 021801:1-10.
2. “Seismic fragility analysis of pressurized piping systems considering ratcheting: A case study”, A. Ravi Kiran, G. R. Reddy and M. K. Agrawal, *International Journal of Pressure Vessels and Piping*, 2019, 169, pp. 26-36.
3. “Ratcheting Based Seismic Performance Assessment of a Piping System: Experiments and analysis”, A. Ravi Kiran, G. R. Reddy, M. K. Agrawal, M. Raj and S. D. Sajish, *International Journal of Pressure Vessels and Piping*, 2019, 177, pp. 103995.
4. “Fatigue-Ratcheting Behavior of 6 in Pressurized Carbon Steel Piping Systems Under Seismic Load: Experiments and Analysis”, A. Ravi Kiran, G. R. Reddy, P. N. Dubey and M. K. Agrawal, *ASME Journal of Pressure Vessel Technology*, 2017, 139, pp. 061801:1-15.
5. “Experimental and numerical studies of inelastic behavior of thin walled elbow and tee joint under seismic load”, A. Ravi Kiran, G. R. Reddy and M. K. Agrawal, *Thin-Walled Structures*, 2018, 127, pp. 700-709.
6. “Experimental and Numerical Studies on Inelastic Dynamic Behavior of Stainless Steel Elbow under Harmonic Base Excitation”, A. Ravi Kiran, G. R. Reddy and M. K. Agrawal, *ASME Journal of Pressure Vessel Technology*, 2018, 140, pp. 021204: 1–9.

Conferences: 02

1. “Prediction of Fatigue-Ratcheting failure of a piping system using Iterative Response Spectrum method”, A. Ravi Kiran, G. R. Reddy and M. K. Agrawal, *Proceedings of 13th International Conference on Vibration Problems (ICOVP-13)*, 2017, IIT Guwahati, India.
2. “Strain Based Seismic Performance Assessment of Pressurized Piping System: Experiments and analysis”, A. Ravi Kiran, G. R. Reddy, M. K. Agrawal, M. Raj and S. D. Sajish, *Proceedings of 16th Symposium on Earthquake Engineering*, 2018, IIT Roorkee, India.



Ravi Kiran Akella

DEDICATIONS

Dedicated to Lord Govinda

ACKNOWLEDGEMENTS

I would like to express my sincere gratitude to **Prof. G. R. Reddy** for his consistent support and guidance throughout this research work. Without his encouragement and motivation, it would have been difficult to accomplish the work of this magnitude.

I would like to thank the doctoral committee (**Prof. B. K. Dutta, Prof. J. Chattopadhyay, Prof. R. Balasubramaniam, Prof. T. A. Dwarakanath** and **Dr. I. A. Khan**) for the guidance, motivation and critical evaluation of my research activities.

I am thankful to my senior colleague **Shri. M. K. Agrawal** for his support during my PhD work. I would like to thank **Dr. M. Hari Prasad** for useful discussions on reliability aspects. Also, sincere thanks to Earthquake Engineering & Vibration Research Centre (EVRC) of Central Power Research Institute (CPRI), Bangalore for their support in carrying out shake table tests. I am also thankful to structural dynamics laboratory, Indira Gandhi Centre for Atomic Research (IGCAR), Kalpakkam for their co-operation during shake table experiments on piping system. A special thanks to **Shri M. A. Khan** and stress laboratory of Reactor Safety Division (RSD) for providing post-yield strain gauges required for the ratcheting tests of piping systems. Support received from the colleagues of BARC, Mumbai is gratefully acknowledged.

I would like to express my deepest gratitude to my parents for their limitless love, faith and enormous support. I am extremely thankful to my wife **Smt. Vijaya Lakshmi** for understanding and continuous support throughout my PhD work. Last but not least, I appreciate the patience and support of my wonderful kids, **Mast. Krishna Teja Akella** and **Mast. Anirudh Akella** during this research work. Their vibrant presence had made the strenuous research activity more joyful.



Ravi Kiran Akella

TABLE OF CONTENTS

ABSTRACT	I
LIST OF FIGURES	III
LIST OF TABLES	VI
ABBREVIATIONS	VII
NOMENCLATURE.....	IX
CHAPTER 1 INTRODUCTION	1
1.1 Risk-based seismic performance assessment of pressurized piping systems considering ratcheting	1
1.2 Problem statement, research objectives and scope of work	2
1.3 Organization of thesis	4
CHAPTER 2 LITERATURE SURVEY.....	6
2.1 Introduction.....	6
2.2 Literature on Seismic Fragility Analysis (SFA) of piping systems	6
2.2.1 Literature on the failure mode considered for SFA.....	6
2.2.2 Literature on the SFA methodology	8
2.3 Literature on predominant failure mode of piping systems under seismic load	9
2.4 Details of seismic ratcheting tests on piping components and systems	14
2.4.1 Ratcheting experiment on pressurized elbow under harmonic excitation.....	15
2.5 Literature on validated numerical tools for simulation of ratcheting in piping components and systems.....	22
2.5.1 Literature on simulation of ratcheting in piping components under static cyclic load 23	
2.5.2 Literature on numerical tools for simulation of ratcheting in piping systems under seismic load	23
2.6 Gap areas and directions for research	25

CHAPTER 3 INCREMENTAL ITERATIVE RESPONSE SPECTRUM (IIRS) METHOD FOR PREDICTION OF RATCHETING27

3.1 Introduction..... 27

3.2 Details of Incremental Iterative Response Spectrum (IIRS) method 29

3.3 Application of IIRS method to predict ratcheting in an elbow under harmonic excitation 31

3.3.1 Stage 1: Cyclic envelope characteristics for the elbow 32

3.3.2 Stage 2: IRS analysis for elbow test setup..... 38

3.4 Outcome and discussion 43

CHAPTER 4 INELASTIC SEISMIC BEHAVIOUR OF AN ELBOW AND A TEE JOINT: EXPERIMENTS AND ANALYSIS USING IIRS METHOD.....45

4.1 Introduction:..... 45

4.2 Experimental study on inelastic seismic behavior of Elbow and Tee joint 45

4.2.1 Details of the test setup 45

4.2.2 Details of seismic ratcheting tests 49

4.2.3 Discussion of test results of elbow and tee joint..... 56

4.2.4 Determination of frequency change of elbow and tee joint using wavelets..... 58

4.2.5 Sine sweep test on tested components post failure 61

4.3 Numerical study of tested elbow and tee joint 62

4.3.1 Ratcheting analysis of elbow using IIRS method 62

4.3.1.1 Determination of cyclic envelope characteristics for the elbow 62

4.3.1.2 Iterative method using response spectrum as input..... 67

4.3.2 Fatigue life evaluation for tee joint 70

4.4 Outcome and discussion 71

CHAPTER 5 SEISMIC PERFORMANCE ASSESSMENT OF PRESSURIZED PIPING SYSTEMS CONSIDERING RATCHETING: EXPERIMENTS AND ANALYSIS USING IIRS METHOD73

5.1 Introduction:..... 73

5.2 Experimental seismic performance assessment of piping system 74

5.2.1 Seismic performance assessment of CSPS-A 74

5.2.1.1 Shake table test of CSPS-A..... 74

5.2.1.2	Wavelet analysis for the evaluation of dominant frequency shift for CSPS-A	80
5.2.1.3	Characterization of ratcheting performance limits	82
5.2.2	Seismic performance assessment of CSPS-B	83
5.2.2.1	Wavelet analysis for the evaluation of dominant frequency shift for CSPS-B	90
5.3	Numerical simulation of tested piping systems.....	92
5.3.1	IIRS analysis of CSPS-A.....	92
5.3.1.1	Detailed cyclic plasticity analysis of elbow	93
5.3.1.2	Iterative analysis of CSPS-A with response spectrum as input	96
5.3.2	IIRS analysis of CSPS-B.....	99
5.3.2.1	Detailed cyclic plasticity analysis of elbow.....	99
5.3.2.2	Iterative analysis of CSPS-B with response spectrum as input.....	103

CHAPTER 6 SEISMIC FRAGILITY ANALYSIS OF PRESSURIZED PIPING SYSTEMS CONSIDERING RATCHETING.....107

6.1.	Introduction:.....	107
6.2.	Details of fragility assessment methodology	108
6.2.1.	Details of floor motion variability.....	109
6.2.2.	Evaluation of variation in damping.....	113
6.2.3.	Numerical tool used for evaluation of ratcheting.....	115
6.2.4.	Ratcheting based Performance Limit States (PLS) for piping systems.....	115
6.2.5.	Evaluation of fragility	116
6.3.	Case study: Fragility assessment for Carbon Steel Piping System (CSPS) and Stainless Steel Piping System (SSPS).....	117
6.3.1.	Fragility assessment for a Carbon Steel Piping System (CSPS)	117
6.3.1.1.	Selection of set of simulations.....	117
6.3.1.2.	IIRS simulations of CSPS	118
6.3.1.3.	Response Surface Method for fragility evaluation.....	122
6.3.1.4.	Generation of fragility curves for CSPS	123
6.3.2.	Case study: Fragility assessment for a Stainless Steel Piping System (SSPS)	127
6.3.2.1.	Selection of set of simulations.....	127
6.3.2.2.	IIRS simulations of SSPS.....	127
6.3.3.	Details of fragility evaluation of SSPS.....	133
6.4.	Outcome and discussion	135

CHAPTER 7 RISK-BASED SEISMIC PERFORMANCE ASSESSMENT OF PRESSURIZED PIPING SYSTEMS CONSIDERING RATCHETING.....	137
7.1 Introduction.....	137
7.2 Methodology for risk assessment.....	137
7.3 Site specific seismic hazard	138
7.4 Seismic risk evaluation	138
7.5 Outcome and discussion	139
CHAPTER 8 CONCLUSIONS, CONTRIBUTIONS AND DIRECTIONS FOR FUTURE RESEARCH	141
8.1 Conclusions	141
8.2 Contributions.....	142
8.3 Recommendations to improve seismic performance of piping systems	143
8.4 Directions for future research:	143
References	145

LIST OF FIGURES

Figure 2.1: Photograph of test setup of elbow	15
Figure 2.2: Schematic of test setup of elbow and location of strain gauges	16
Figure 2.3: Hoop Strain time history at crown of elbow.....	17
Figure 2.4: Photograph of piping system.....	18
Figure 2.5: Schematic and dimensions of the piping system.....	18
Figure 2.6: Test Response spectra for 2% damping.....	18
Figure 2.7: Hoop Strain time history at crown of elbow.....	19
Figure 2.8: Axial Strain time history at horizontal anchor location.....	20
Figure 2.9: Photograph of SSPS	20
Figure 2.10: Test Response Spectra (TRS) for 2% damping.....	21
Figure 2.11: Hoop Strain time history at crown of elbow.....	22
Figure 2.12: Water jet through crack at crown of SSPS elbow	22
Figure 2.13: Deformation of piping system using spring model	24
Figure 2.14: Spring model to replace elbow	24
Figure 3.1: Flow chart of IIRS method	31
Figure 3.2: FE model of elbow	32
Figure 3.3: Assumed thickness variation in the elbow	33
Figure 3.4: Mesh convergence study for elbow	33
Figure 3.5: Limit displacement for the elbow.....	34
Figure 3.6: Load Line Displacement time history at the free end of the elbow model.....	35
Figure 3.7: Comparison of Chaboche model	36
Figure 3.8: Cyclic moment-rotation curves for the elbow with uniform thickness	36
Figure 3.9: Cyclic moment-rotation curves for the elbow with thickness variation	37
Figure 3.10: Cyclic moment- strain curves for the elbow with uniform thickness	37
Figure 3.11: Cyclic moment- strain curves for the elbow with thickness variation.....	37
Figure 3.12: Envelope Strain-Moment-Rotation characteristics for the elbow	38
Figure 3.13: FE model of elbow with springs.....	38
Figure 3.14: Variation of stiffness in IIRS analysis.....	40
Figure 3.15: Response spectrum for harmonic excitation with amplitude of 0.2g	43
Figure 3.16: Comparison of predicted strain accumulation at flank of the elbow with test results	43
Figure 4.1: Photograph of test setup of elbow	47
Figure 4.2: Schematic of test setup of elbow and location of strain gauges	48
Figure 4.3: Photograph of test setup of tee joint	48
Figure 4.4: Schematic of test setup of tee joint and location of strain gauges	48
Figure 4.5: Shake table input acceleration time history in X-direction (horizontal).....	49
Figure 4.6: Shake table input acceleration time history in Y-direction (vertical).....	50
Figure 4.7: Shake table input acceleration time history in Z-direction (horizontal)	50
Figure 4.8: Test Response Spectra for 2% damping	50
Figure 4.9: Hoop strain history (SG-1H) at first crown of elbow	52
Figure 4.10: Axial strain history (SG-2A) at first crown of elbow	53
Figure 4.11: Hoop strain history (SG-3H) at second crown of elbow	53
Figure 4.12: Axial strain history (SG-4A) at second crown of elbow	54
Figure 4.13: Hoop strain history (SG-T1H) at front portion of location-A at tee junction.....	54
Figure 4.14: Axial strain history (SG-T2A) at front portion of location-A at tee junction.....	55
Figure 4.15: Hoop strain history at rear portion of	55

Figure 4.16: Water jet through crack at crown of elbow	56
Figure 4.17: Crack at the weld location of tee and pipe.....	56
Figure 4.18: Plot of peak strains in each level of excitation for elbow and tee tests	57
Figure 4.19: TFR of hoop strain signal of SG-1H during the first 100s duration.....	59
Figure 4.20: TFR of hoop strain of SG-1H during the last 100s duration	59
Figure 4.21: TFR of hoop strain signal of SG-T1H during the first 100s duration	60
Figure 4.22: TFR of hoop strain of SG-T1H during the last 100s duration.....	61
Figure 4.23: Schematic of secant stiffness.....	61
Figure 4.24: FE model of the elbow	63
Figure 4.25: Thickness variation in elbow.....	63
Figure 4.26: Load Line Displacement time history at the elbow tip.....	64
Figure 4.27: Comparison of experimental stabilized hysteresis loop with Chaboche model	64
Figure 4.28: Cyclic moment-rotation curves for the elbow with uniform thickness	65
Figure 4.29: Cyclic moment-rotation curves for the elbow with thickness variation	65
Figure 4.30: Cyclic moment- strain curves for the elbow with uniform thickness	66
Figure 4.31: Cyclic moment- strain curves for the elbow with thickness variation.....	66
Figure 4.32: Envelope Strain-Moment-Rotation characteristics for the elbow	67
Figure 4.33: FE model of the elbow	69
Figure 4.34: Comparison of predicted strain accumulation.....	70
Figure 5.1: Photograph of CS piping systems (CSPS-A) test setup	74
Figure 5.2: Dimensions of CSPS-A and location of instruments.....	75
Figure 5.3: Comparison of TRS with RRS for 2% damping	76
Figure 5.4: X- direction acceleration time history (horizontal)	77
Figure 5.5: Y- direction acceleration time history (horizontal)	77
Figure 5.6: Z- direction acceleration time history (Vertical)	77
Figure 5.7: Hoop strain time histories at first crown location (SG-1) of elbow-1	79
Figure 5.8: Hoop strain time histories at second crown location (SG-2) of elbow-1	80
Figure 5.9: Photograph of rupture at crown.....	80
Figure 5.10: TFR of SG-1 strain signal during first 250s duration.....	81
Figure 5.11: TFR of SG-1 strain during the last 200s duration	81
Figure 5.12: Test setup of CSPS-B	84
Figure 5.13: Dimensions of CSPS-B and location of strain gauges.....	85
Figure 5.14: Table excitation in horizontal direction (X-axis)	85
Figure 5.15: Table excitation in horizontal direction (Y-axis)	86
Figure 5.16: Table excitation in vertical direction (Z-axis).....	86
Figure 5.17: Test Response spectra for 2% damping.....	86
Figure 5.18: Hoop strain time history at crown location (SG-1) of elbow-1	88
Figure 5.19: Hoop strain time history at crown location (SG-5) of elbow-2	89
Figure 5.20: Comparison of hoop strain time histories at two crown locations.....	89
Figure 5.21: Photograph of crack at crown of the elbow	90
Figure 5.22: Hoop strain time history at Tee junction (SG-3)	90
Figure 5.23: TFR of strain at tee joint during the first 200s duration	91
Figure 5.24: TFR of strain at tee joint during the last 160s duration	92
Figure 5.25: Finite element model of elbow	93
Figure 5.26: Line model of piping system	93
Figure 5.27: Comparison of Chaboche model and uniaxial stabilized hysteresis loop under symmetric strain cycling.....	94

Figure 5.28: Evaluation of elbow tip limiting displacement.....	94
Figure 5.29: Cyclic displacement time history at elbow tip.....	95
Figure 5.30: Cyclic moment-rotation curves for the CSPS-A elbow.....	95
Figure 5.31: Cyclic moment- strain curves for the CSPS-A elbow	96
Figure 5.32: Cyclic envelope ϵ -M- θ characteristic of CSPS- A elbow.....	96
Figure 5.33: Comparison of predicted peak strains with experimental results	98
Figure 5.34: FE model of CSPS-B elbow	100
Figure 5.35: Line model of CSPS-B with combination of springs	100
Figure 5.36: Evaluation of limit displacement of CSPS-B elbow	101
Figure 5.37: Tip displacement time history for ratcheting analysis.....	101
Figure 5.38: Cyclic moment-rotation curves for CSPS-B elbow.....	102
Figure 5.39: Cyclic moment- strain curves for CSPS-B elbow	102
Figure 5.40: Envelope Strain-Moment-Rotation characteristics for CSPS-B elbow	103
Figure 5.41: Comparison of predicted strain accumulation at crown with test results (CSPS-B).....	105
Figure 6.1: Flow chart showing fragility assessment methodology.....	110
Figure 6.2: FE model of typical Indian PHWR reactor building	112
Figure 6.3: Damping values of tested components and piping systems with frequency.....	114
Figure 6.4: Histogram of damping values from shake table tests	115
Figure 6.5: FRS of twenty records for 0.058% damping	119
Figure 6.6: FRS of twenty records for 2.2% damping	119
Figure 6.7: FRS of twenty records for 4.342% damping	119
Figure 6.8: Maximum ratcheting strain in elbow-1 of CSPS for fifth DOE case of mean damping and mean frequency under 20 FRS.....	120
Figure 6.9: The floor excitation levels (ZPA of FRS) for PLS-1 in all nine DOE cases	121
Figure 6.10: The floor excitation levels (ZPA of FRS) for PLS-2.....	121
Figure 6.11: The floor excitation levels (ZPA of FRS) for PLS-3 in all nine DOE cases	122
Figure 6.12: Fragility curves for first limit state, PLS-1 (1% strain limit)	126
Figure 6.13: Fragility curves for second limit state, PLS-2 (5% strain limit).....	126
Figure 6.14: Fragility curves for third limit state, PLS-3 (codal stress limit).....	127
Figure 6.15: Comparison of Chaboche model with results from uniaxial cyclic tests.....	128
Figure 6.16: Applied displacement at elbow tip	128
Figure 6.17: Cyclic strain-moment-rotation curves for elbow.....	129
Figure 6.18: Comparison of predicted peak strain with test results	129
Figure 6.19: Maximum ratcheting strain in elbow-1 of SSPS for DOE case.....	130
Figure 6.20: The floor excitation levels (ZPA of FRS) for PLS-1 in all nine DOE cases	131
Figure 6.21: The excitation levels (ZPA of FRS) for PLS-2 (5% ratcheting) in all nine DOE cases	131
Figure 6.22: The excitation levels (ZPA of FRS) for performance level based on codal stress limit (PLS-3) in all nine DOE cases.....	132
Figure 6.23: Fragility curves for 1% strain performance level (PLS-1)	134
Figure 6.24: Fragility curves for 5% strain performance level (PLS-2)	134
Figure 6.25: Fragility curves for performance level based on codal stress limit (PLS-3)	135
Figure 7.1: Frame work for risk assessment of piping systems	137
Figure 7.2: Seismic hazard plot of a Peninsular Indian (PI) site.....	138
Figure 7.3: AEP of SSPS and CSPS-B for the three PLS	139

LIST OF TABLES

Table 2.1: Loading details for ratcheting test of the elbow.....	16
Table 2.2: Details of various levels of base excitation.....	19
Table 2.3: Details of various levels of base excitation.....	21
Table 3.1: Natural frequencies and mass participation for the elbow.....	39
Table 3.2: Results of IIRS analysis for the elbow (uniform thickness).....	41
Table 3.3: Results of IIRS analysis for the elbow (thickness variation).....	41
Table 4.1: Loading details for ratcheting test of elbow and tee joint.....	51
Table 4.2: Results of IRS analysis for elbow with uniform thickness.....	68
Table 4.3: Fatigue life evaluation for various levels of excitation of tee joint.....	71
Table 5.1: Comparison of frequencies (f) from sine sweep test and analysis.....	76
Table 5.2: Loading details for CSPS-A test.....	78
Table 5.3: Loading details for CSPS-B test.....	87
Table 5.4: Details of iterations for CSPS-A.....	97
Table 5.5: Details of iterations for CSPS-B.....	104
Table 6.1: Details of intra plate earthquake records.....	111
Table 6.2: Details of tested piping components and systems.....	113
Table 6.3: Different cases of Design of Experiments (DOE).....	118
Table 6.4: Polynomial coefficients for all PLS.....	123
Table 6.5: The parameters for log-normal fragility function for three PLS of CSPS.....	125
Table 6.6: Polynomial coefficients for response surfaces of different PLS.....	132
Table 6.7: Log-normal fragility function parameters for three performance levels.....	133

ABBREVIATIONS

<i>AEP</i>	Annual Exceedance Probability
<i>ASME</i>	The American Society of Mechanical Engineers
<i>B&PV</i>	Boiler and Pressure Vessel
<i>CPRI</i>	Central Power Research Institute
<i>CSPS</i>	Carbon Steel Piping System
<i>CUF</i>	Cumulative Usage Factor
<i>DOE</i>	Design of Experiments
<i>EPRI</i>	Electric Power Research Institute
<i>EQ</i>	Earthquake
<i>FE</i>	Finite Element
<i>FFT</i>	Fast Fourier Transform
<i>FRS</i>	Floor Response Spectrum
<i>ICW</i>	Inner Containment Wall
<i>IDA</i>	Incremental Dynamic Analysis
<i>IGCAR</i>	Indira Gandhi Centre for Atomic Research
<i>IIRS Method</i>	Incremental Iterative Response Spectrum Method
<i>IS</i>	Internal Structure
<i>JSME</i>	Japan Society of Mechanical Engineers
<i>LB</i>	Lower Bound
<i>MECOS</i>	Metallic Component Margins
<i>NB</i>	Nominal Bore
<i>NUPEC</i>	Nuclear Power Engineering Corporation

<i>OCW</i>	Outer Containment Wall
<i>OECD-NEA</i>	Organization for Economic Co-operation and Development— Nuclear Energy Agency
<i>PBD</i>	Performance Based Design
<i>PHWR</i>	Pressurized Heavy Water Reactor
<i>PI</i>	Peninsular India
<i>PLS</i>	Performance Limit States
<i>PRA</i>	Probabilistic Risk Assessment
<i>PSHA</i>	Probabilistic Seismic Hazard Analysis
<i>RB</i>	Reactor Building
<i>RRS</i>	Required Response Spectrum
<i>RSM</i>	Response Surface Method
<i>SFA</i>	Seismic Fragility Analysis
<i>SG</i>	Strain Gauge
<i>SMER</i>	Surface Mounted Electrical Resistance
<i>SSC</i>	Structures, Systems and Components
<i>SSPS</i>	Stainless Steel Piping System
<i>TES</i>	Twice Elastic Slope
<i>TFR</i>	Time-Frequency Representation
<i>TRS</i>	Test Response Spectrum
<i>UB</i>	Upper bound
<i>WT</i>	Wavelet Transform
<i>ZPA</i>	Zero Period of Acceleration

NOMENCLATURE

$a_1, a_2 \text{ \& } a_3$	Constants for exponential fit
\hat{a}	Excitation level in terms of ZPA
$A(g)$	Amplitude of excitation
A_m	Median of the fragility function
α_i	Back stress
b	Parameter which changes wavelet shape
B_1, B_2'	Primary Stress Index
β	Standard deviation of $\ln \hat{a}$
β_w	Parameter which controls the shape of the wavelet
$c_1, c_2, c_3, c_4, c_5 \text{ \& } c_6$	Constants for response surface polynomials
C_2	Secondary stress index
C_i, γ_i	Chaboche parameters
D_o	Elbow outer diameter
δ_L	Limit displacement
$\Delta\varepsilon$	Strain amplitude
E	Error sum of squares
ε	Strain
ε_x	Uniaxial strain
ε_x^p	Uniaxial plastic strain
ε_L^p	Amplitude of uniaxial plastic strain
f	Natural frequency (Hz)
h	Elbow parameter
$H(\lambda)$	Hazard
I	Moment of Inertia
j	Iteration number
k_0	Constant

k	Slope of the hazard curve in log-log scale
k_{Rz}	Rotational stiffness of elbow
K_2	Peak stress index
K_e	Plastic correction factor
λ	Spectral acceleration
m, n	Parameters representing frequency and time in wavelet analysis
M	Elbow moment from response spectrum analysis
M_c	Cyclic envelope moment of elbow from ratcheting analysis
M_{max}	Maximum magnitude
n_i	Number of load cycles
N	Total number of samples
N_i	Number of cycles for fatigue failure
p	Number of variables
P	Pressure
P_f	Conditional probability of exceedance of a performance level for a given excitation level, \hat{a}
$P_{F/\lambda}$	Fragility
ϕ	Bend angle
Φ	Standard normal cumulative distribution function
r_m	Mean radius of elbow
R	Elbow bending radius
R^2	Coefficient of determination
R_{epi}	Epi-central distance
S_a	Alternating stress
S_m	Permissible stress intensity
S_n	Primary stress plus secondary stress
T	Total sum of squares
σ	Linear stress in pipe
σ_0	Cyclic yield stress

σ_x	Uniaxial stress
σ_y	Yield stress
ψ	Wavelet function
t	Elbow thickness
θ	Angle of cross section
θ_e	Rotation in elbow
u_L	Limit displacement
U	Cumulative usage factor
U_i	Usage factor
$W(a, b)$	Wavelet transform with 'a' as a scaling parameter and 'b' is a translation parameter
x_1, x_2	Normalized parameters
ξ	Damping of the piping components/ systems
Z	Section modulus of pipe

CHAPTER 8 CONCLUSIONS, CONTRIBUTIONS AND DIRECTIONS FOR FUTURE RESEARCH

The research carried out as a part of this doctoral program produced certain important outcome as follows:

Studies on risk-based seismic performance assessment of pressurized piping systems considering ratcheting are presented. Supported by experimental and numerical investigations, initially seismic performance of piping components and systems with an emphasis on ratcheting is studied. Later, a methodology is developed for seismic fragility assessment considering ratcheting and applied to typical piping systems. Finally, seismic risk is evaluated by convoluting a typical site specific hazard curve with fragility curves. The conclusions of this research work are listed below.

8.1 Conclusions

This research has generated some novel outcomes which can be beneficial for the scientific community and future research. They are listed below.

1. From the wavelet analysis, it is found that the dominant frequency of the piping systems before ratcheting failure is only 2-4% less than the initial value; whereas for piping components, the reduction is in the range of 13-15%. This is due to load re-distribution and redundancy at system level. Also, it is concluded that the ratcheting failure of pressurized piping systems is a local phenomenon and there is only a slight variation in global stiffness.
2. Incremental Iterative Response Spectrum (IIRS) method evolved in this research is validated with experimental results and it is concluded that this method can be used for simulation of ratcheting in pressurized piping systems under seismic load. This method can also be used to evaluate fragility considering ratcheting.

From the numerical studies using IIRS method, it is concluded that thickness distribution in elbow has a significant influence on ratcheting strain.

3. In the case study of seismic fragility analysis, it is found that excitation levels with 5% ratcheting limit for stainless steel piping system is 13-15% higher than those for carbon steel piping system. Hence, it is concluded that stainless steel piping systems requires relatively higher levels of excitation to attain a ratcheting performance limit state than carbon steel piping systems. This is attributed to cyclic hardening in stainless steels, which reduces rate of ratcheting.
4. From the case study on seismic risk, it is found that annual exceedance probability for stainless steel piping system is less than that of carbon steel piping system for all performance limits. Hence, it is concluded that seismic risk for stainless steel piping systems is relatively lower than that of carbon steel piping systems.
5. Seismic risk for stainless steel and carbon steel piping systems of the case study, considering 5% ratcheting limit is 18% and 21% of that of design stress limit respectively. Hence, it is concluded that consideration of ratcheting reduces conservatism in seismic risk assessment of piping systems.

8.2 Contributions

The following are specific innovative and novel contributions from the research work carried out as part of PhD.

1. An experimentally validated numerical tool known as Incremental Iterative Response Spectrum (IIRS) method has been evolved to carry out seismic performance assessment of pressurized piping systems considering ratcheting.

2. At present, no ratcheting based criterion is available in the design codes. Ratcheting performance limit of 5% has been proposed to qualify the piping systems for Safe Shut down Earthquake (SSE).
3. A methodology for seismic fragility assessment, which is required for evaluation of seismic risk of piping systems considering ratcheting, has been evolved. This methodology can be applied to any general piping system for evaluation of seismic fragility and risk if site specific hazard information is known.

8.3 Recommendations to improve seismic performance of piping systems

Based on the research work carried out, the following recommendations are provided to improve the seismic performance of piping systems:

1. As fatigue-ratcheting is predominant failure mode of piping systems under seismic load, it is recommended to use ratcheting based limits for seismic design of piping systems.
2. It is recommended to use IIRS method for evaluation of ratcheting in the piping systems under seismic load.
3. It is recommended to consider ratcheting for seismic risk assessment of piping systems to reduce conservatism.

8.4 Directions for future research:

Present research focused on evaluation of seismic risk and fragility curves for pressurized piping systems considering ratcheting. Supported by several experimental and numerical studies, several logical conclusions were drawn. Also, case studies were presented to demonstrate the methodology. However, the following areas require further research for a better understanding:

1. In the present work, experimental and numerical studies were carried out for piping components and systems at room temperature. In future, high temperature effects can be studied.
2. The present studies are carried out with uniform base excitation. In future, studies can be carried out using multi-support excitation and seismic anchor movement.
3. In the present work Fatigue-Ratcheting interaction is not studied. Such interaction effects can be studied in future.

ABSTRACT

Seismic performance assessment of pressurized piping systems is a vital requirement to ensure the safety of nuclear facilities. Risk-based seismic performance assessment of pressurized piping systems is an evolving area to achieve predictable and desirable performance under different levels of earthquakes with a targeted risk. Such an assessment necessitates site specific hazard and fragility information of performance limit states based on actual failure mode. As the predominant failure mode of pressurized piping systems under seismic load is ratcheting, it is required to generate seismic fragility curves of piping systems considering ratcheting. In the literature on Seismic Fragility Analysis (SFA) of piping systems, failure criterion used was plastic collapse, which was the assumed failure mode by earlier version of design code. No studies have reported for seismic fragility analysis of piping systems considering ratcheting, which is actual failure mode. Also, the ASME nuclear piping design code has provided ratcheting based design criterion which was later discontinued due to insufficient experimental data and lack of validated numerical tools.

Hence, the first objective of the present work is to evaluate ratcheting based performance levels of piping systems, which requires validated numerical tools. This objective is met by carrying out experimental and numerical studies on pressurized piping components and systems. Initially, ratcheting behaviour in a carbon steel elbow and tee joint under incremental seismic excitation is studied. Later ratcheting response of pressurized piping systems under incremental excitation is investigated.

The second objective is to develop a methodology for ratcheting based SFA of pressurized piping systems. In the present work, a methodology is developed for SFA of pressurized piping systems considering ratcheting. In this procedure, Response Surface Method (RSM) along with Monte Carlo simulations are used for fragility evaluation. Variation in damping is evaluated from the experimental studies on piping components and systems and statistical parameters are obtained. Floor motion variation is obtained by carrying out time history analyses of a typical Reactor Building under twenty intra plate earthquake records. The methodology has been illustrated for SFA of carbon steel and stainless steel piping systems, which were considered for an international benchmark exercise on seismic margin assessment. Subsequently, the fragility curves of the piping systems are convoluted with hazard curves for a typical Peninsular Indian site to obtain seismic risk in terms of annual exceedance probability of ratcheting based performance limits. Recommendations for carrying out seismic performance, fragility and risk assessments of pressurized piping systems considering ratcheting have been provided.

CHAPTER 1 INTRODUCTION

1.1 Risk-based seismic performance assessment of pressurized piping systems considering ratcheting

The performance assessment of pressurized piping systems during an earthquake is necessary to ensure safety of nuclear facilities. Risk-based seismic performance assessment is an emerging approach to achieve predictable and desirable performance of the pressurized piping systems under different levels of earthquakes with a targeted risk. This assessment is more detailed and comprehensive than deterministic assessment in which the piping systems are studied for a specific seismic event. This approach is being adopted by ASCE Standard 43-05 [1] as well as Regulatory Guide 1.208 [2]. Kennedy [3] provided the technical basis for this probabilistic approach given in ASCE 43-05. The objective of such an assessment is to achieve a target seismic risk, defined as annual exceedance probability of a performance limit state during design of Structures, Systems and Components (SSC) of nuclear facilities. This assessment necessitates site specific hazard and fragility information of performance limit states based on actual failure mode. Site specific hazard curves provide the annual frequency of exceedance of a given level of ground motion, which is obtained from Probabilistic Seismic Hazard Analysis (PSHA). The fragility curves are usually expressed in terms of conditional probability of exceedance (P_f) of a performance limit state for a given seismic input level. As the predominant failure mode of pressurized piping systems under seismic load is ratcheting, it is required to generate seismic fragility curves of piping systems considering ratcheting. This requires numerical tool validated with experimental results for predicting ratcheting in piping components and systems.

1.2 Problem statement, research objectives and scope of work

Risk-based seismic performance assessment of piping systems comprises of two steps; first one is evaluation of site specific seismic hazard curves and the second one is the generation of fragility curves of piping systems. Hazard curves, $H(\lambda)$ provides the annual frequency of exceedance of a given level of ground motion, λ and these curves are obtained from Probabilistic Seismic Hazard Analysis (PSHA). On the other hand, fragility curves, $P_f(\lambda)$ provides the conditional probability of exceedance of a performance limit state of piping system for a given level of ground motion, λ . Seismic risk is obtained by the convolution of hazard curves with fragility information. Usually seismic risk is measured in terms of Annual Exceedance Probability (AEP) (Kennedy [3]) and is evaluated by risk integral given below:

$$AEP = \int_0^{\infty} H(\lambda) \left(\frac{dP_{F/\lambda}}{d\lambda} \right) d\lambda \quad (1.1)$$

Where,

λ is the ground motion parameter,

$H(\lambda)$ is the site specific seismic hazard at λ ,

$P_{F/\lambda}$ is the conditional exceedance probability (fragility) of a performance limit state of piping system for a given level of ground motion, λ

and $\frac{dP_{F/\lambda}}{d\lambda}$ is the derivative of the fragility with respect to ground motion parameter.

Kennedy and Ravindra [4], Ju and Gupta [5], Firoozabad et. al. [6], Zentner [7] and Schueller et. al. [8] worked on Seismic Fragility Analysis (SFA) of pressurized piping systems. However, in these studies, failure criterion used was plastic collapse, which was the assumed failure mode by earlier version of ASME nuclear piping design code (before 1995) [9]. From few experimental studies carried out by EPRI [10] it was

concluded that predominant failure mode of pressurized piping systems under seismic load is fatigue-ratcheting. Accordingly, the 1995 version of ASME nuclear piping design code [9] has incorporated ratcheting by increasing permissible stress limits and provided an alternate strain based criterion of 5% ratcheting limit for Level-D event. In the literature, no studies have reported SFA of pressurized piping systems considering ratcheting, which is actual failure mode. Hence, there is a need to develop methodology for SFA of pressurized piping systems considering ratcheting. So, the first objective is to evaluate ratcheting based performance levels of piping systems under seismic load. This requires validated numerical tools based on ratcheting. Also, the alternate ratcheting strain based criterion was not present in subsequent edition of ASME code, while retaining the stress criterion by modifying stress indices. This may be due to insufficient experimental data and lack of validated numerical tools. Also these provisions are still under debate by several regulatory agencies. Hence, there is a need to develop numerical tools validated with experimental results for predicting the ratcheting in piping systems.

The second objective is to develop a methodology for ratcheting based SFA of pressurized piping systems. This requires ratcheting based performance limit states, characterization of variation in seismic input and piping parameters. Finally, site specific hazard curves are required for convoluting with fragility curves to evaluate seismic risk.

The objectives and scope of the present research are summarized as follows:

- a. To develop validated numerical tool for simulation of ratcheting in pressurized piping systems: To address this requirement, experimental and numerical studies are to be carried out on ratcheting in pressurized piping components and systems.

- b. To develop methodology for SFA of pressurized piping systems considering ratcheting, which is the predominant failure mode under seismic load: To address this requirement, a methodology is to be developed for SFA of piping systems considering ratcheting. Performance limit states for ratcheting, variation in seismic input and piping parameters are required to be obtained.
- c. To evaluate seismic risk of pressurized piping systems considering ratcheting: To address this requirement, site specific hazard curves are to be obtained. Later seismic risk can be evaluated by convoluting these hazard curves with fragility information.

1.3 Organization of thesis

This thesis mainly deals with risk-based seismic performance assessment of pressurized piping systems considering ratcheting. Chapter 1 comprises three sections. The first section introduces risk-based seismic performance assessment of piping systems considering predominant failure mode of ratcheting. The next section explains the objectives and research significance. The last section gives the details of organization of thesis.

The detailed literature survey on seismic risk, fragility analysis of piping systems and experimental & numerical studies on ratcheting is provided in Chapter 2. The limitations of existing literature, gap areas and scope of present work are also elaborated in this chapter. A numerical tool known as Incremental Iterative Response Spectrum (IIRS) method is used to simulate ratcheting in pressurized piping components and systems. The details and application of IIRS method for prediction of ratcheting are given in Chapter 3. Ratcheting simulation using IIRS method is illustrated for an elbow, which was tested earlier under harmonic excitation.

Experimental and numerical studies on inelastic dynamic behaviour of an elbow and a tee joint under seismic loading are described in Chapter 4. The details of seismic performance assessment for pressurized piping systems considering ratcheting are provided in Chapter 5. Details of shake table tests on piping systems and numerical assessment using IIRS method are given in this Chapter. Also, ratcheting strain based seismic performance assessment is discussed in this Chapter. The details of Seismic Fragility Analysis of pressurized piping systems considering ratcheting are provided in Chapter 6. This Chapter presents the methodology for seismic fragility analysis of pressurized piping systems considering ratcheting. Seismic fragility curves are generated for typical carbon steel and stainless steel piping systems. Variation in damping is evaluated from the statistical analysis of damping values obtained from several shake table experiments on piping systems and components. Floor response spectra at steam generator elevation of a typical Indian PHWR containment under twenty intra plate earthquake records are used for the assessment. Performance of the piping systems is characterized in terms of design stress limit and two strain based limits. Chapter 7 provides the details of risk-based seismic performance assessment of pressurized piping systems considering ratcheting. This chapter illustrates the risk assessment for the piping systems utilizing the fragility curves and typical site specific hazard curve. Conclusions, contributions and directions for future research are provided in Chapter 8.

CHAPTER 2 LITERATURE SURVEY

2.1 Introduction

Risk-based seismic performance assessment of piping systems is attracting the attention of researchers as it is more detailed and comprehensive than deterministic assessment. Several studies were carried out on Seismic Fragility Analysis (SFA) of piping systems, which is a vital requirement for the risk assessment. Section 2.2 describes the literature on SFA of piping systems. This topic is subdivided into two parts. The first part describes the failure mode considered and the later one about SFA methodology. As the failure mode considered for SFA of piping systems significantly influence the results, more emphasis is given for the predominant failure mode of piping systems under seismic load. Section 2.3 discusses the studies carried out on predominant failure mode of piping systems under seismic load. The details of seismic ratcheting tests for piping components and systems are provided in Section 2.4. Finally, the literature on validated numerical tools for simulation of ratcheting in piping systems under seismic load is given in Section 2.5.

2.2 Literature on Seismic Fragility Analysis (SFA) of piping systems

Kennedy and Ravindra [4], Ju and Gupta [5], Firoozabad et. al. [6], Zentner [7] and Schueller et. al. [8] worked on SFA of piping systems. SFA comprises of two major components. First one is failure mode of piping systems and the second one is methodology. The details of failure mode and methodology adopted in the literature are discussed in this section.

2.2.1 Literature on the failure mode considered for SFA

Kennedy and Ravindra [4] developed seismic fragilities for nuclear power plant structures, equipment and piping systems. In this study, the piping fragility was based

on ASME code specified stress limit, which was based on static collapse. Fragility parameters for a safety class-II piping systems of a typical nuclear power plant were presented in the study. This study recommended to reduce the conservatism in the present seismic design practices by suitably accounting the inelastic energy absorption.

Ju and Gupta [5] generated seismic fragility curves for threaded Tee-joint connections of hospital piping systems. In this study, monotonic moment (M)-rotation (θ_e) curves were used to define the limit states. Plastic collapse moment given by ASME code was considered as ‘first leakage’, It was obtained from the twice elastic slope method (TES), in which plastic collapse moment equals to the twice the initial slope of the M- θ_e curve. Also, other limit states considered were ‘moderate damage’ and ‘severe damage’ corresponding to 2.5 times and 3 times of initial slope respectively. From this study, it was observed that system fragility for the same performance limit state differs significantly from decoupled analysis of the component. This study noted that the interaction effects between the main line piping system and branch piping have significant influence over seismic fragilities.

Firoozabad et. al. [6] carried out seismic fragility analysis of a typical NPP piping system. A BNL benchmark piping system was considered for this assessment. In this study also, static collapse was the assumed failure mode for the piping components. The twice elastic slope method (TES) adopted by ASME code was used for the calculation of plastic limit load. From this study, it was observed that conditional probability of failure for a straight pipe is relatively higher than that of corresponding elbow.

Zentner [7] provided a methodology and case study for numerical computation of seismic fragilities of NPP equipment and piping system. In this study, the author considered the allowable stress limit of RCC-MR code as the failure criterion. The

fragility curves using this criterion were highly conservative as the ductility effects were not considered.

Schueller et. al [8] carried out a study on fragility of primary piping of nuclear power plants. In this study, two failure criteria were considered: First one is leakage and second one is breakage of piping, in which stress based limits were used.

It is observed that many of these studies, the failure criterion considered was plastic collapse. This was the assumed failure mode by earlier version of ASME code code (before 1995) [9].

2.2.2 Literature on the SFA methodology

In the study of seismic fragilities for nuclear power plant structures, equipment and piping systems by Kennedy and Ravindra [4], a methodology based on available data along with extrapolation of design data was used. The fragility curves generated using actual data are accurate; however major limitation is the availability of large number of samples for fragility evaluation. In this study safety factor method is used. This is relatively simplified approach based on the seismic margin assessment, with several simplified assumptions such as linear relation between input and output parameters.

Ju and Gupta [5] generated seismic fragility curves for threaded Tee-joint connections using Monte-Carlo simulation method. Zentner [7] also used Monte-Carlo method for generation of fragility curves. In this method, the uncertainty in input parameters is addressed by randomly generating values for several scenarios of the problem. It has an advantage of generating probability from the results of several scenarios regardless of specific probability distribution. However, the limitation of this method is the requirement of large number of simulations.

Towashiraporn [11] used Response Surface Method (RSM) for generating seismic fragilities of buildings. The RSM uses Design of Experiments (DOE) techniques to identify efficient set of simulations and then use regression analysis to create a polynomial approximation of analysis results over variable space. The details of DOE were provided by Montgomery [12]. The advantage of this method is that structural/ piping response is required to be computed for only few set of simulations, when compared to conventional Monte-Carlo simulations.

There are two approaches for carrying out dynamic structural analysis for fragility evaluation. The first procedure is Incremental Dynamic Analysis (IDA) (Vamvatsikos and Cornell [13]; Mitropoulou and Papadrakakis [14]; Baker [15]) where the structure is subjected to one or more ground motion records each scaled to different levels of intensity, resulting in response plotted with respect to intensity level. The other one is multiple stripes analysis carried out by Jalayer [16], in which structure is analyzed at specified set of ground motion levels, each has a unique ground motion set. IDA is most commonly used approach for carrying out the dynamic structural analysis Baker [15].

2.3 Literature on predominant failure mode of piping systems under seismic load

Central Electricity Generating Board (CEGB), Berkeley, UK conducted series of experimental studies with an objective of reducing conservatism in seismic design of piping systems. Beaney [17] carried out preliminary tests on un-pressurized straight pipes and bends under cyclic loading. No significant damage was observed when excitation applied till the levels of Safe Shutdown Earthquake (SSE). Beaney [18] studied the effects of pressure on the resonant response of straight pipes by applying high levels of sinusoidal excitation at their ends. It was observed that the pressure has

caused hoop-wise expansion which is limited by material strain hardening. Further, Beaney [19] carried out tests on plain pipes and pipes with a thinned section. Later, Beaney [20] conducted cyclic tests on elbows and observed that strain accumulation was less than 1%. Though several tests were carried out, detailed information on ratcheting strain time histories are not available.

Electric Power Research Institute (EPRI) [10] initiated research to study the failure mechanisms of piping components and systems under seismic load. It was observed that ASME code acceptance criteria were based on static loadings which protects against pressure rupture, plastic collapse and fatigue. The primary focus of this research was to develop improved piping design rules to reduce the conservatism for reversed dynamic loads.

Accordingly, EPRI has carried out experiments on piping components and systems to find out the failure modes of nuclear piping under seismic load. The EPRI components tests [21] were carried out on tees, elbows, reducers, nozzles and integral attachments. From these tests, it was observed that the dominant failure mode of piping components subjected to building filtered dynamic loads is fatigue ratcheting and not the plastic collapse. At system level, carbon steel and stainless steel piping systems (six-inch diameter, schedule 40) were tested and details are given in EPRI system test report [22]. The objective of these tests was to confirm the behaviour observed in component tests. From these system level tests also, fatigue-ratcheting was the observed failure mode. Hence, it was concluded from EPRI tests, that the failure mode of piping under high dynamic reversed loading is always fatigue, ratcheting or combination of the two, and not the plastic collapse. However, data of strain time histories of these tests are not available. The details are summarized in EPRI report on Fatigue-Ratchet tests [23].

Based on these tests, EPRI report on Piping Design Rules Revisions [24] and Tagart et. al. [25] recommended code rule changes. This study has provided simple stress evaluation of modified equation (9) of the code to control the cumulative ratcheting strain. Also, a cumulative strain limit of 5% was recommended.

Accordingly, the 1995 version of ASME nuclear piping design code [9] incorporated ratcheting for Level-D seismic event. However, these codal provisions have undergone several changes and a brief description of these changes is given below:

Prior to 1995, nuclear piping design for seismic loading was based on prevention of Plastic Collapse. Equation (9) of NB-3600, Section-III, ASME Boiler & Pressure Vessel code (Prior to 1995) [9] is given in equation (2.1). The allowable primary stress for level D service condition was $3S_m$ where S_m is allowable stress-intensity.

$$B_1 \frac{PD_0}{2t} + B_2 \frac{M_i D_0}{2I} \leq 3S_m \quad (2.1)$$

The limit on primary plus secondary stress intensity of $3S_m$ has been placed at a level which ensures shakedown to elastic action after a few repetitions of the stress cycle except in regions containing significant local structural discontinuities or local thermal stresses (NB-3227.6).

Subsequently, it was postulated that cause of failure of piping components is Fatigue-Ratcheting, and not the plastic collapse. The 1995 ASME Boiler & Pressure Vessel code, Section-III, has incorporated the reverse dynamic loading and ratcheting into the code. Equation (2.2) gives the revised version of equation (2.1). The allowable primary stress for level D service condition is increased to $4.5S_m$ where S_m is allowable stress intensity.

$$B_1 \frac{PD_0}{2t} + B_2 \frac{M_i D_0}{2I} \leq 4.5S_m \quad (2.2)$$

This new limit is intended to ensure plastic shake down, defined as an event when ratcheting ceases to occur after a few cycles. The code also provides an alternate strain based approach (NB-3228.6), which states the average through wall ratcheting strain should not exceed 5% in 10 cycles of loading for level D service condition. In the 2001 edition of the code, the primary stress limit for level D loading has brought back to $3S_m$ but with modified B_2 indices (referred as B_2' indices) and the equation (2.3) gives the modified version of equation (2.2). However, the alternate strain based approach has not been altered.

$$B_1 \frac{PD_0}{2t} + B_2' \frac{M_i D_0}{2I} \leq 3S_m \quad (2.3)$$

In the further revision of the code, stress based approach has been continued and strain based approach has been removed. This may be due to insufficient experimental data and lack of validated numerical tools. Also, the basis of these changes is still under debate and hence experimental and numerical studies are required to be carried out to understand the Fatigue-Ratcheting phenomenon.

Kot et. al. [26] carried out experiments on piping systems to study the piping response under high level seismic loads. From these tests, few qualitative observations made are: (a) Pipe strains and deformations at seismic excitation levels of 300% Safe Shutdown Earthquake (SSE), are about 0.3% and at 800% SSE are about 1%. (b) Pipe failures at higher seismic excitation levels of about 800% SSE is highly unlikely.

The Nuclear Power Engineering Corporation (NUPEC) [27] carried out a series of tests on piping components and systems. It was observed that pipe failures in these

tests were characterized as through-wall cracks occurred as a result of fatigue-ratcheting.

Touboul et. al. [28] carried out quasi-static cyclic tests on pressurized elbows to study failure mode and to validate the computational tools. Details of local strain accumulation are not available from these tests. However, a gross diametric change (crown to crown diameter) of 1% to 15% was observed. Failure in the form of longitudinal cracks was observed on elbow flanks. Using these test results, Touboul et. al. [29] observed that seismic margins using RCC-MR code [30] and ASME class 2 [9] equations were same.

Yahiaoui et. al. carried out cyclic tests on carbon steel and stainless steel elbow under internal pressure and resonant dynamic in-plane bending [31] and out-of-plane bending [32]. From these tests, it was observed that overall range of displacement was increased with input excitation.

Moreton et. al. [33] proposed a methodology to evaluate the onset of ratcheting using the experiments of Yahiaoui et. al. on carbon steel and stainless steel pressurized elbows.

Chen et. al. [34] carried out ratcheting tests on carbon steel elbows under static cyclic bending loading. It was observed that the ratcheting strain rate was increased with increase in the amplitude of cyclic bending load at constant pressure or with an increase in the internal pressure at constant amplitude of cyclic bending load.

Vishnuvardhan et. al. [35] carried out tests on straight pipes and elbows under internal pressure and static cyclic load. In these tests, ratcheting failures of straight pipes were observed by occurrence of through-wall cracks or bursting with

simultaneous ballooning. In case of elbows, ratcheting failures were observed by the occurrence of through-wall crack with simultaneous ballooning.

Boussaa et. al. [36] carried out dynamic tests on pressurized elbows to study the fatigue-ratcheting failure mode. The tests were conducted under repeated seismic excitation till failure. The failures were observed by the occurrence of through wall cracks at flank location of elbow.

Slagis [37] reviewed the experimental data from available test programmes. The author observed that type of failure and seismic margin depends significantly on piping geometry, configuration as well as on the method of manufacture. The author remarked that critical parameters, which control the seismic response, are natural frequency and hoop stress. The fundamental frequencies of pipes in these tests were in the range of 5 to 10 Hz and material yield strength varies from 146 to 335 MPa. In these tests, slight variation (around 5%) is observed in frequency with loading amplitude (from 0 to 4g). The author also has observed that straight pipe has a seismic margin of 14 over Level-D permissible limit. For elbow, a margin of 14 was observed over Level-D allowable stress. The author has also noted that collapse is also a potential failure mode for certain configurations in the EPRI tests [10]. This recommends further studies to understand the failure mode of piping systems under seismic load.

2.4 Details of seismic ratcheting tests on piping components and systems

From the earlier experiments on piping components and systems, failure mode of piping under high dynamic reversed loading was identified. However, detailed information on ratcheting strain time histories of these tests are not available. As earthquake induces dynamic loading on piping components, it is necessary to study the ratcheting response in piping components and systems under dynamic loading. The

details of ratcheting tests on piping components and systems under incremental base excitation are provided below.

2.4.1 Ratcheting experiment on pressurized elbow under harmonic excitation

Earlier, Muthumani et. al. [38] carried out shake table tests on a pressurized 90⁰ long radius stainless steel (SS 304L) elbow under incremental harmonic excitation till failure. The outer diameter and nominal thickness of the elbow are 89 mm 5.5 mm respectively. The photograph and schematic of the test set up are shown in Figure 2.1 and Figure 2.2 respectively. The elbow is filled with water and pressurized up to 18 MPa to induce hoop stress of design limit, $1S_m$. From sine sweep test, the first natural frequency of the test model was 2.25 Hz.

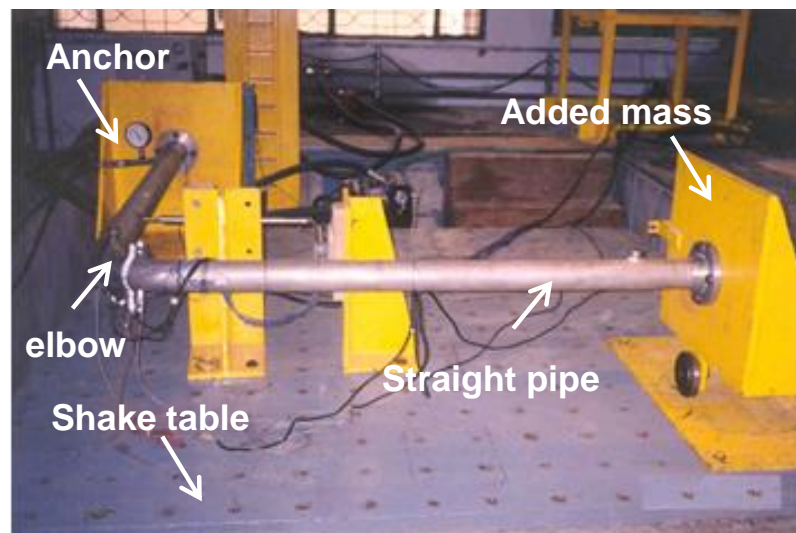


Figure 2.1: Photograph of test setup of elbow

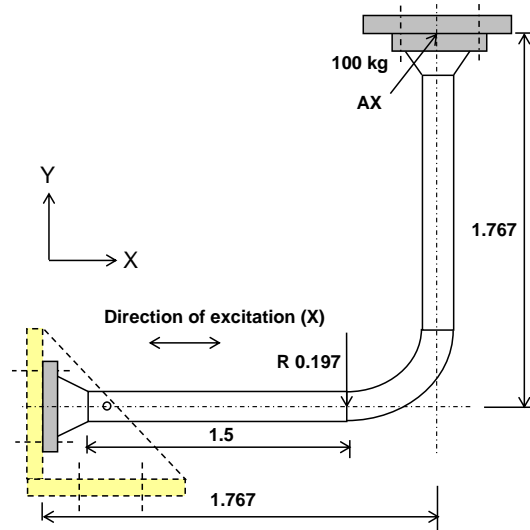


Figure 2.2: Schematic of test setup of elbow and location of strain gauges

Ratcheting test is conducted on the pressurized elbow by applying incremental harmonic excitation in X-direction at first resonant frequency and the details of loading are given in Table 2.1.

Table 2.1: Loading details for ratcheting test of the elbow

S. No.	Amplitude (g)	Internal pressure (MPa)	No. of Cycles
1	0.2	18	60
2	0.4	18	60
3	0.6	18	60
4	0.8	18	60
5	1.0	18	300
6	1.0	23	180
7	1.0	25	220

The resulting hoop strain time history at crown of elbow is plotted in Figure 2.3. During 221st cycle with 1g excitation, failure has occurred at weld joint between elbow and pipe resulting in a sudden drop in measured dynamic strain values as observed from Figure 2.3. It is to be noted that this failure has occurred at a pressure of 25 MPa, which is higher than design pressure. As the level of excitation could not be increased beyond the shake table capacity of 1g, the test is continued till failure with this constant

excitation at higher pressures. The hoop strain at crown of elbow is around 5% prior to failure.

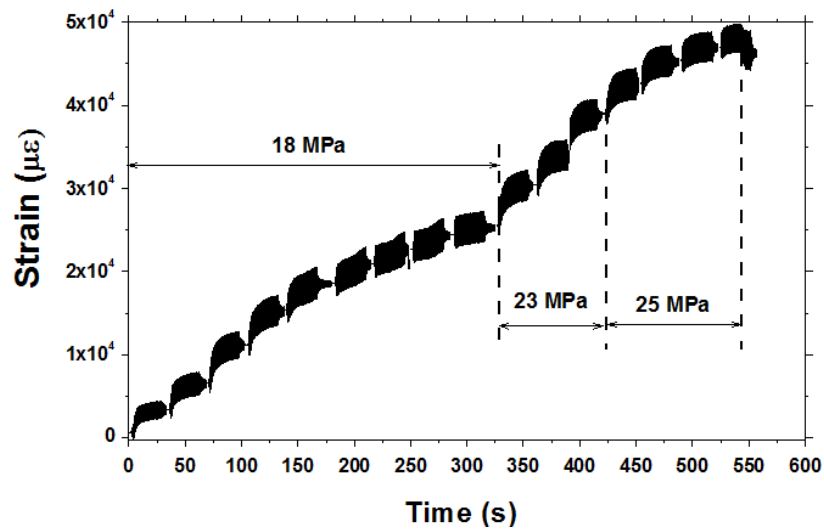


Figure 2.3: Hoop Strain time history at crown of elbow

2.4.2 Ratcheting experiments on pressurized piping systems under seismic load

Ratcheting experiments were carried out on 3 inch and 6 inch piping systems. The details are provided below.

2.4.2.1 Ratcheting experiments on 3-inch carbon steel piping system under seismic load

A three dimensional carbon steel pressurized piping system (size: 3" NB and schedule 40) shown in Figure 2.4 was tested by Ravi Kiran et. al. [39] under increasing seismic load. Schematic and dimensions of the piping system are provided in Figure 2.5. It was pressurized with water and subjected to incremental tri-axial earthquake load with Test Response Spectra (TRS) shown in Figure 2.6, till failure.



Figure 2.4: Photograph of piping system

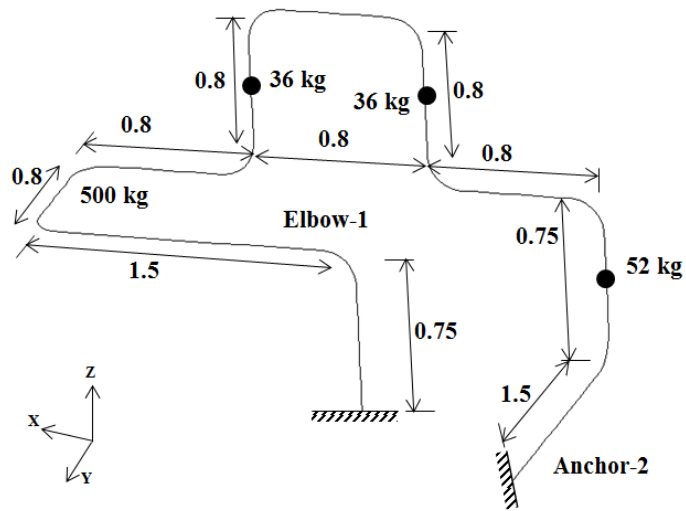


Figure 2.5: Schematic and dimensions of the piping system

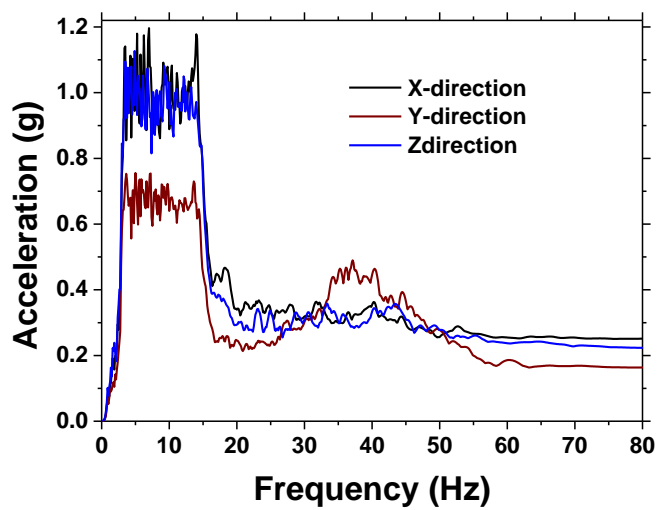


Figure 2.6: Test Response spectra for 2% damping

The details of various levels of base excitation are provided in Table 2.2. The resulting hoop strain time history at crown of elbow is shown in Figure 2.7. It is observed that the strain gauge was de-bonded during excitation with 0.75g ZPA and the strain measured was about 0.3%. The axial strain time history at horizontal anchor location is given in Figure 2.8 and it is observed that this gauge was failed during excitation with 1.75g ZPA, after recording a strain of about 1%. During the third input time history which is compatible 2g ZPA, a crack is formed at a weld location of elbow-1 and water jet has come out.

Table 2.2: Details of various levels of base excitation

ZPA of TRS (g)	Pressure (MPa)	No. of base excitation time histories
0.25	21.3	6
0.5	21.3	3
0.75	21.3	12
1	21.3	9
1.25	21.3	9
1.5	21.3	9
1.75	21.3	9
2	21.3	3

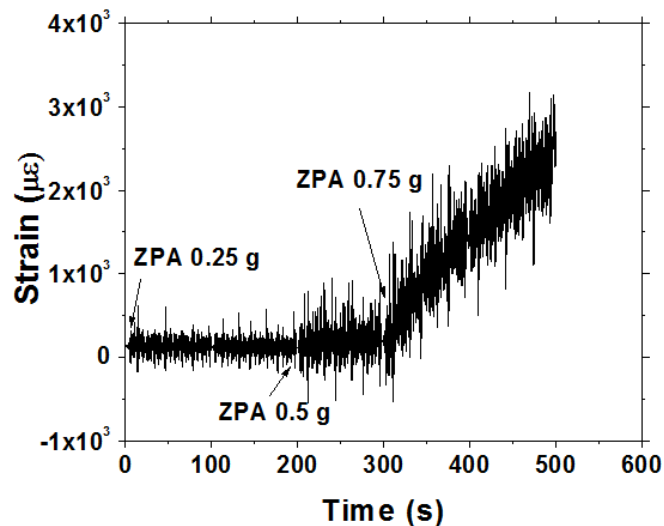


Figure 2.7: Hoop Strain time history at crown of elbow

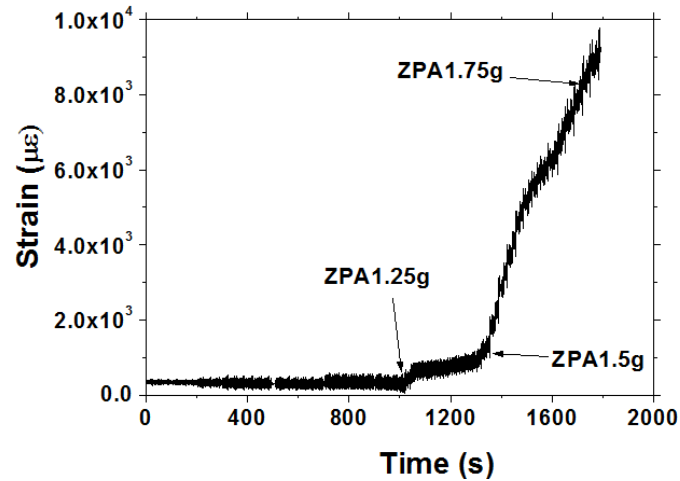


Figure 2.8: Axial Strain time history at horizontal anchor location

2.4.2.2 Ratcheting tests on 6 in stainless steel piping system under seismic load

Two sets of pressurized stainless steel (grade SS304L) piping systems (size: 6” NB and schedule 40) shown in Figure 2.9 were tested by Ravi Kiran et. al. [40] under increasing seismic load. To understand the fatigue-ratcheting phenomenon at system level, these shake table tests were carried out on pressurized piping system of stainless steel material, which was designated as Stainless Steel Piping System (SSPS). It was pressurized with water and subjected to incremental tri-axial earthquake load with Test Response Spectra (TRS) shown in Figure 2.10, till failure.



Figure 2.9: Photograph of SSPS

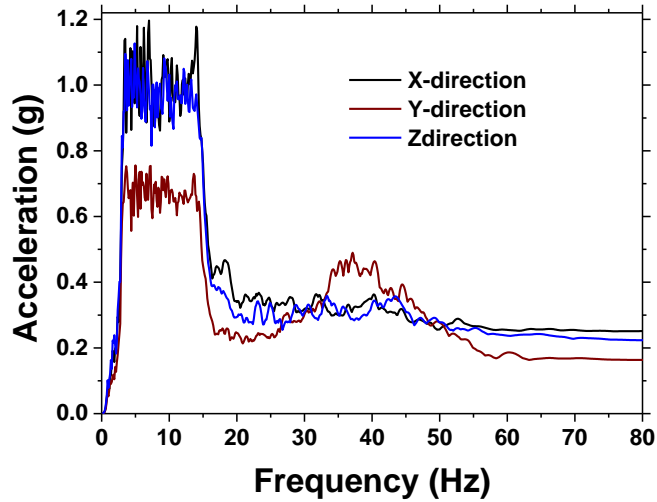


Figure 2.10: Test Response Spectra (TRS) for 2% damping

The details of various levels of base excitation are provided in Table 2.3.

Table 2.3: Details of various levels of base excitation

ZPA (g)	Internal Pressure (MPa)	No. of base excitation time histories
1	12	5
1.25	12	5
1.5	12	5
1.75	12	5
2	12	5
2.25	12	5
2.5	12	5
2.5	14	30
2.5	16	8

The resulting hoop strain time history at crown of elbow in two tests is shown in Figure 2.11. The maximum strain at the crown location of elbow in test-1 is 1.45%. Early strain gauge failure occurred in test-2. During the third input time history which is compatible 2g ZPA, water jet has come out through wall crack at crown location of elbow as shown in Figure 2.12.

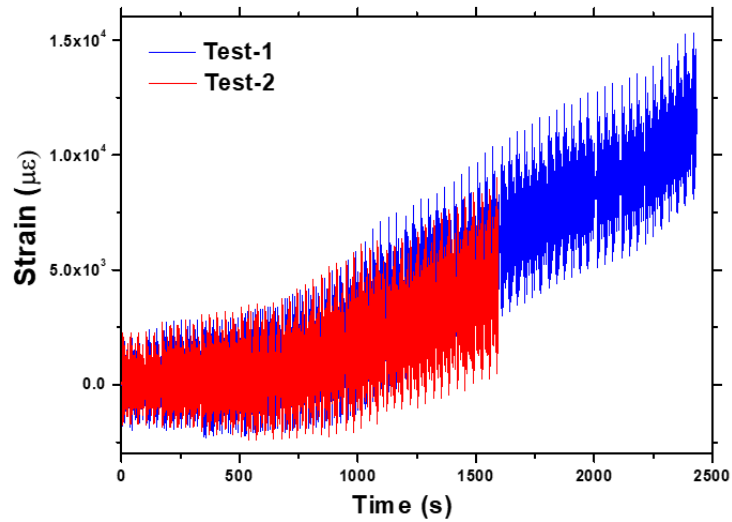


Figure 2.11: Hoop Strain time history at crown of elbow



Figure 2.12: Water jet through crack at crown of SSPS elbow

2.5 Literature on validated numerical tools for simulation of ratcheting in piping components and systems

Literature on numerical tools for simulation of ratcheting in piping systems is broadly categorized into two groups: a) Literature on simulation of ratcheting in piping components under static cyclic load b) Literature on numerical tools for simulation of ratcheting in piping systems under seismic load.

2.5.1 Literature on simulation of ratcheting in piping components under static cyclic load

Hassan et. al. [41] presented analysis of straight pipes under static cyclic loading using a kinematic hardening rule based on Armstrong-Frederick model [42].

Kulkarni et. al. [43] carried out analysis of a straight pipe under static cyclic loading using Chaboche [44] model. However, this study has provided the results for the first 90 cycles. It was observed that the simulation under predicts ratcheting in the beginning for the first 40 cycles and later, slightly over predicts the experimental results. The simulation was also carried out for an elbow under first 120 cycles of harmonic base excitation using equivalent static cyclic load approximation. It was observed that the simulation over predicts ratcheting beyond 100 cycles.

Ravi Kiran et. al. [45] further continued the analysis of a straight pipe under static cyclic loading beyond 90 cycles using Chaboche [44] model. It was observed that this model over-predicts the ratcheting in straight pipe at higher cycles, near ratcheting failure.

DeGrassi et. al. [46] carried out non-linear pre-test analysis of NUPEC piping programme [27] using Chaboche model.

2.5.2 Literature on numerical tools for simulation of ratcheting in piping systems under seismic load

Jaquay et. al. [47] provided an incremental hinge technique for the analysis of piping systems under seismic loading. This is a seismic response prediction method based on a simplified plastic system analysis utilizing response spectrum as input. The simplified plastic system analysis was carried out using incremental response spectrum analysis. The yielded components were replaced with hinge elements when a predefined

hinge moment is reached. This hinge moment value is selected to result in inelastic energy absorption of the same magnitude as observed in piping component dynamic tests and analyses.

Ravi Kiran et. al. [48] applied this incremental hinge technique with a modification to analyze the three inch piping system. In this study, the modification proposed was to use a spring model comprising of three translational and three rotational springs to replace critical elbow. A typical deformation of the piping system using this spring model is shown in Figure 2.13 and details of spring model are given in Figure 2.14.

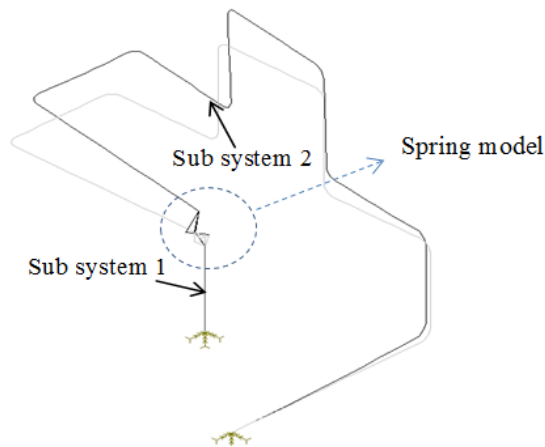


Figure 2.13: Deformation of piping system using spring model

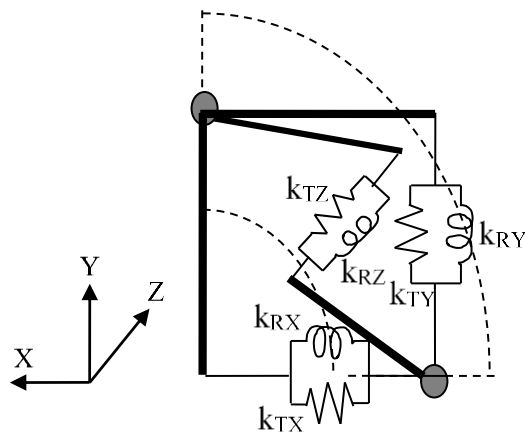


Figure 2.14: Spring model to replace elbow

Hanspal [49] further modified this incremental hinge technique by considering the hinge moment as that corresponds to 5% strain and not from the static collapse. In this modification, iterations were carried out till the formation of single hinge in the piping system, unlike in original incremental hinge technique where the system is said to be failed until the formation of two hinges [48].

Touboul et. al. [50] remarked that enhanced and simplified numerical methods are required to be developed in order to take into account the plasticity effects.

2.6 Gap areas and directions for research

As described in Section 2.2, majority of studies on seismic fragility analysis of piping systems have considered plastic collapse as failure mode. No studies have reported on seismic fragility analysis considering ratcheting, which is actual failure mode. This necessitates a more comprehensive research on SFA using this predominant failure mode.

Also, the ASME code has initially provided ratcheting based design criterion which was further discontinued due to insufficient experimental data and lack of validated numerical tools. Hence, there is a need to develop numerical tools for simulation of ratcheting and validate with experimental results for carrying out seismic performance assessment of piping systems. Also, the numerical tool for simulation of ratcheting is required to be suitable for most widely adopted Incremental Dynamic Analysis (IDA) procedure for fragility evaluation.

Hence, the first objective of the present research is to develop validated numerical tool for simulation of ratcheting in pressurized piping systems. This objective is met by carrying out experimental and numerical studies on ratcheting in pressurized piping components and systems. The next major goal is to carry out Seismic Fragility Analysis

(SFA) of pressurized piping systems considering ratcheting, which is the predominant failure mode under seismic load. This requirement is fulfilled by developing a methodology for SFA of piping systems considering ratcheting. The validated numerical tool is used for simulation of ratcheting. Also, performance limit states for ratcheting, variation in seismic input and piping parameters are obtained. The final task is the evaluation of seismic risk. This is fulfilled by the convolution of fragility information with seismic hazard curves.

CHAPTER 3 INCREMENTAL ITERATIVE RESPONSE SPECTRUM (IIRS) METHOD FOR PREDICTION OF RATCHETING

3.1 Introduction

Seismic Fragility Analysis (SFA) of piping systems considering ratcheting requires validated numerical tools to simulate ratcheting in the piping systems. Also, there is a need for a numerical tool which can be used by designers to predict ratcheting in piping components for a possible use of ratcheting based criterion.

The ratcheting behavior of pressurized piping systems under seismic load can be obtained using detailed non-linear time history analysis or by simplified numerical tools. Detailed non-linear time history analysis provides seismic response at each instant of time, whereas simplified numerical tools using response spectrum provide the peak seismic response. Non-linear time history analysis can be carried out using either full non-linear Finite Element (FE) models or sub-structuring concepts. Hassan et. al. [41] and Kulkarni et. al. [43] carried out quasi-static cyclic analysis of piping components using full non-linear FE models to simulate ratcheting. However, ratcheting simulation of long piping systems under random excitation by non-linear time-history analysis using full models is cumbersome, expensive and requires advanced computing facilities. Alternatively, sub-structuring concepts can be used to obtain the ratcheting behavior of critical components like elbows, by the use of multi-point constraints at the junctions of straight pipes and elbows of piping system. DeGrassi et. al. [46] attempted to use such techniques for simplified piping configurations. Incremental hinge technique by Jaquay et. al. [47] is a seismic response prediction method based on a simplified plastic system analysis utilizing response

spectrum as input. Ravi Kiran et al. [48] have applied this incremental hinge technique with a modification of replacement of critical elbow with spring model comprising of three translational and three rotational springs. In this study, the spring constants are evaluated from static analysis. Hanspal [49] has further modified this incremental hinge technique by considering the hinge moment as that corresponds to 5% accumulated strain and not from the static collapse. These concepts are clubbed in a numerical procedure termed as Incremental Iterative Response Spectrum (IIRS) method for evaluation of ratcheting in piping systems under incremental seismic load. In this method, the spring stiffness is updated using the envelope cyclic characteristics, obtained from cyclic plasticity analysis. The first advantage of IIRS method is that the designers can use the existing response spectrum analysis for prediction of ratcheting in piping system. The second advantage of IIRS method compared to detailed FEA is its suitability for fragility analysis of piping systems based on ratcheting failure, which requires large number of simulations. Sub-structuring with multi point constraints needs time history analysis to predict ratcheting behaviour and it is not straight forward to perform response spectrum analysis. To overcome this, in IIRS method, components are analyzed separately under cyclic load and pressure. Moment – rotation and strains are related with spring characteristics considering ratcheting.

In the literature, Incremental Dynamic Analysis (IDA) was widely used for SFA of steel and RC structures. In IDA, the structure is subjected to one or more ground motion records each scaled to different levels of intensity, resulting in response plotted with respect to intensity level. Due to its suitability for IDA, IIRS method is considered for evaluation of ratcheting strains in piping systems. In this method, the piping system is subjected to incremental seismic excitation and the resulting peak strain response is plotted with respect to the chosen ground motion parameter.

The details of IIRS method are provided in the next section. Subsequently, this method is demonstrated for an elbow pipe system, which was tested earlier by Muthumani et. al. [38] under incremental harmonic base excitation.

3.2 Details of Incremental Iterative Response Spectrum (IIRS) method

The flow chart of IIRS method for evaluation of ratcheting in piping systems is shown in Figure 3.1. Typically piping systems comprise of straight pipes, elbows and tee joints. Elbows and tee joints are relatively highly stressed when compared to straight portions due to geometry. Hence, ratcheting occurs more significantly in these components when compared with straight pipes. IIRS method is used to find out ratcheting in the highly stressed component (typically elbow) of the piping system. It is a linearization technique in which the local inelastic response of the component is obtained iteratively using the linear response spectrum analysis. It comprises of two stages. In the first stage, envelope characteristics are generated from the cyclic analysis of the component (typically elbow). Two straight pipe segments are attached to both ends of elbow and the whole elbow pipe system is modeled using shell elements. The model is subjected to incremental monotonic tip displacement and the resulting load-displacement curve is plotted. The limiting displacement is obtained by the intersection of two tangents. Later, cyclic analysis of the elbow pipe system is carried out by applying incremental cyclic tip displacement. Chaboche nonlinear kinematic hardening material model [44] is used for the analysis. The resulting moment-rotation and moment-strain hysteresis plots are obtained. Cycle by cycle peak value is extracted from these loops to obtain envelope moment-rotation-strain curves.

In the second stage, ratcheting strains are obtained from the iterative response spectrum analysis of the line model of piping system using the envelope characteristics. The line model of the piping system is obtained using pipe and elbow elements.

Response spectrum analysis of the line model is carried out to identify the critical elbows. The line model is updated by replacing the critical elbows with a combination spring model. This combination spring model comprises of three translational, three rotational springs connected by rigid links. Response spectrum analysis of the updated line model of the piping system is carried out. The resulting moment-rotation values for the elbow are obtained from this analysis. Corresponding to this rotation, the envelope moment value of the elbow is obtained from the envelope moment-rotation-strain curves generated in first stage. This envelope moment is compared with the moment of the line model. If the error is more than the chosen threshold (1%), the rotational stiffness is revised by multiplying its previous value with the ratio of envelope moment to the moment from response spectrum analysis. Then, response spectrum analysis is repeated for second iteration. The moment-rotation values of the elbow are obtained and compared with corresponding envelope moment-rotation values. If the error is less than the threshold, the convergence is attained and ratcheting strain corresponding to this moment is obtained from the envelope cyclic curve of the elbow. Later, the excitation level is increased to next level and the iterative response spectrum analysis is repeated. Finally, the peak ratcheting strain is plotted with respect to excitation level.

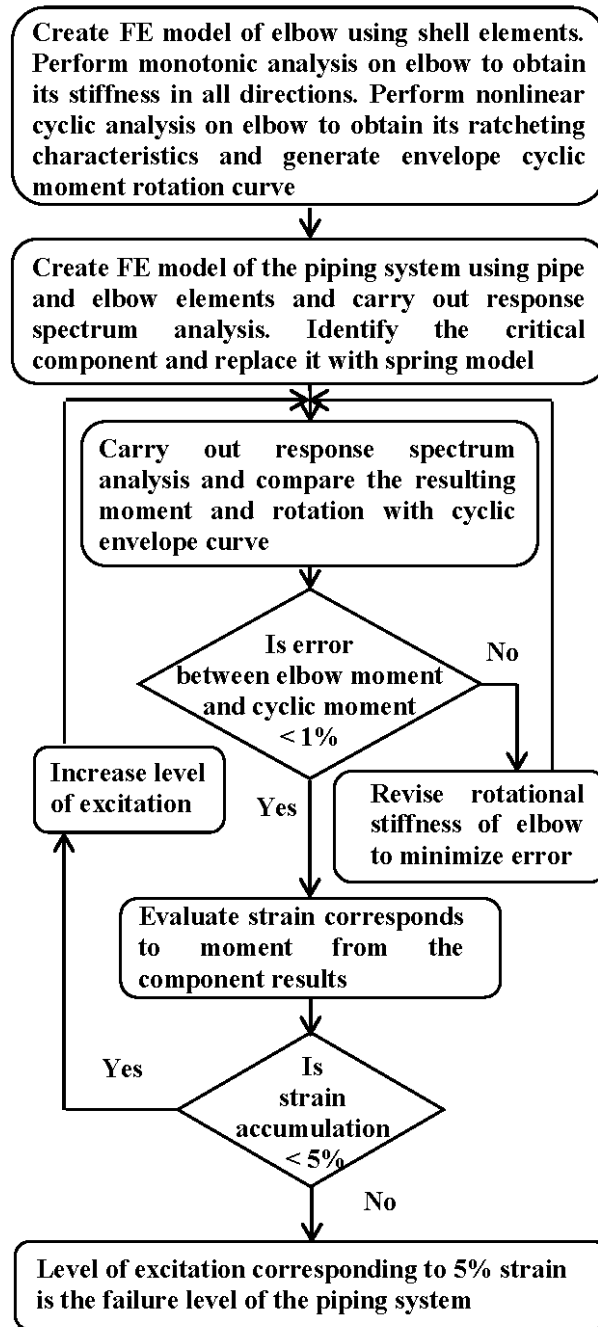


Figure 3.1: Flow chart of IIRS method

3.3 Application of IIRS method to predict ratcheting in an elbow under harmonic excitation

IIRS method is applied to predict ratcheting in a stainless steel elbow pipe system, which was tested earlier by Muthumani et. al. [38] under incremental harmonic base excitation. Schematic of test setup of elbow and location of strain gauges is shown in Figure 2.4. The test specimen was a 90° long radius elbow with an outer diameter 89

mm and nominal thickness of 5.5 mm. It comprises of two straight pipes, large radius elbow and a lumped mass. The material of the elbow is stainless steel (SS 304L). This is analyzed using IIRS method which comprises of two stages. In the first stage, envelope characteristics are generated from the cyclic analysis of elbow and in second stage; ratcheting peak ratcheting strains are calculated from the iterative response spectrum analysis of the line model of piping systems/components using the envelope characteristics. The details are provided below.

3.3.1 Stage 1: Cyclic envelope characteristics for the elbow

Ratcheting simulation is carried out for the elbow. Shell elements are used to model the elbow and the finite element (FE) model is shown in Figure 3.2.

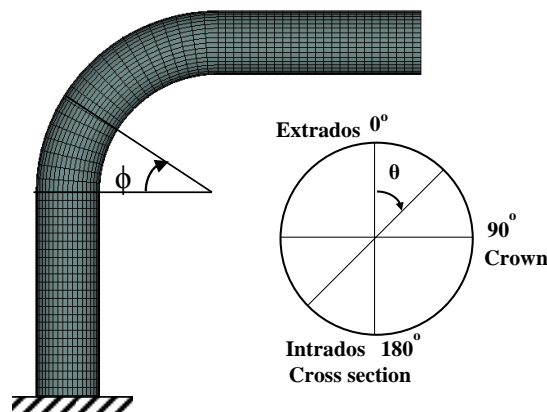


Figure 3.2: FE model of elbow

Hassan et. al. [41], Kulkarni et. al. [43] and DeGrassi et. al. [46] used four node shell elements for ratcheting simulation in piping components under cyclic loading. It was concluded from these studies, that the predicted ratcheting response by four node shell elements compared well with experiments results. Hence, four node shell element with six degrees of freedom is used in the present work. Thickness variation in the elbow, which is idealized from the measurement on similar elbow, is shown in Figure

3.3. This assumed thickness variation is plotted for different cross section angles (θ) and bend angles (ϕ) as shown.

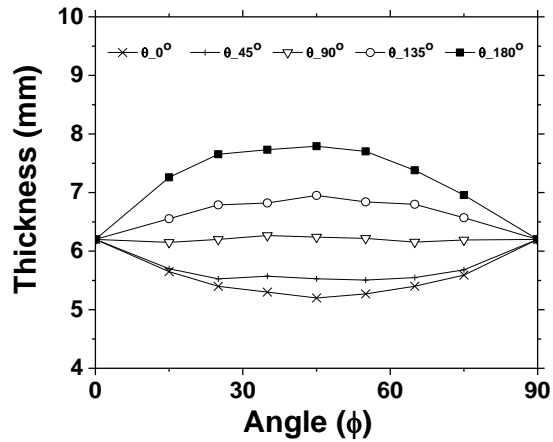


Figure 3.3: Assumed thickness variation in the elbow

Mesh convergence study is carried out for elbow to minimize the discretization error. Initially the elbow is modeled using coarse mesh and a force of 4 kN is applied at the tip. The resulting tip displacement is obtained. Later, the mesh density is increased and tip displacement is obtained under the same force at elbow tip. The resulting tip displacement variation with mesh density is shown in Figure 3.4. It is observed that convergence is obtained for mesh with 768 degrees of freedom (DOF). This is the minimum DOF required. However, for ratcheting analysis, FE model with 18936 DOF is used.

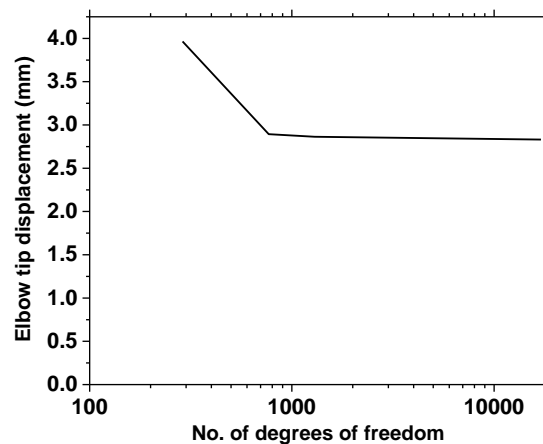


Figure 3.4: Mesh convergence study for elbow

The FE model is subjected to internal pressure for generating hoop stress equals to design stress of $1S_m$ based on yield stress. Static nonlinear analysis is conducted to get limit displacement (δ_L) by applying an incremental force at the elbow tip. The limit displacement for the elbow is 12.7 mm, which is determined by intersecting tangent method as shown in Figure 3.5.

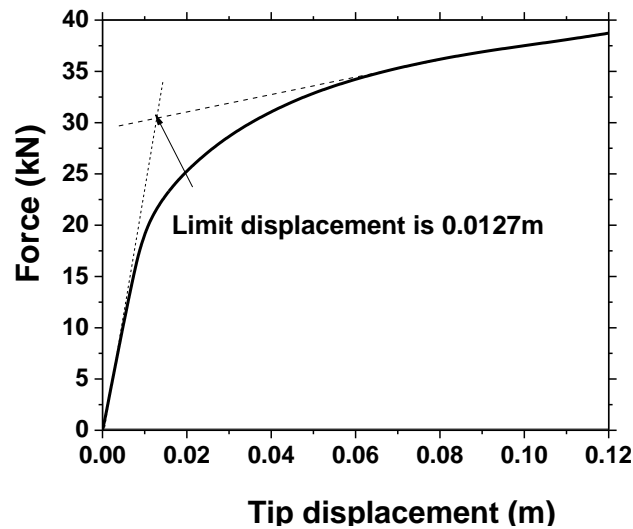


Figure 3.5: Limit displacement for the elbow

Cyclic plasticity analysis is carried out by applying design level internal pressure and incremental cyclic tip displacement. Using 10% incremental limit displacement, the cyclic tip displacement given in Figure 3.6 is applied to the elbow and analysis is performed. Analysis of the elbow is carried out with uniform nominal thickness as well as with variable thickness using linear interpolation for intermediate locations.

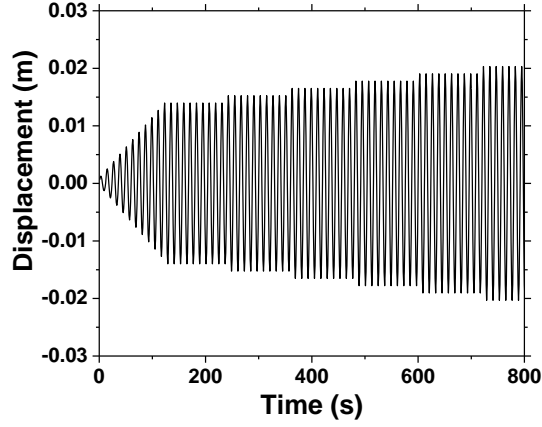


Figure 3.6: Load Line Displacement time history at the free end of the elbow model

The simulation is carried out using Chaboche model, which requires six parameters (C_i and γ_i , $i=1,2$ and 3), which are obtained from the experimental uniaxial hysteresis loop using equations given below:

$$\sum_{i=1}^3 \alpha_i + \sigma_0 = \sigma_x \quad (3.1)$$

$$d\alpha_i = \frac{2}{3} C_i d\varepsilon_p - \gamma_i \alpha_i d\varepsilon_p \quad (3.2)$$

$$\alpha_i = \frac{C_i}{\gamma_i} \left[1 - 2 \exp\left\{ -\gamma_i (\varepsilon_x^p - (-\varepsilon_L^p)) \right\} \right], \text{ for } i=1 \text{ and } 2 \quad (3.3)$$

$$\alpha_3 = C_3 \varepsilon_L^p \quad (3.4)$$

The detailed evaluation procedure and significance of all these parameters is given by Chaboche [44]. In the three decomposed Chaboche model, the stabilized hysteresis loop is divided into three portions. The value of C_1 is evaluated from the slope of the curve at onset of yielding. The value of γ_1 is chosen to stabilize the hardening of α_1 which is obtained from Eq. (3.3) quickly. The values of C_2 and γ_2 are evaluated from the above equations to match the non-linear portion of the hysteresis loop. Finally, the third linear portion of the curve at high strain values is used for evaluation of α_3 . The

straight line drawn parallel to this linear portion of loop gives α_3 and the slope gives the value of C_3 . The Chaboche parameters obtained are: $C_1=1085000$, $C_2=43000$, $C_3=4100$, $\gamma_1=271250$, $\gamma_2=500$, $\gamma_3=9$ [43] and the comparison of Chaboche model with experimental stabilized hysteresis loop is shown in Figure 3.7.

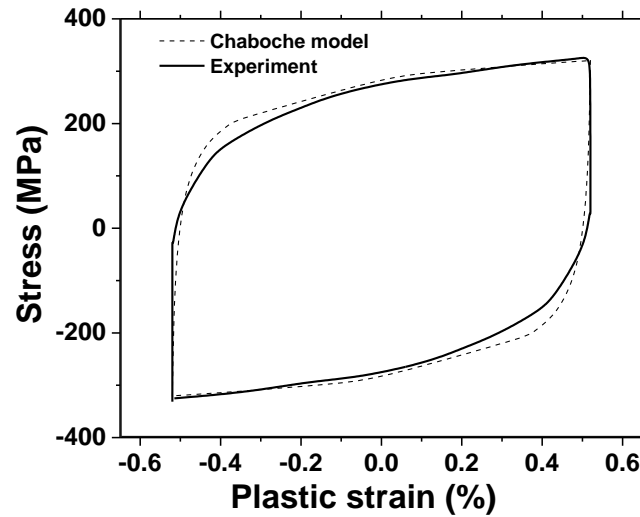


Figure 3.7: Comparison of Chaboche model with Experimental stabilized hysteresis loop

The cyclic moment- rotation curves for the elbow with uniform and thickness variation are shown in Figure 3.8 and Figure 3.9 respectively. The cyclic moment-strain curves for the elbow with uniform and thickness variation are shown in Figure 3.10 and Figure 3.11 respectively.

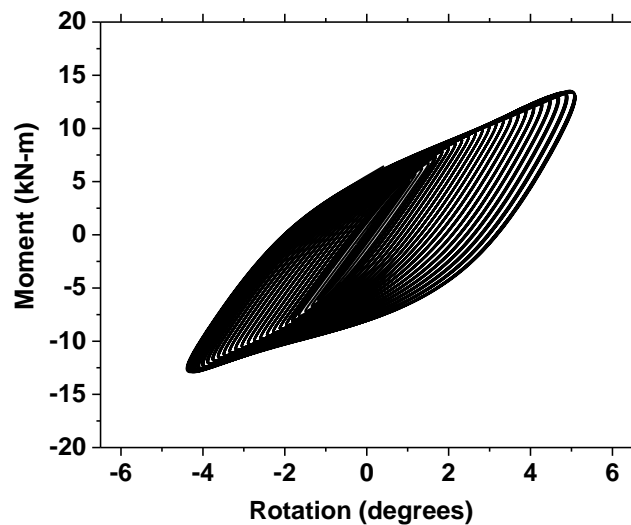


Figure 3.8: Cyclic moment-rotation curves for the elbow with uniform thickness

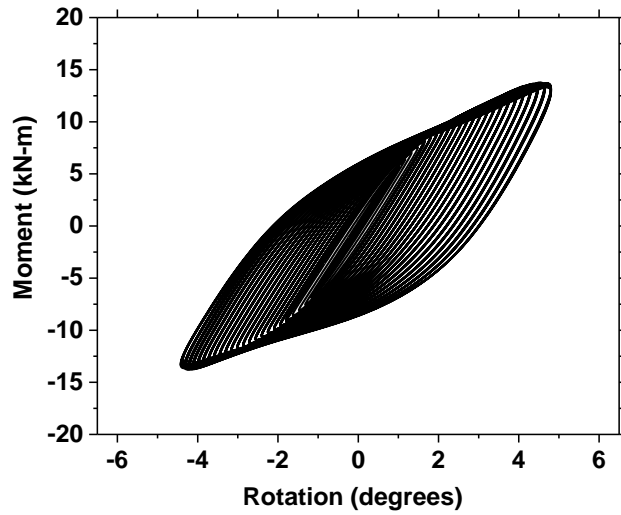


Figure 3.9: Cyclic moment-rotation curves for the elbow with thickness variation

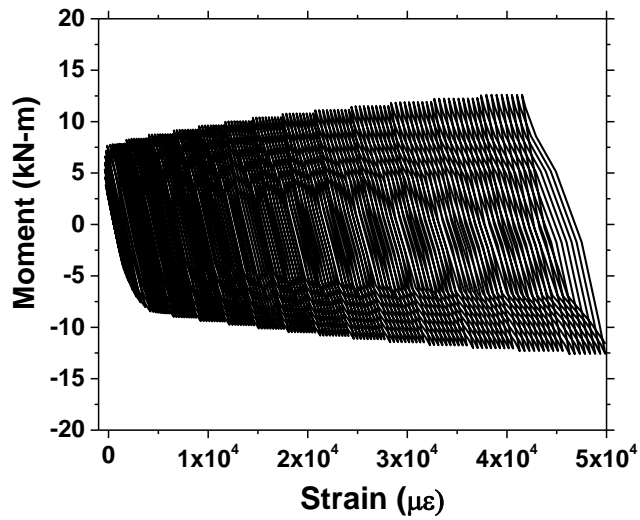


Figure 3.10: Cyclic moment- strain curves for the elbow with uniform thickness

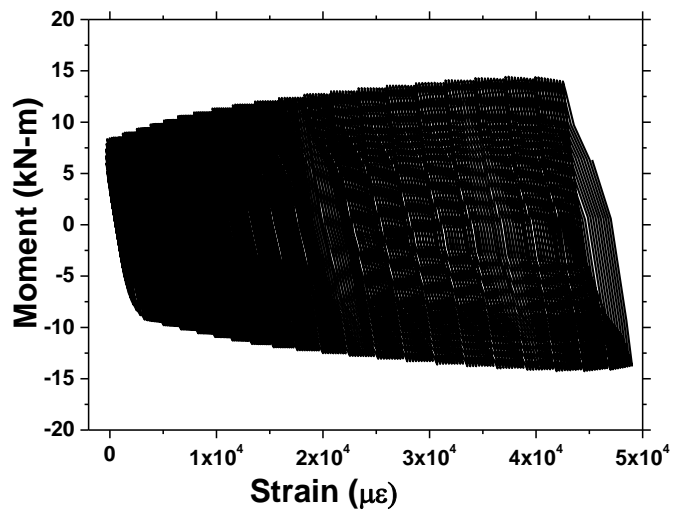


Figure 3.11: Cyclic moment- strain curves for the elbow with thickness variation

Envelope Strain-Moment-Rotation characteristics of the elbow are obtained by joining the peaks of cyclic rotation-moment and moment-strain curves and are shown in Figure 3.12.

3.3.2 Stage 2: IRS analysis for elbow test setup

FE model of the elbow test setup using spring model is shown in Figure 3.13. In this model, elbow is represented using combination of translational and rotational springs. The spring constants are obtained from the static analysis of the elbow.

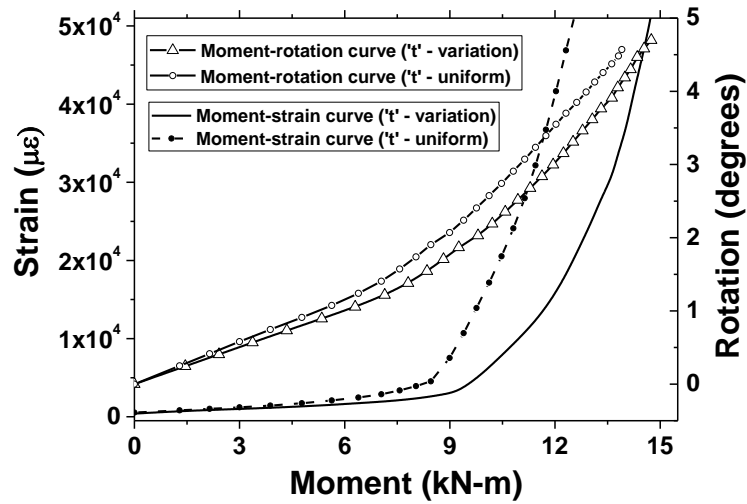


Figure 3.12: Envelope Strain-Moment-Rotation characteristics for the elbow

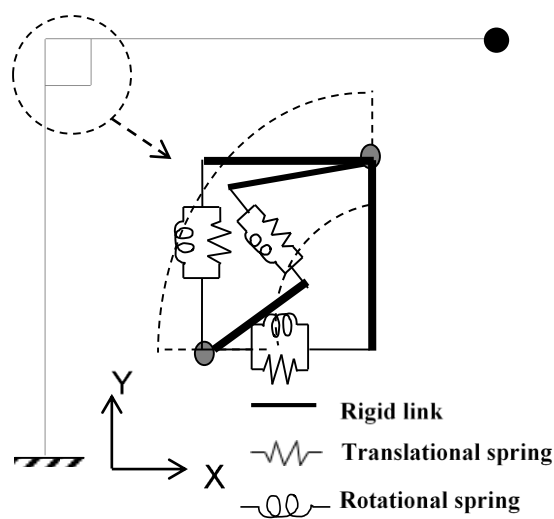


Figure 3.13: FE model of elbow with springs

The analysis is carried out by applying incremental displacement at elbow tip. The initial slope of the load-displacement curve gives the translational spring stiffness while the slope of moment-rotation curve gives the rotational spring stiffness. The analysis is carried out for both in-plane and out-of-plane directions to obtain stiffness values of all three translational and three rotational springs. Natural frequencies and mass participation in three directions for the elbow are given in Table 3.1.

Table 3.1: Natural frequencies and mass participation for the elbow

S. No.	f (Hz) Analysis (Experiment)	% mass participation in X- direction	% mass participation in Y- direction	% mass participation in Z- direction
1	2.16 (2.25)	10.0	68.8	1.5E-12
2	6.85	81.1	7.8	2.7e-9
3	16.17	1.0E-8	3.0E-8	24.3

The first natural frequency of the elbow using spring model is 2.16 Hz. This is closer to 2.25 Hz, which was obtained from sine sweep test. This mode has 68.8 % mass participation in Y-direction. IIRS analysis is carried out on the elbow with a pressure of 18 MPa (same as that of experiment) and increasing harmonic base motion. Response spectrum for excitation with frequency of 2.16 Hz and amplitude of 0.2g is shown in Figure 3.15, which is obtained from the peak response of single DOF oscillator under harmonic base excitation with a constant frequency. Cyclic characteristics of the elbow for uniform thickness from first phase of analysis are used.

Base motion with 0.2g ZPA is applied to the model shown in Figure 3.13 and response spectrum analysis is carried out. The resulting in plane moment (M) and rotation (θ_c) are 4.517 kN•m and 1.48×10^{-2} rad respectively. The cyclic moment (M_c) corresponds to this rotation is 4.521 kN•m, resulting in an error of 0.09%, which is less

than chosen convergence limit. Ratcheting strain for 0.2g ZPA is 0.2%, which is obtained from Figure 3.12 corresponding to this moment. Base motion is increased to 0.4g ZPA and response spectrum analysis is carried out. The resulting ‘M’ and ‘ θ_e ’ are 9.034 kN•m and 2.96×10^{-2} rad respectively. The ‘ M_c ’ corresponds to this rotation is 7.709 kN•m, resulting in an error of 17.17%, which is more than chosen convergence limit. In the second iteration, the stiffness is revised to 0.261 MN•m/rad, and response spectrum analysis is carried out. The resulting ‘M’ and ‘ θ_e ’ are 8.038 kN•m and 3.086×10^{-2} rad respectively. The ‘ M_c ’ corresponds to this rotation is 7.926 kN•m, resulting in an error of 1.41%, which is slightly more than chosen convergence limit. In the third iteration, the stiffness is revised to 0.257 MN•m/rad and resulting ‘M’ and ‘ θ_e ’ are 7.949 kN•m & 3.094×10^{-2} rad respectively. The ‘ M_c ’ corresponds to this rotation is 7.941 kN•m, resulting in an error of 0.1%, which is less than chosen convergence limit. Ratcheting strain for 0.4g ZPA is 0.42%, which is obtained from Figure 3.12 corresponding to this moment. IRS analysis is done for the remaining base motion with ZPA from 0.6g to 1.0 g. Variation of stiffness in IIRS analysis for various levels of excitation is shown in Figure 3.14.

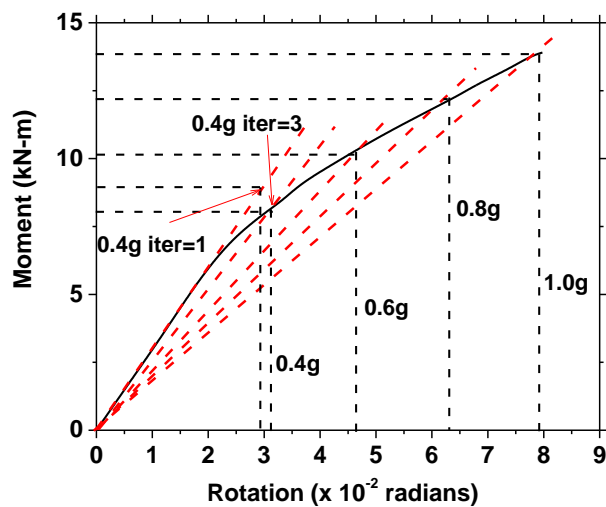


Figure 3.14: Variation of stiffness in IIRS analysis

For the base motion of 1.0g ZPA, ratcheting strain of 7.4% is obtained from the converged moment of 13.3 kN•m. The level of excitation corresponding 5% strain is 0.86g, which is obtained from interpolation. Details of iterations are provided in Table 3.2.

Table 3.2: Results of IIRS analysis for the elbow (uniform thickness)

Table excitation level, ZPA (g)	Iter. no.	k_{Rz} (MN•m/rad)	M (kN•m)	θ_e ($\times 10^{-2}$ rad)	M_c (kN•m)	Error (%)	ϵ_{elb} ($\mu\epsilon$)
0.2	1	0.31	4.517	1.48	4.521	0.09	2010
0.4	1	0.31	9.034	2.96	7.709	17.17	4195
	2	0.261	8.038	3.086	7.926	1.41	
	3	0.257	7.949	3.094	7.941	0.10	
0.6	1	0.257	11.924	4.64	10.060	18.53	18600
	2	0.22	10.310	4.75	10.184	1.24	
	3	0.21	10.194	4.76	10.188	0.06	
0.8	1	0.21	13.591	6.34	11.764	15.53	39020
	2	0.19	11.778	6.35	11.768	0.08	
1.0	1	0.19	14.722	7.93	13.408	9.80	74700
	2	0.17	13.280	7.87	13.337	0.43	

Similarly IIRS analysis has been carried out using the elbow characteristics of thickness variation and the results are given in Table 3.3.

Table 3.3: Results of IIRS analysis for the elbow (thickness variation)

Table excitation level (g)	Iter. no.	k_{Rz} (MN•m/rad)	M (kN•m)	θ_e ($\times 10^{-2}$ rad)	M_c (kN•m)	Error (%)	ϵ_{elb} ($\mu\epsilon$)
0.2	1	0.351	4.954	1.42	4.963	0.18	1550
0.4	1	0.351	9.909	2.84	8.518	16.33	3020
	2	0.302	8.959	2.97	8.766	2.20	

	3	0.295	8.823	2.99	8.803	0.23	
0.6	1	0.295	13.234	4.48	11.152	18.67	12250
	2	0.249	11.618	4.67	11.384	2.06	
	3	0.244	11.425	4.69	11.404	0.18	
0.8	1	0.244	15.234	6.25	12.977	17.39	25660
	2	0.208	13.204	6.35	13.067	1.05	
	3	0.205	13.072	6.35	13.069	0.02	
1.0	1	0.205	16.340	7.94	14.488	12.78	43900
	2	0.182	14.457	7.93	14.471	0.10	

The resulting ratcheting strains are compared with experimental strains and the comparison is shown in Figure 3.16. It can be seen that analysis with IIRS method has predicted slightly higher ratcheting strains except for lower levels of excitation. The test was carried out under harmonic excitation at a constant frequency of 2.25 Hz. However, due to slight frequency reduction of elbow at higher excitation, the dynamic amplification in test is lesser than resonant amplification. Hence, the strains in test are lesser than IIRS method. Also, this difference is because the experimental uni-axial stabilized hysteresis loop used for evaluation of Chaboche parameters was considered from the literature and not from the same elbow. Also, it is observed that elbow with thickness variation has predicted lower strains compared to that of uniform thickness. Hence, it can be concluded that ratcheting in elbow depends on the thickness variation. It can also be seen from Figure 3.16 that the resulting peak strain plotted over amplitude of excitation is similar to results from IDA. Hence, it is concluded that IIRS method is similar to IDA and can be used to carry out seismic fragility analysis of pressurized piping systems.

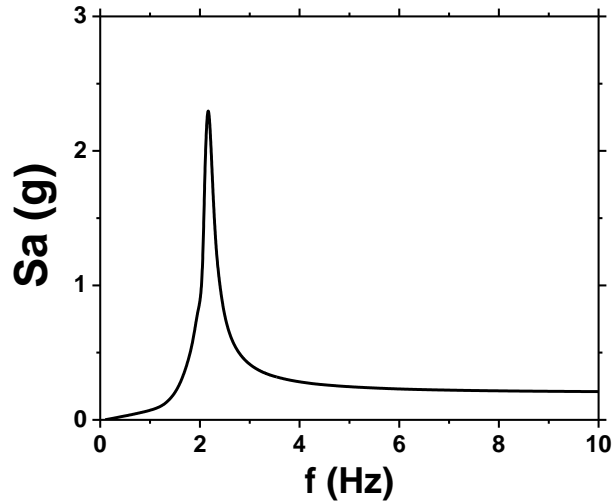


Figure 3.15: Response spectrum for harmonic excitation with amplitude of 0.2g

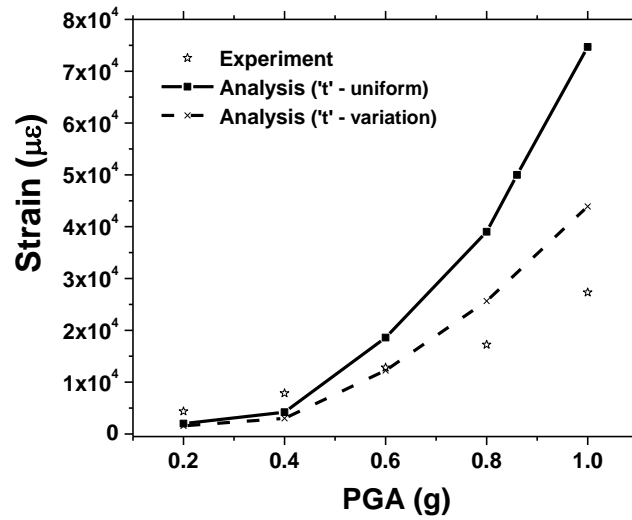


Figure 3.16: Comparison of predicted strain accumulation at flank of the elbow with test results

3.4 Outcome and discussion

This chapter presents the details of numerical tool for evaluation of ratcheting in pressurized piping systems under seismic load. The methodology has been illustrated for a stainless steel elbow under incremental harmonic excitation. The research carried out has highlighted the following salient aspects:

Simulation based Seismic Fragility Analysis (SFA) of piping systems considering ratcheting requires Incremental Dynamic Analysis (IDA) with validated numerical tool. Incremental Iterative Response Spectrum (IIRS) method, which uses response spectrum as input is found to be suitable for IDA of piping systems for evaluation of ratcheting.

In this method, the piping system is subjected to incremental seismic excitation and the resulting peak strain response can be plotted with respect to the chosen ground motion parameter.

This method is illustrated for an elbow under harmonic base excitation and peak strain accumulation is obtained for each of the incremental excitation. It is observed that elbow with thickness variation has predicted lower strains compared to those of uniform thickness. From this analysis, strain accumulation in elbow is observed to be dependent on thickness variation. It can be seen that analysis with IIRS method has predicted slightly higher ratcheting strains except for lower levels of excitation. This is because of lesser dynamic amplification in test by slight frequency reduction of elbow at higher excitation. Also, this difference is because the experimental uni-axial stabilized hysteresis loop used for evaluation of Chaboche parameters was considered from the literature and not from the same elbow.

CHAPTER 4 INELASTIC SEISMIC BEHAVIOUR OF AN ELBOW AND A TEE JOINT: EXPERIMENTS AND ANALYSIS USING IIRS METHOD

4.1 Introduction:

It is well known that piping components such as elbows and tee joints are relatively highly stressed when compared to straight portions due to geometry. Hence, study of ratcheting in these components is a vital requirement for better understanding of seismic response of piping systems. In the present study, ratcheting response is studied for a carbon steel elbow and tee joint under incremental table excitation.

4.2 Experimental study on inelastic seismic behavior of Elbow and Tee joint

Shake table tests are carried out on pressurized carbon steel elbow and tee using the seismic test facility at Central Power Research Institute (CPRI), Bangalore. The size of the shake table is 3m x 3m and has ten-ton load capacity.

4.2.1 Details of the test setup

A 90° short radius elbow and 90° tee joint are used for the test. Both the components have same size of DN 80 mm and schedule 40 (outer diameter of 89 mm and 5.5 mm nominal thickness). The material of the elbow and tee is carbon steel of grade SA 106 Gr B. The photograph and schematic of test setup for elbow are shown in Figure 4.1 and Figure 4.2 respectively. Straight pipes of more than thrice diameter of pipe are attached to elbow. The photograph and schematic of test setup for tee joint are shown in Figure 4.3 and Figure 4.4 respectively.

Bottom end of the elbow setup is anchored to the shake table and the top end is connected to a rigid attachment carrying 25kg and 105 kg masses at both ends. Two

ends of the tee joint are anchored to shake table and the top end is connected to rigid attachment having 25 kg and 125 kg at both ends. The purpose of added masses in the test setup is to obtain the frequencies of piping components in the same range of typical frequencies of nuclear power plant piping systems. Four post yield Surface Mounted Electrical Resistance (SMER) strain gauges are installed on two crown locations of elbow to obtain strain in hoop and axial or meridional directions.

Specifications of strain gauges are given below:

- a. Gauge resistance: $120 \pm 0.5 \Omega$
- b. Gauge factor: 2.15 ($\pm 2\%$)
- c. Strain limit: 20% (post yield gauges)
- d. Type of mounting: Surface mounting
- e. Wheatstone bridge circuit arrangement: Quarter-bridge

Accelerometers with measurement range of ± 10 g are used in the shake table tests. In addition, laser displacement sensors with measurement range of ± 75 mm are used in these tests. The strain gauges in hoop direction are denoted as SG-1H & SG-3H, while in axial direction gauges are denoted by SG-2A & SG-4A at two crown locations. For tee joint, two post yield strain gauges, SG-T1H and SG-T3H are mounted to measure hoop strain at front and rear portions of location-A respectively. Another gauge, SG-T2A is pasted in axial direction at the front portion of location-A.

Initially the elbow and tee are filled with water and sine sweep test with amplitude of 0.05g is carried out in the frequency range of 1-50 Hz to evaluate free vibration characteristics. One fourth octave per minute is the sweep rate of the test. Both ends of the 3 inch NB, schedule 40 elbow are attached with straight pipes of same size. An inverted 'L'- shape straight pipe attachment of size 1.05 m x 0.3 m is connected to the top end of the elbow setup as shown. Pipes of 3 inch NB, Schedule

160 sizes are used for the attachment. A straight pipe of 2 inch NB, schedule 40 is diagonally connected to the attachment for improving rigidity. In the tee joint test setup, all three ends of 3 inch NB, schedule 40 tee joint are connected to straight pipes of same size. An 'I' – shape straight pipe attachment of 1.4 m length is connected to the top end of the tee joint setup. Pipe of 3 inch NB, Schedule 160 size is used for the attachment. The purpose of these attachments is to induce in-plane and out of plane moment to the components under tri-axial excitation. The components are filled with water and sine sweep tests are carried out to obtain free vibration characteristics. The first three frequencies of elbow are 4.4 Hz, 4.6 Hz and 27.2 Hz. For tee joint, the frequencies are 4.2 Hz and 5.3 Hz.

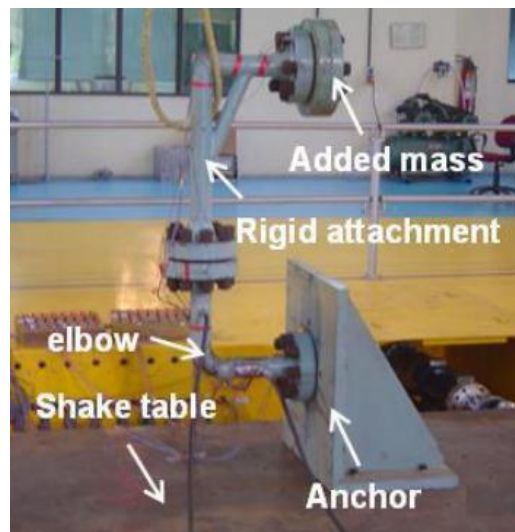


Figure 4.1: Photograph of test setup of elbow

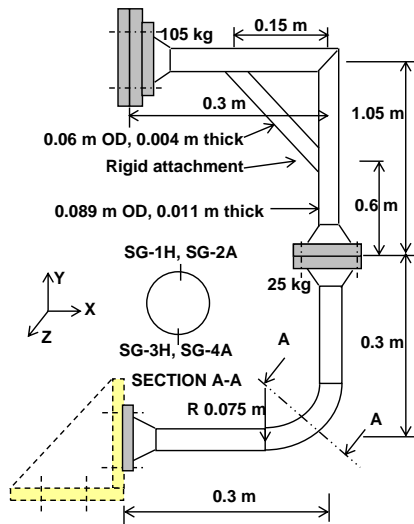


Figure 4.2: Schematic of test setup of elbow and location of strain gauges

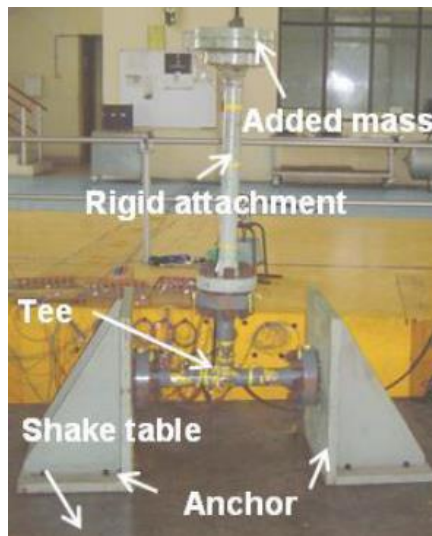


Figure 4.3: Photograph of test setup of tee joint

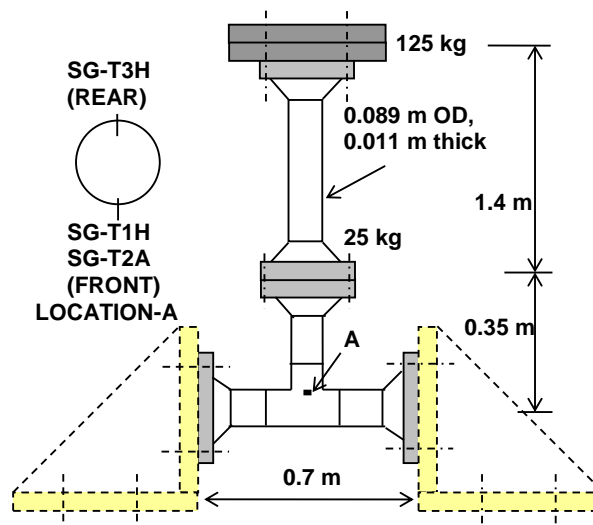


Figure 4.4: Schematic of test setup of tee joint and location of strain gauges

4.2.2 Details of seismic ratcheting tests

Increasing amplitude tri-axial seismic excitation is applied to the pressurized piping components to obtain its ratcheting response. Shake table input acceleration time history in horizontal (X) direction is shown in Figure 4.5. The time histories in vertical (Y) and other horizontal (Z) directions are shown in Figure 4.6 and Figure 4.7 respectively.

Corresponding Test Response Spectra (TRS) in three directions for 2% damping are shown in Figure 4.8. The TRS in vertical (Y) direction is considered lower than that of horizontal direction. It is observed that the piping components will be subjected to maximum dynamic amplification as their fundamental frequencies correspond to the peak response zone of the TRS. The components are subjected to this increasing base excitation and the response is measured. Loading details are summarized in Table 4.1.

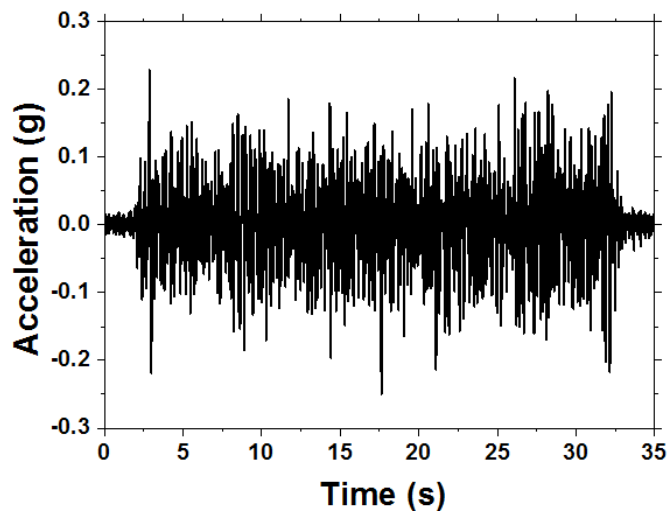


Figure 4.5: Shake table input acceleration time history in X-direction (horizontal)

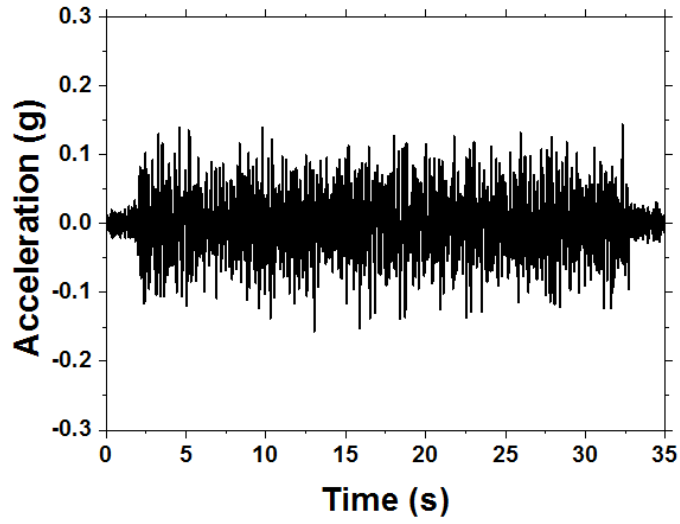


Figure 4.6: Shake table input acceleration time history in Y-direction (vertical)

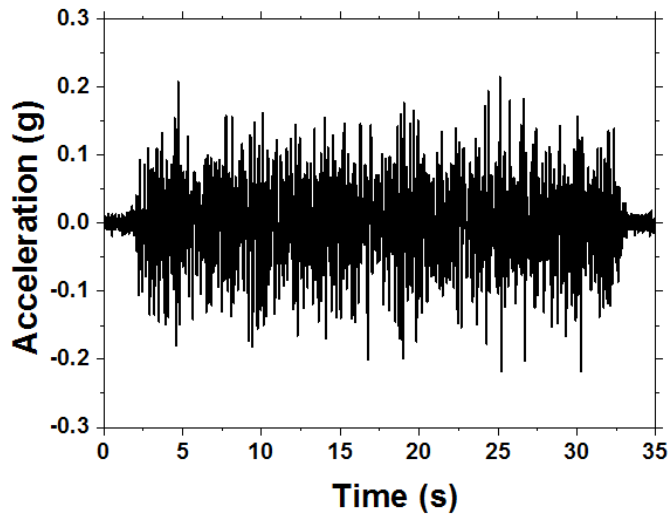


Figure 4.7: Shake table input acceleration time history in Z-direction (horizontal)

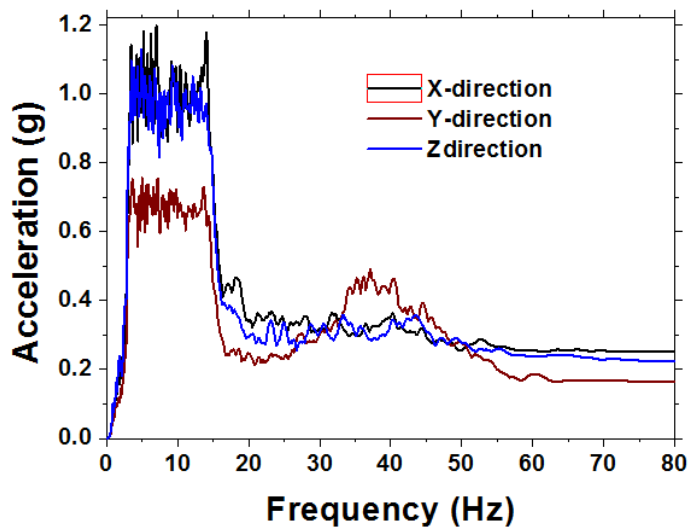


Figure 4.8: Test Response Spectra for 2% damping

To avoid P- Delta effect, center of gravity of 105 kg lumped mass (which govern the total moment) is passing through the support. This ensures that no extra moment and stresses will result in the piping under gravity. Under dynamic situation, maximum deflection is 132.8 mm corresponding to base excitation with ZPA of 2.25g (peak spectral acceleration of 10.35g corresponds to first frequency of 4.4 Hz). Corresponding moment is 153.1 N-m. Whereas moment through horizontal force is about 13917 N-m, which is much higher than that of gravity load. In addition the failure is due to ratcheting locally not static collapse. In the present test, vertical configuration is chosen to avoid several limitations with horizontal configurations. In horizontal configurations, P- Delta effect occurs if the lumped mass is not supported for self-weight. If the lumped mass is supported, additional frictional force will obstruct the motion of lumped mass as observed in experiment of stainless steel elbow at SERC, Chennai [38].

The test is started by applying this base excitation for five times and the response of the elbow is recorded. Later the ZPA of excitation is increased to 0.5g and subsequently increased till 2.25g with an increment of 0.25g. During ratcheting tests, strains at various locations are monitored and strain accumulation is used as the criterion for repeating each excitation level. If very little strain accumulation takes place during a particular excitation level after five passes, the amplitude is increased to next level.

Table 4.1: Loading details for ratcheting test of elbow and tee joint

Level of table excitation, ZPA (g)	p (MPa)	No. of passes for Elbow	Linear stress as per design code ($\times S_m$)	No. of passes for tee joint	Linear stress as per design code ($\times S_m$)
0.25	21.3	5	1.05	5	1.45
0.5	21.3	5	2.11	5	2.27
0.75	21.3	5	3.16	5	3.09

1.0	21.3	5	4.22	5	3.92
1.25	21.3	5	5.27	5	4.74
1.5	21.3	5	6.33	9	5.57
1.75	21.3	5	7.38	9	6.39
2.0	21.3	10	8.43	1	7.21
2.25	21.3	1	9.49	-	-

Hoop and axial strain time histories of first crown location of elbow (SG-1H, SG-2A) are shown in Figure 4.9 and Figure 4.10 respectively. The maximum strains for SG-1H are 1735 $\mu\epsilon$, 2455 $\mu\epsilon$ and 2800 $\mu\epsilon$ for excitations with ZPA of 0.25g, 0.5g and 0.75g respectively. No strain accumulation is observed in hoop direction till excitation of 1g ZPA. During excitation of 1g ZPA, strain accumulation has started and reached a maximum value of 4170 $\mu\epsilon$. Peak strains for 1.25g ZPA and 1.5g ZPA are 10450 $\mu\epsilon$ and 16330 $\mu\epsilon$ respectively and the strain gauge, SG-1H has de-bonded during excitation with 1.5g ZPA. A very little strain accumulation with a peak value of 6100 $\mu\epsilon$ has been observed in axial direction for gauge SG-2A.

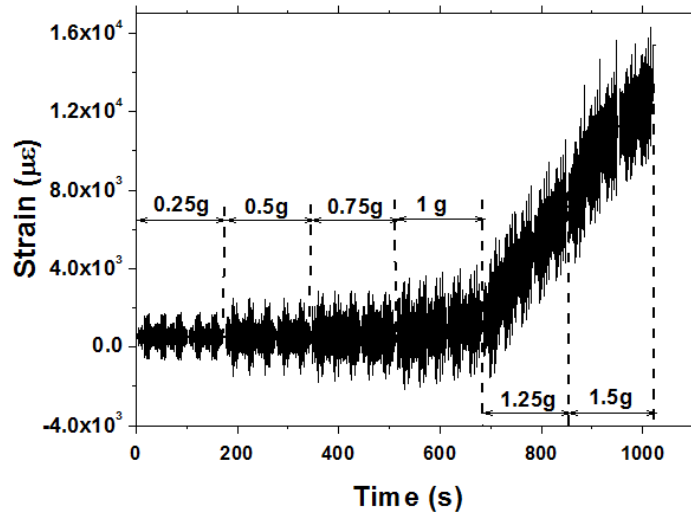


Figure 4.9: Hoop strain history (SG-1H) at first crown of elbow

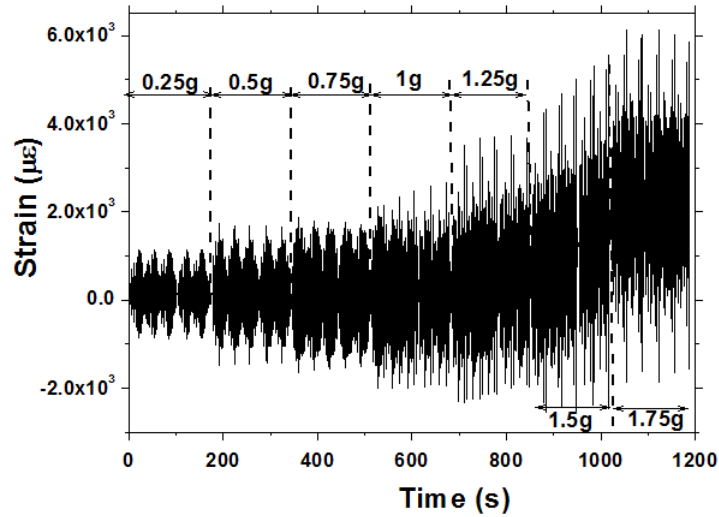


Figure 4.10: Axial strain history (SG-2A) at first crown of elbow

Hoop and axial strain time histories of second crown location of elbow (SG-3H, SG-4A) are shown in Figure 4.11 and Figure 4.12 respectively. De-bonding of SG-3H is occurred after observing a peak strain of 10140 $\mu\epsilon$ during 1.25g excitation. It is observed that negligible strain accumulation has occurred in axial direction for other gauge, SG-4A.

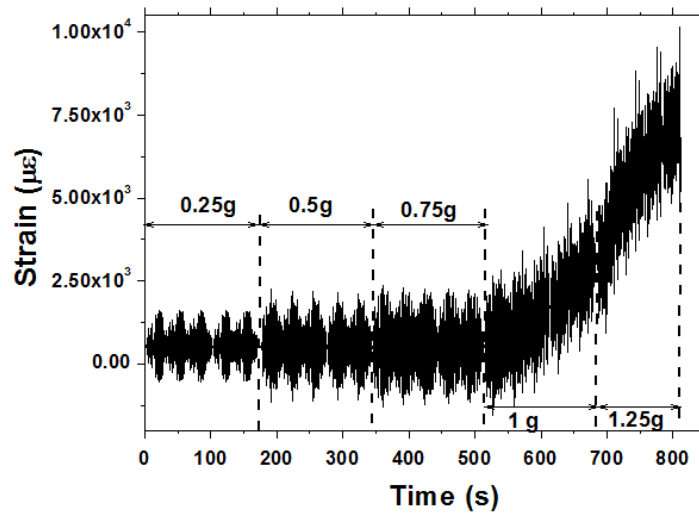


Figure 4.11: Hoop strain history (SG-3H) at second crown of elbow

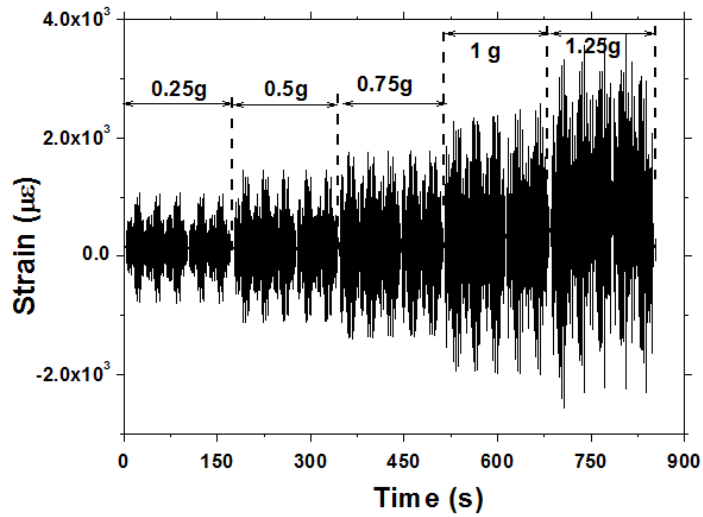


Figure 4.12: Axial strain history (SG-4A) at second crown of elbow

Hoop and axial strain time histories at front portion of location-A at tee junction (SG-T1H, SG-T2A) are shown in Figure 4.13 and Figure 4.14 respectively. A maximum strain of 7160 $\mu\epsilon$ with little accumulation is noticed in hoop direction at junction of tee joint at the end of the test. No strain accumulation is observed in axial direction.

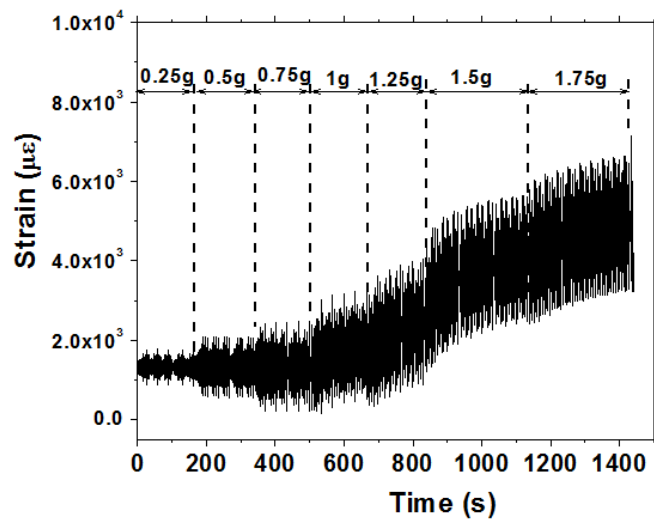


Figure 4.13: Hoop strain history (SG-T1H) at front portion of location-A at tee junction

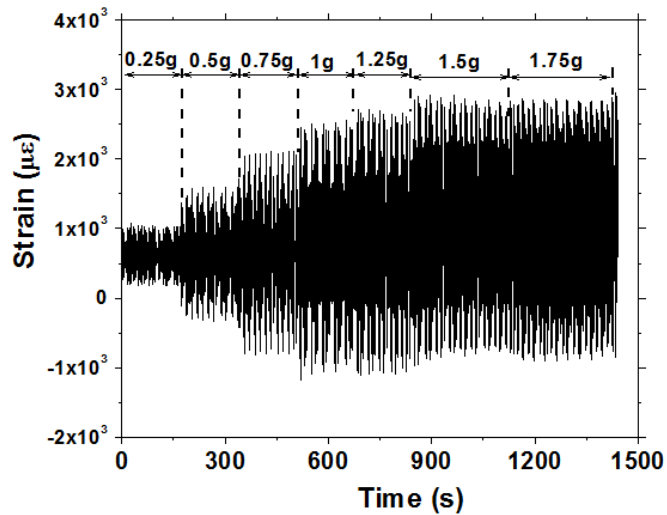


Figure 4.14: Axial strain history (SG-T2A) at front portion of location-A at tee junction

Hoop strain history at rear portion of location-A at tee junction (SG-T3H) is shown in Figure 4.15. At this location, the strain has reached a maximum value of 5760 $\mu\epsilon$ with little accumulation. Also, the strain saturation or shake down behavior is noticed at these two diametrically opposite locations of tee junction.

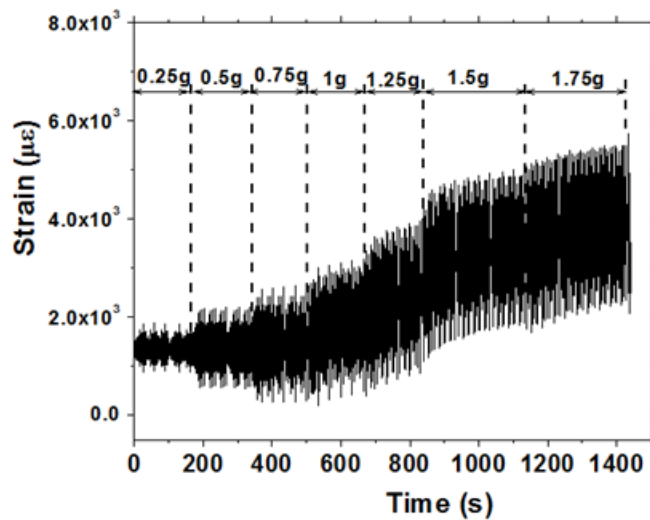


Figure 4.15: Hoop strain history at rear portion of location-A (SG-T3H) at tee junction

A crack is developed at crown of the elbow and water jet came out, during first wave with excitation of 2.25g ZPA. This is the expected location of failure for elbow as the stress intensification is high for crown under bending load due to ovalization.

Similar failures at crown were also observed in earlier tests by Firoozabad et. al. [51] and Varelis et. al. [52] on elbows under quasi static cyclic loading. For tee joint, weld failure has occurred between tee and pipe during the first excitation of 2g ZPA. The photographs of water jet through crown of elbow and crack at weld location are shown in Figure 4.16 and Figure 4.17 respectively.



Figure 4.16: Water jet through crack at crown of elbow



Figure 4.17: Crack at the weld location of tee and pipe

4.2.3 Discussion of test results of elbow and tee joint

The plot of peak strains in hoop direction at two crowns of elbow (SG-1H & SG-3H) and tee joint (SG-T1H & SG-T3H) with respect to each level of base excitation in

Figure 4.18. Due to strain gauge failure (SG-1H) during elbow test after base excitation level with ZPA of 1.5g, an exponential fit is used to extrapolate the peak strains for base excitation levels between 1.75g and 2.25g ZPA at which failure has occurred. The exponential fit used is;

$$\varepsilon = a_1 \exp(A(g)/a_2) + a_3 \quad (4.1)$$

The extrapolated ratcheting strains for base excitation levels of 1.75g, 2g and 2.25g are 30000 $\mu\varepsilon$, 55000 $\mu\varepsilon$ and 103000 $\mu\varepsilon$ respectively. This infers a significant accumulation of strain at crown of elbow. Hence, it can be concluded that the local strain accumulation at crown has resulted in ratcheting failure of elbow.

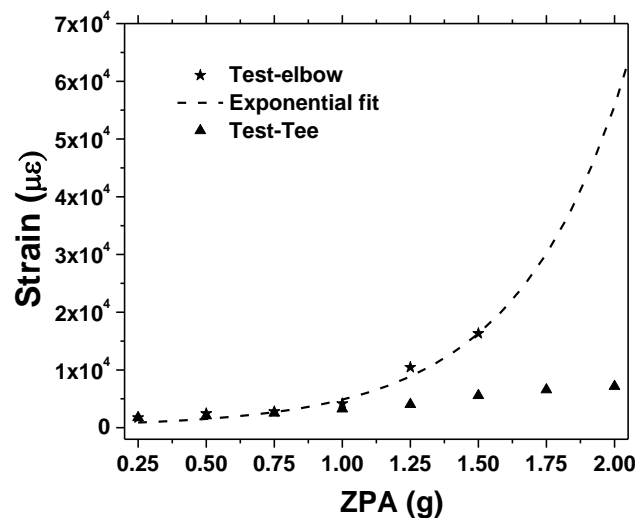


Figure 4.18: Plot of peak strains in each level of excitation for elbow and tee tests

In contrast to this, a very little strain accumulation with a peak strain of 7160 $\mu\varepsilon$ has been observed at the junction of tee joint before failure. Due to very little ratcheting and shake down behaviour, it can be inferred that fatigue has caused the failure in the tee joint. Hence, it is concluded that ratcheting dominant fatigue-ratcheting is the failure mode for elbow under internal pressure and seismic load. Also, it is concluded that fatigue is the predominant failure mode for tee joint under internal pressure and seismic load.

4.2.4 Determination of frequency change of elbow and tee joint using wavelets

As the piping components are loaded into plastic domain during the ratcheting tests, it is imperative to study the change of their natural frequencies. Frequency changes of elbow and tee joint during the ratcheting tests are determined by applying wavelets to strain signals. This wavelet analysis is similar to Fast Fourier transform (FFT) analysis of a test signal to obtain frequency content. However, the only advantage of wavelet analysis is its ability to provide simultaneous time frequency representation, while FFT analysis gives only frequency representation. Time-frequency representation (TFR) of any signal $f(t)$ is provided by wavelet transform (WT), which is defined as:

$$W(a,b) = \frac{1}{\sqrt{|a|}} \int f(t) \psi\left(\frac{t-b}{a}\right) dt \quad (4.2)$$

where, $\psi\left(\frac{t-b}{a}\right)$ is the wavelet function. 'a' is a scaling parameter which evaluates frequency while 'b' is a translation parameter which measures time. Morlet wavelet function [53] is considered to obtain simultaneous TFR of strain signals for elbow and Tee joint, and is given by,

$$\psi\left(\frac{t-b}{a}\right) = \exp\left(\frac{-\beta_w^2(t-b)^2}{a^2}\right) \cos\left(\frac{\pi(t-b)}{a}\right) \quad (4.3)$$

Where, β_w controls the shape of the wavelet.

Wavelet analysis has been carried out for the hoop strain signal of ratcheting test on elbow (SG-1H) given in Figure 4.9. TFR for first hundred second duration of the hoop strain during ratcheting test with 0.25g ZPA is shown in Figure 4.19.

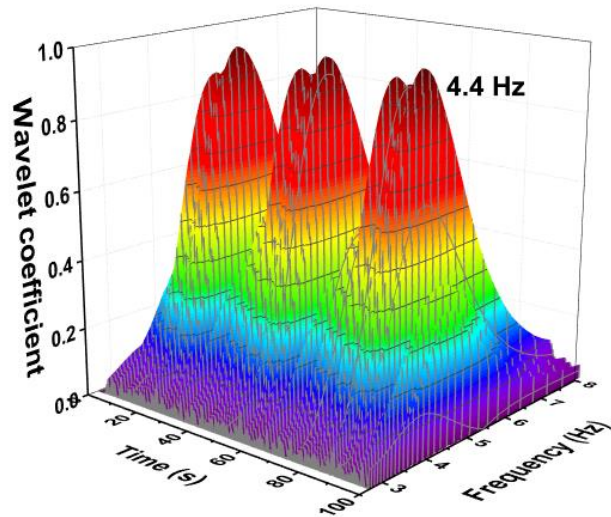


Figure 4.19: TFR of hoop strain signal of SG-1H during the first 100s duration

The predominant frequency obtained from the TFR during this excitation of 0.25g ZPA is 4.4 Hz. This is matching with the natural frequency of 4.4 Hz, which was obtained from the sine sweep test before ratcheting test. The strain gauge, SG-1H has de-bonded during excitation with 1.5g ZPA. TFR for last hundred second duration of the available hoop strain data during ratcheting test with 1.5g ZPA is shown in Figure 4.20. The predominant frequency obtained from the TFR during this excitation of 1.5g ZPA is 3.8 Hz. Hence, the dominant frequency has been reduced by 13.6% in this test. This reduction of frequency can be attributed to plasticity during the tests.

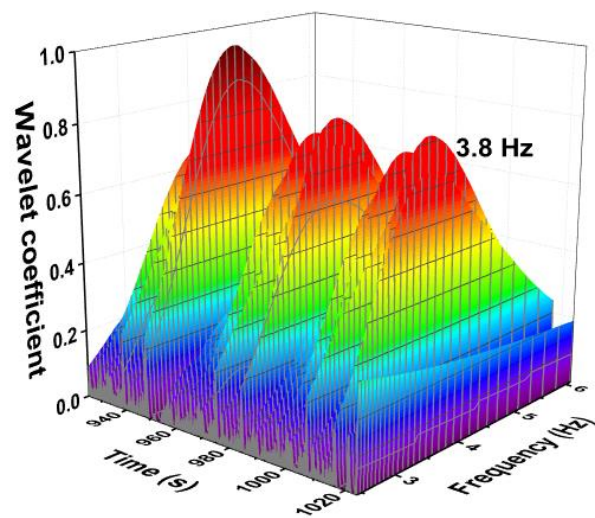


Figure 4.20: TFR of hoop strain of SG-1H during the last 100s duration

Similarly, wavelet analysis has also been carried out for the hoop strain signal of ratcheting test on tee joint (SG-T1H) given in Figure 4.13. TFR for first hundred second duration of the hoop strain during ratcheting test with 0.25g ZPA is shown in Figure 4.21. The predominant frequency obtained from the TFR during this excitation of 0.25g ZPA is 4.55 Hz, which is slightly higher than frequency obtained from the sine sweep test before ratcheting test.

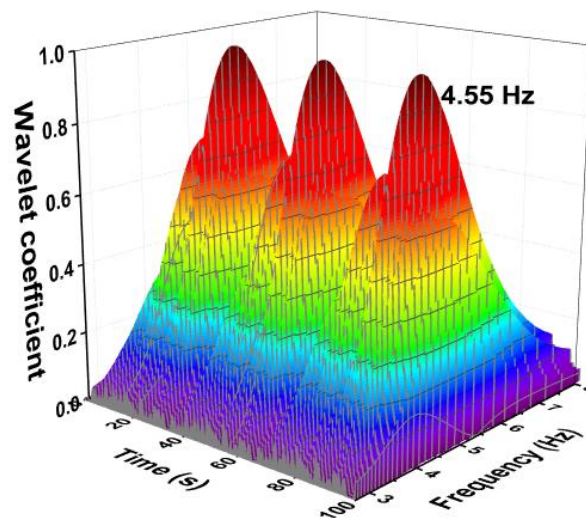


Figure 4.21: TFR of hoop strain signal of SG-T1H during the first 100s duration

TFR for last hundred second duration of the available hoop strain data during ratcheting test with 1.75g ZPA is shown in Figure 4.22. The predominant frequency obtained from the TFR during this excitation of 1.75g ZPA is 3.875 Hz. Hence, the dominant frequency has been reduced by 14.8% in this test. This is due to plasticity during the tests.

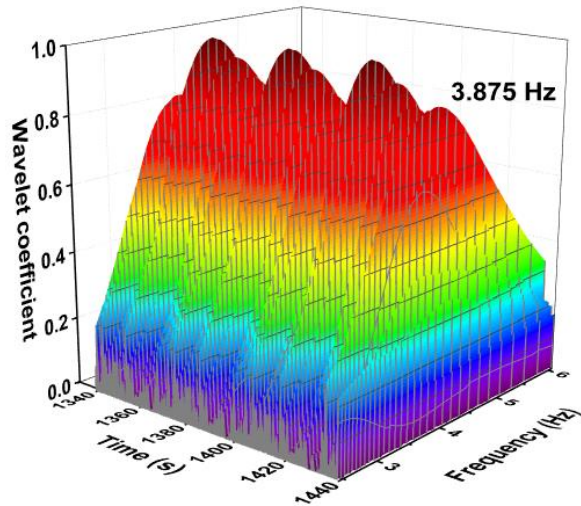


Figure 4.22: TFR of hoop strain of SG-T1H during the last 100s duration

Schematic of secant stiffness is shown in Figure 4.23. The secant stiffness value is considerably lower than initial stiffness if plastic collapse is considered for evaluation of limit load. Hence, consideration of secant stiffness would result in considerably higher frequency reduction, when compared with observed frequency shift.

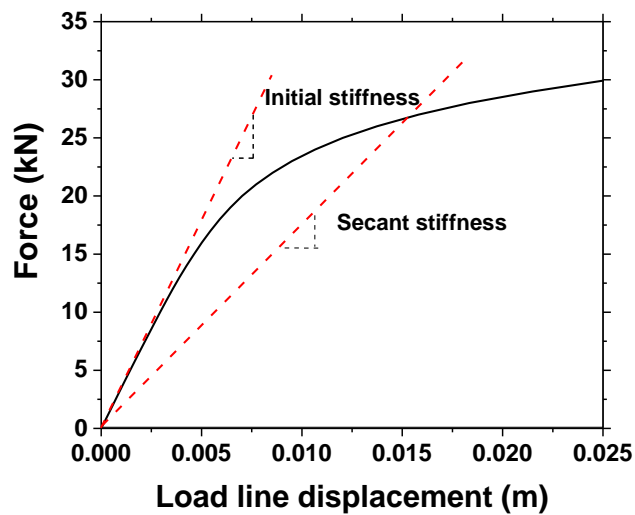


Figure 4.23: Schematic of secant stiffness

4.2.5 Sine sweep test on tested components post failure

Sine sweep tests have been carried out on the tested components post failure to obtain the frequency changes. This test has been carried out with amplitude of 0.05g in the frequency range of 1-50 Hz. The first two natural frequencies from the sine sweep

test of the elbow post failure are 4.09 Hz and 4.125 Hz respectively. The frequency of 4.09 Hz is slightly higher than 3.8 Hz as obtained from wavelet analysis of available final stage of elbow strain signal. This is because the elbow is in elastic region for the lower excitation level of 0.05g for sine sweep test and plastic region for the higher excitation level of 1.5g ZPA. The two natural frequencies of the tee joint post failure from sine sweep test are 3.9 Hz and 5.09 Hz respectively. This frequency of 3.9 Hz is slightly higher than 3.875 Hz obtained from wavelet analysis of final stage of tee strain signal. This is because the tee joint is in elastic region for the lower excitation level of 0.05g for sine sweep test and plastic region for the higher excitation level of 1.75g ZPA.

4.3 Numerical study of tested elbow and tee joint

Simplified numerical procedures are required to evaluate ratcheting strains in elbows and also for possible use of strain based design criterion. Response spectrum analysis is the most common and simple method used by designers to analyze piping components under seismic load to carry out seismic design checks. As the ratcheting is significant for elbow under seismic load, the strain accumulation in the elbow is evaluated using IIRS method with response spectrum as input. As fatigue is significant for tee joint, a simplified fatigue life assessment of tee has been presented. The details are given below.

4.3.1 Ratcheting analysis of elbow using IIRS method

Ratcheting simulation of the elbow is carried out using Incremental Iterative Response Spectrum (IIRS) method. In this method, first the envelope cyclic characteristics are determined and later these characteristics are used in the iterative method with response spectrum as input. The details of the analysis are given below.

4.3.1.1 Determination of cyclic envelope characteristics for the elbow

Cyclic characteristics are determined from the ratcheting simulation of the elbow. Chaboche non-linear kinematic hardening model [44] is used for simulation and

the finite element (FE) model of the elbow is shown in Figure 4.24. Ultrasonic thickness measurement of the elbow has been carried out at different angles of cross section (θ) and bend angle (ϕ) and the measured thickness is plotted in Figure 4.25.

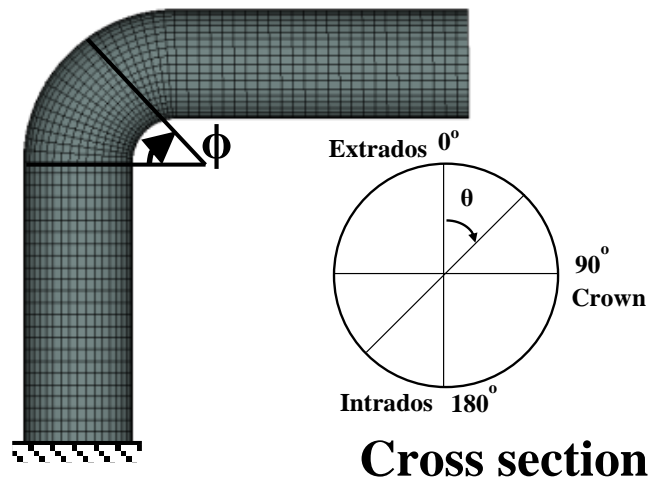


Figure 4.24: FE model of the elbow

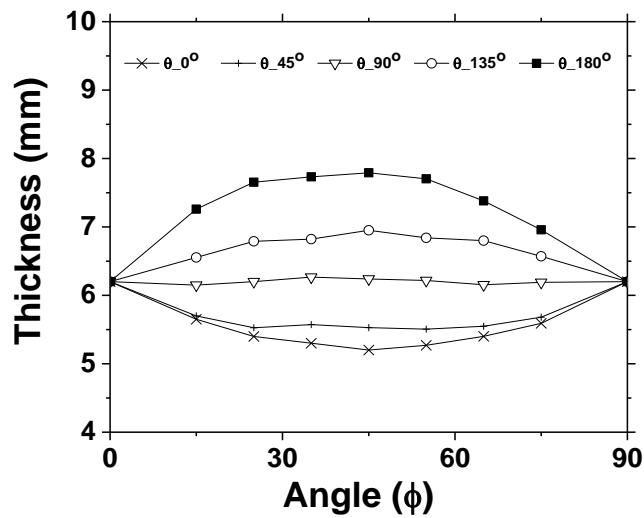


Figure 4.25: Thickness variation in elbow

Nonlinear static analysis is conducted to determine the limit displacement (δ_L) of the elbow. The tangents for elastic and inelastic regions of load-displacement curve intersect at 6.5 mm, which is considered as limit displacement (δ_L). Ratcheting simulation is done by applying internal pressure to generate design stress of $1S_m$ and

incremental cyclic displacement of $0.1\delta_L$. The applied cyclic load line displacement at elbow tip is shown in Figure 4.26.

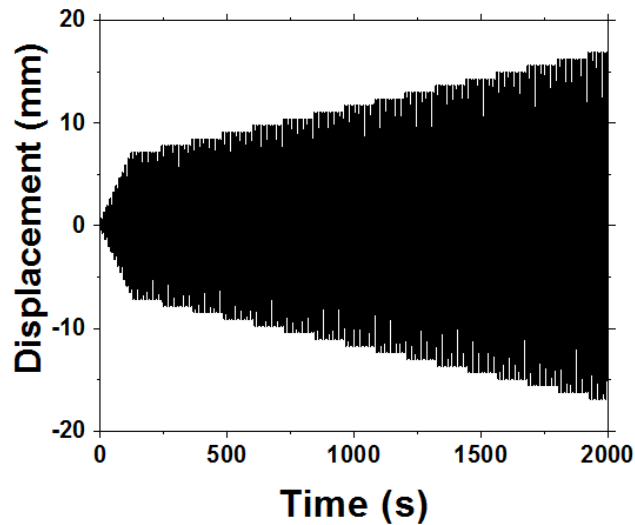


Figure 4.26: Load Line Displacement time history at the elbow tip

The Chaboche parameters obtained are, $C_1=1123000$, $C_2=55500$, $C_3=6000$, $\gamma_1=280750$, $\gamma_2=550$, $\gamma_3=9$ [43] and the comparison of Chaboche model with experimental stabilized hysteresis loop is shown in Figure 4.27.

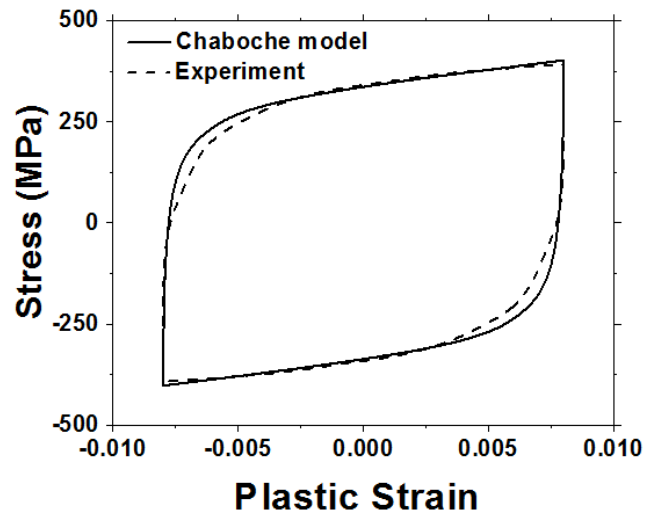


Figure 4.27: Comparison of experimental stabilized hysteresis loop with Chaboche model

Ratcheting simulation is conducted with uniform thickness as well as with measured thickness variation. The cyclic moment-rotation curves are obtained for the

elbow with uniform nominal and variable thicknesses, and are shown in Figure 4.28 and Figure 4.29 respectively.

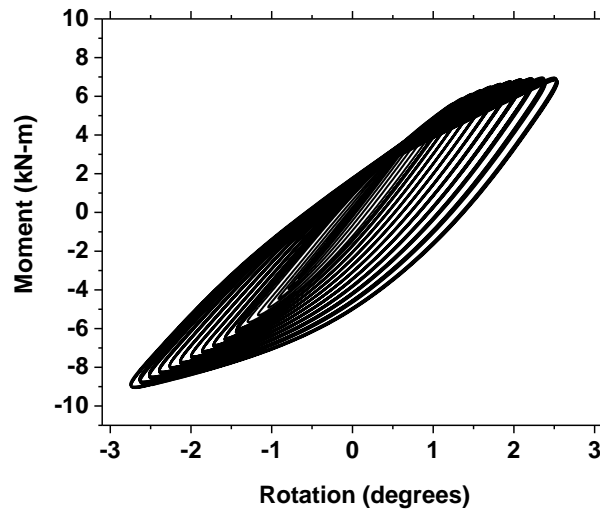


Figure 4.28: Cyclic moment-rotation curves for the elbow with uniform thickness

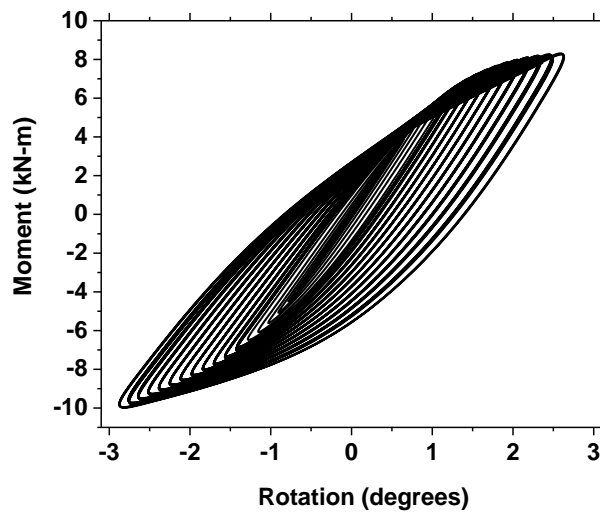


Figure 4.29: Cyclic moment-rotation curves for the elbow with thickness variation

The cyclic moment- strain curves for the elbow with uniform nominal and variable thicknesses are plotted in Figure 4.30 and Figure 4.31 respectively.

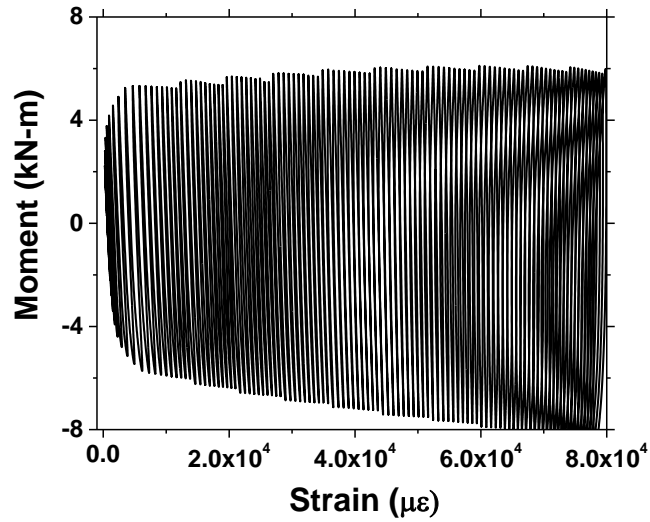


Figure 4.30: Cyclic moment- strain curves for the elbow with uniform thickness

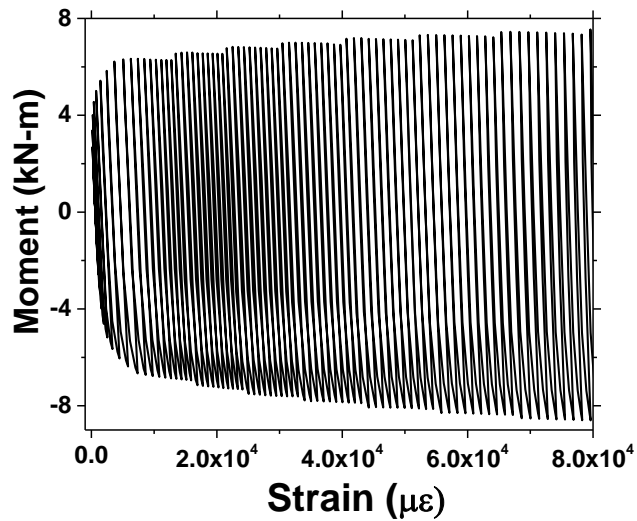


Figure 4.31: Cyclic moment- strain curves for the elbow with thickness variation

Envelope Strain-Moment-Rotation characteristics for the elbow are obtained by joining the peaks of cyclic rotation-moment and moment-strain curves and are shown in Figure 4.32. It can be seen that the elbow with actual thickness is slightly stiffer than that of uniform thickness. This is due to the higher thickness at the intrados resulting during pipe bending process.

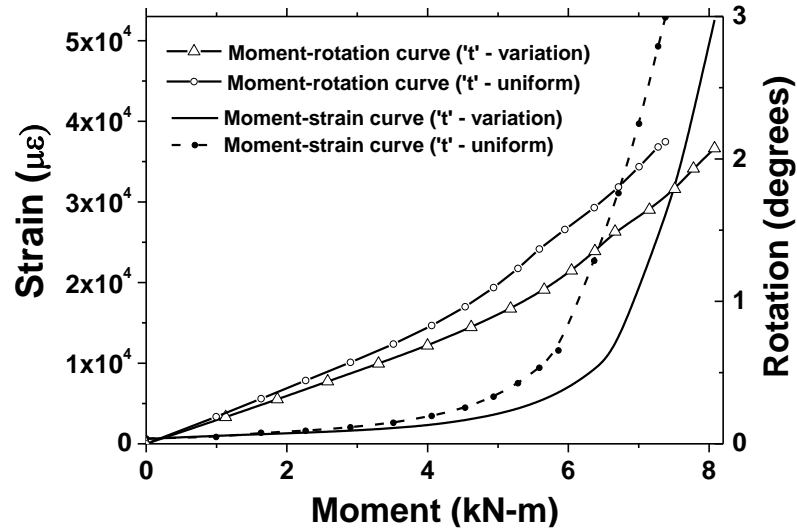


Figure 4.32: Envelope Strain-Moment-Rotation characteristics for the elbow

4.3.1.2 Iterative method using response spectrum as input

FE model of the test setup of elbow using springs is shown in Figure 4.33, in which the elbow is modeled with three translational and three rotational springs. The first natural frequency of elbow with spring model is 4.59 Hz and is closer to 4.4 Hz. The second natural frequency by spring model is 4.84 Hz and compares well with 4.6 Hz by sine sweep test. The third frequency of 26.5 Hz by analysis is slightly less than that of test. The test setup has a total lumped mass of 130 kg (105 kg +25 kg) and total distributed mass of 84 kg. The extra lumped masses are attached to obtain typical natural frequencies of actual piping systems.

Iterative analysis is carried out on elbow with a pressure of 21.3 MPa and incremental base motion. The cyclic characteristics of the elbow of uniform thickness from first phase of analysis are used. Base motion with 0.25g ZPA is applied to the model shown in Figure 4.33 and response spectrum analysis (ASCE 4-98 [54]; Reddy et. al. [55]) is carried out. The resulting moment (M) and rotation (θ_e) are 1.816 kN•m and 0.58×10^{-2} rad respectively. M_c corresponds to this rotation is 1.816 kN•m. Hence the error is nil, and strain for 0.25g ZPA is 1040 $\mu\epsilon$, which is obtained from Fig. 17 corresponding to this moment. For the excitation with 0.5g ZPA, M and θ_e are 3.633

kN•m and 1.17×10^{-2} rad respectively. M_c corresponds to this rotation is 3.408 kN•m. Hence, the error is 6.59% and in next iteration, rotational stiffness is revised as 0.291 MN•m/rad and the error is reduced to 0.77%, which is less than assumed value for convergence (1%). Hence, solution is converged and the strain corresponds to this moment is 1530 $\mu\epsilon$. The method is continued for the remaining base motion corresponding to ZPA of 0.75g to 1.25 g. For the base motion of 1.25g ZPA, ratcheting strain of 56650 $\mu\epsilon$ is obtained from the converged moment of 8.543 kN•m. Results of iterative analysis for the elbow with uniform thickness are provided in Table 4.2.

Table 4.2: Results of IRS analysis for elbow with uniform thickness

Table excitation level, ZPA (g)	Iter. no.	k_{Rz} (MN•m/rad)	M (kN•m)	θ_e ($\times 10^{-2}$ rad)	M_c (kN•m)	Error (%)	ϵ_{elb} ($\mu\epsilon$)
0.25	1	0.31	1.816	0.58	1.816	0	1040
0.5	1	0.31	3.633	1.17	3.408	6.60	1530
	2	0.291	3.607	1.24	3.579	0.78	
0.75	1	0.291	5.410	1.86	4.928	9.78	3095
	2	0.265	5.352	2.02	5.232	2.29	
	3	0.259	5.338	2.06	5.307	0.58	
1.0	1	0.259	7.118	2.75	6.439	10.55	17500
	2	0.234	7.032	3.00	6.802	3.38	
	3	0.227	7.003	3.09	6.924	1.14	
	4	0.224	6.993	3.12	6.966	0.39	
1.25	1	0.224	8.742	3.90	7.937	10.14	56650
	2	0.203	8.635	4.25	8.337	3.57	
	3	0.196	8.595	4.38	8.488	1.26	
	4	0.194	8.581	4.43	8.543	0.44	

Similarly, iterative analysis has been carried out using elbow characteristics for actual thickness variation. The comparison of resulting ratcheting strains with experimental results for different levels of excitation is shown in Figure 4.34. It is noticed that the IIRS method using uniform thickness has conservatively predicted higher strain accumulation when compared with experimental strains of elbow. The elbow with actual thickness variation has predicted lower strains compared to that of uniform nominal thickness, but still conservatively predicted higher strains when compared with test results. Hence, it can be concluded thickness distribution has a significant influence on strain accumulation in elbow. Also, it is noticed that the IIRS method with response spectrum as input has conservatively predicted the experimental results. Hence, it can be concluded that this numerical tool can be used to predict ratcheting strain in elbow which in turn can be used for a possible strain based design criterion for seismic load.

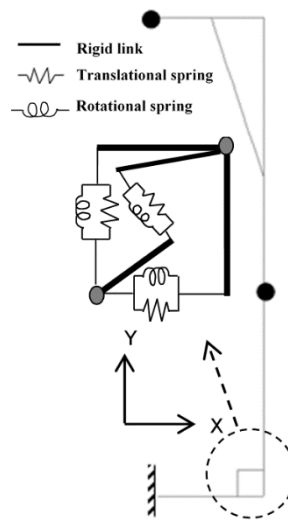


Figure 4.33: FE model of the elbow

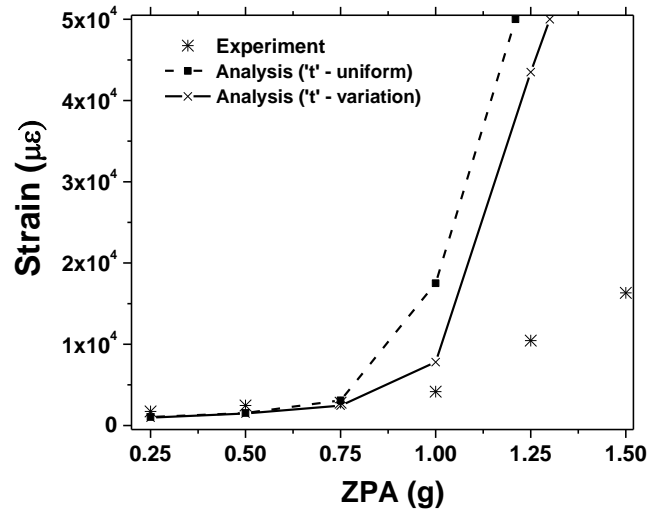


Figure 4.34: Comparison of predicted strain accumulation at crown of CS elbow with test results

4.3.2 Fatigue life evaluation for tee joint

Fatigue life evaluation for tee joint is carried out using methodology provided by Urabe et. al. [56] and Asada et. al. [57] and fatigue failure level is evaluated by considering a limit of unity for Cumulative Usage Factor (CUF). Alternating stress amplitude, S_a with constant pressure is obtained using the equation given below:

$$S_a = K_2 C_2 \frac{M}{Z} \quad (4.4)$$

where, K_2 is peak stress index (unity for tee joint) and M is moment determined from the response spectrum analysis of tee joint. Plastic correction is required for S_a when primary stress plus secondary stress (S_n) is more than $3S_m$ and is given by,

$$S_l = K_e S_a \quad (4.5)$$

where,

$$K_e = 1 + (q - 1) \left(1 - \frac{3S_m}{S_n} \right) \text{ for } (S_n \geq 3S_m) \quad (4.6)$$

$$= 1 \text{ for } (S_n < 3S_m)$$

and q is 3.1.

Number of cycles for fatigue failure, N_i against each alternating stress amplitude, S_i are determined from the design fatigue curve of ASME code [9]. Usage factor and CUF are evaluated using,

$$U_i = \frac{n_i}{N_i} \text{ and } U = \sum \frac{n_i}{N_i} \quad (4.7)$$

Fatigue life evaluation for various levels of excitation is given in Table 4.3.

Table 4.3: Fatigue life evaluation for various levels of excitation of tee joint

ZPA (g)	n_i	S_a (MPa)	K_e	N_i	CUF
0.25	50	275	1	8420	0.01
0.5	50	550	1.51	375	0.14
0.75	50	825	2.04	65	0.91
1.0	50	1100	2.31	25	>1

Ten cycles are considered for each seismic wave. The CUF is 0.01 and 0.14 for base excitation with ZPA of 0.25g and 0.5g respectively. The CUF is increased to 0.91 for excitation with ZPA of 0.75g and has reached unity during first wave for excitation with ZPA of 1.0g, which is the estimated fatigue failure level. Actual failure of the tee joint has occurred during first wave of excitation with 2.0g ZPA. Hence, the fatigue life estimation procedure has conservatively predicted the fatigue failure of the tee joint.

4.4 Outcome and discussion

This chapter presents the details of inelastic seismic behaviour of an elbow and a tee joint. The research carried out has highlighted the following salient aspects:

It is well known that strain accumulation at crown results in ratcheting failure of elbow. In the present work also, significant strain accumulation is observed in hoop direction at crown before ratcheting failure in elbow test. Progressive strain accumulation without shake down is observed in the elbow test. In the tee joint test, little strain accumulation with saturation or shake down is observed before weld joint failure at tee and pipe junction. Hence, it is concluded fatigue is the predominant failure

mode for tee joint under internal pressure and seismic load. Also, very less ratcheting strain is noticed in axial direction for both elbow and tee tests.

Wavelets are used to determine the dominant frequency reduction of the components during testing. It is observed that the dominant frequency has been reduced by 13-15% due to stiffness reduction because of plasticity.

The tested components are analyzed using IIRS method. The analysis has been carried out with uniform thickness and actual thickness distribution. It is observed that elbow with actual thickness distribution has predicted lower strains compared to those of uniform thickness. Hence, it is concluded that thickness distribution in elbow has a significant influence on ratcheting strain. The strains evaluated by IIRS method compares well with experimental strains and hence it is concluded that this method using response spectrum as input can be used to evaluate ratcheting strains in piping components under seismic load. Fatigue life assessment of tee joint has been carried out using a simplified approach, which has conservatively estimated the fatigue failure.

CHAPTER 5 SEISMIC PERFORMANCE ASSESSMENT OF PRESSURIZED PIPING SYSTEMS CONSIDERING RATCHETING: EXPERIMENTS AND ANALYSIS USING IIRS METHOD

5.1 Introduction:

In EPRI tests [10] on piping components and systems, fatigue-ratcheting was observed to be the predominant failure mode under seismic load. Based on these studies, ASME code revised the permissible stress limit for Level-D load. Also, the code has provided an alternate ratcheting based criterion which limits the through wall ratcheting to 5% for Level-D event. The same failure mode was also observed in the NUPEC tests [27]. This ratcheting based criterion was not continued in the further editions of the code. This is due to limited test data on ratcheting and lack of validated numerical tools. To meet this objective as well as to evaluate the ratcheting based performance, experimental and numerical studies are carried out on piping systems.

SFA based on Ratcheting requires,

- i. Ratcheting based Performance Limit States (PLS)
- ii. Large number of simulations to take care of uncertainty

Hence, next objective of the study is to characterize ratcheting based PLS and obtain a suitable numerical tool. Response spectrum analysis is most widely used by designers to carry out design checks of piping systems for seismic load. Hence, IIRS method which uses response spectrum as input is chosen for evaluation of ratcheting in piping systems.

5.2 Experimental seismic performance assessment of piping system

Shake table tests are carried out on two configurations of Carbon Steel Piping Systems (CSPS) to understand their seismic performance. The first one is denoted as CSPS-A and second one by CSPS-B. The details are provided subsequently.

5.2.1 Seismic performance assessment of CSPS-A

A shake table facility of structural dynamics laboratory, Indira Gandhi Centre for Atomic Research (IGCAR), Kalpakkam is used to carry out test on CSPS-A. The size of the shake table is 5m x 5m and has a capacity of 100 tons.

5.2.1.1 Shake table test of CSPS-A

The test is conducted on a Carbon Steel Piping System (CSPS-A) of grade SA 106 Gr B. The size of the CSPS-A is 150 DN and schedule 80 (168 mm outside diameter and 11 mm nominal thickness). It comprises of nine short radius elbows. The photograph and schematic are shown in Figure 5.1 and Figure 5.2 respectively.



Figure 5.1: Photograph of CS piping systems (CSPS-A) test setup

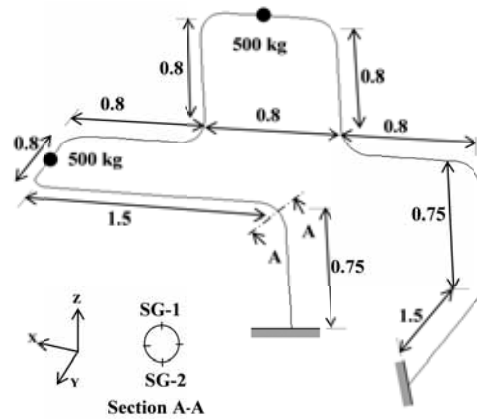


Figure 5.2: Dimensions of CSPS-A and location of instruments

Two ends of the system are connected rigidly to the shake table. One is connected horizontally while the other connected vertically as shown in Figure 5.1. Stationary discs of 500 kg each are connected at two locations of the system as shown to obtain typical frequencies of industrial piping systems. Strain response in hoop direction at two crowns of highly stressed elbow (Sec. A-A) is measured by post yield surface mounted electrical resistance strain gauges. They are denoted by SG-1 and SG-2. Specifications of strain gauges are given below:

- a. Gauge resistance: $120 \pm 0.5 \Omega$
- b. Gauge factor: $2.15 (\pm 2\%)$
- c. Strain limit: 20% (post yield gauges)
- d. Type of mounting: Surface mounting
- e. Wheatstone bridge circuit arrangement: Quarter-bridge

Accelerometers with measurement range of ± 10 g are used in the shake table tests. In addition, laser displacement sensors with measurement range of ± 150 mm are used in these tests. The critical elbow is designated as elbow-1. A pneumatically operated hydraulic pump is used to pressurize the CSPS-A up to its design pressure of

20 MPa. Dominant frequencies of CSPS-A are evaluated from sine sweep test and are given in Table 5.1. The first three frequencies of the system are 5.2 Hz, 8.9 Hz and 14.9 Hz.

Table 5.1: Comparison of frequencies (f) from sine sweep test and analysis

S. No.	f (Hz) from sine sweep test	f (Hz) from analysis
1	5.2	5.5
2	8.9	8.2
3	14.9	14.6

Increasing amplitude tri-axial seismic excitation is applied to the pressurized CSPS-A to obtain its ratcheting response. The Required Response Spectrum (RRS) chosen is from the peak broadened FRS of a typical RB and is shown in Figure 5.3 for a damping of 2%. The vertical RRS is taken as 2/3rd of horizontal RRS.

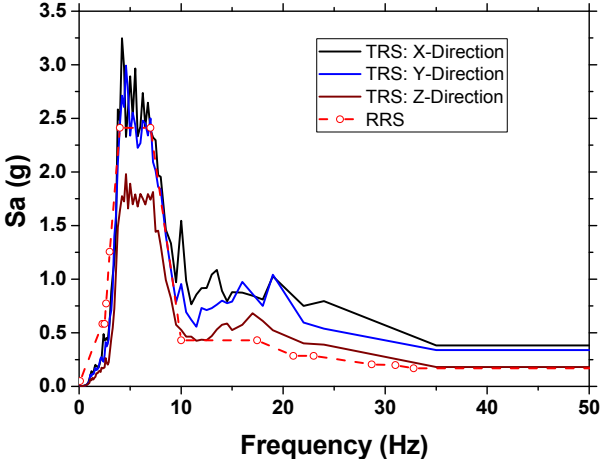


Figure 5.3: Comparison of TRS with RRS for 2% damping

Spectrum compatible input acceleration time histories are generated and are shown in Figure 5.4, Figure 5.5 and Figure 5.6 for X, Y and Z directions respectively.

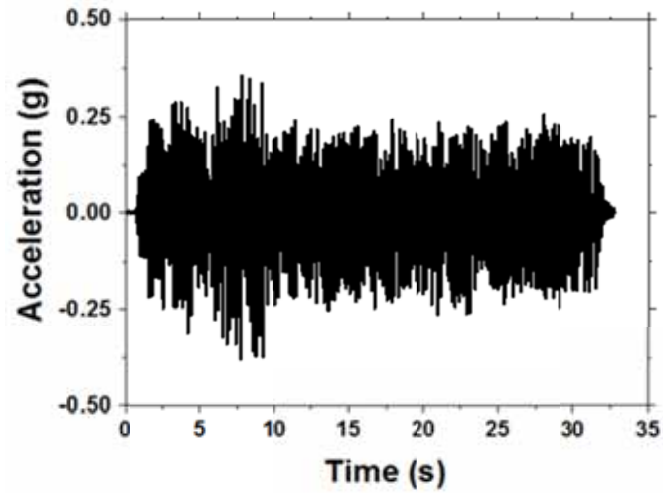


Figure 5.4: X- direction acceleration time history (horizontal)

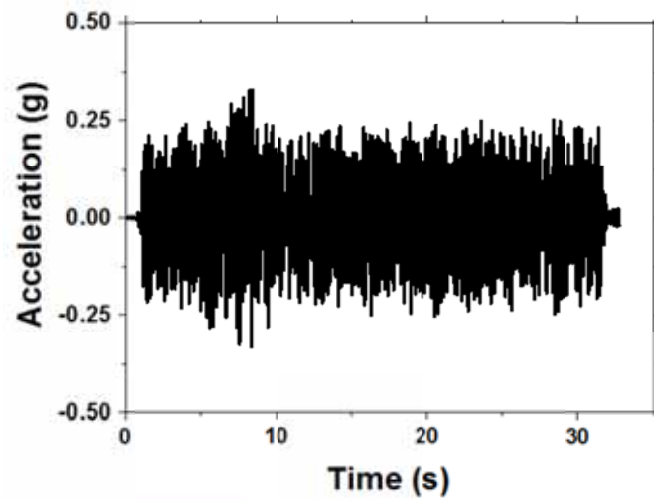


Figure 5.5: Y- direction acceleration time history (horizontal)

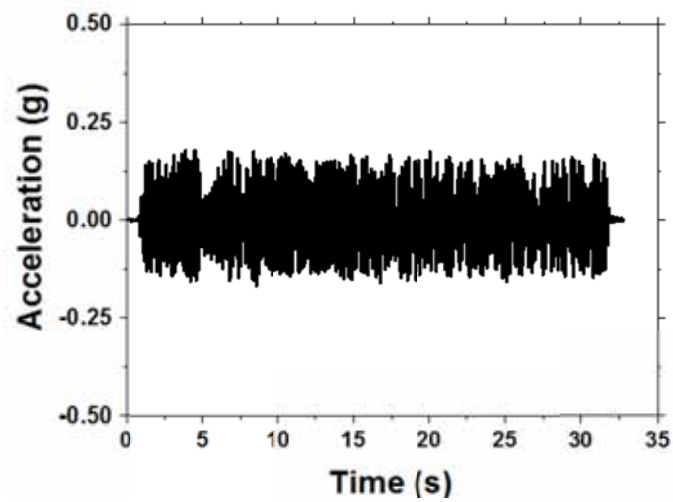


Figure 5.6: Z- direction acceleration time history (Vertical)

Test Response Spectrum (TRS) obtained from the realized shake table input is compared with RRS as shown in Figure 5.3. CSPS-A is subjected to this increasing base excitation and the response is measured. Loading details of CSPS-A test are summarized in Table 5.2.

Table 5.2: Loading details for CSPS-A test

S. No	ZPA (g)	P (MPa)	No. of waves	Linear stress as per design code (x S_m)
1.	0.35	20	5	1.959
2.	0.5	20	7	2.795
3.	0.75	20	4	4.188
4.	1.0	20	5	5.582
5.	1.25	20	5	6.976
6.	1.25	25	3	6.978

The experiment is begun with a pressure of 20 MPa and five passes of table excitation with 0.35g ZPA are applied. Later, the amplitude of table excitation is enhanced to 0.5g and seven passes are given. Further high amplitudes of 0.75g to 1.25g are applied with an incremental excitation of 0.25g. Finally, the pressure is raised to 25 MPa and table excitation of 1.25g ZPA is continued. The pressure is increased because of the acceleration limit of shake table. Linear stress evaluation has been carried out using ASME code design equation given below, is used to calculate linear stresses for each excitation.

$$\sigma = B_1 \frac{PD_0}{2t} + B_2' \frac{M_i D_0}{2I} \quad (5.1)$$

For the present elbow: Outside dia. (D_0) is 168 mm, thickness (t) is 11 mm, bend radius (R) is 150 mm and the elbow parameter ($h = tR/r_m^2$) is 0.27. For this elbow, B_1 ($-0.1+0.4h$) and B_2' ($0.87/h^{2/3}$) values are 0.0067 and 2.1 respectively. The stresses in elbow-1 corresponding to each table excitation are provided in Table 5.2. The design limit of $3S_m$ ($S_m = 138.3$ MPa for SA106 Gr B) is exceeded for table excitation of 0.5g

ZPA. It is also observed that the stress in the elbow is increased only by 0.03% (0.002 S_m) for 25% internal pressure raise (from pressure of 20 MPa to 25 MPa), corresponds to excitation of 1.25g ZPA. From the earlier shake table tests on elbow [38], it was observed that rate of ratcheting increases significantly with an increase in internal pressure. Hence, it can be inferred that an alternate criterion is essential for dealing with protection against ratcheting. In RCC-M code [58], the contribution of stress due to pressure is more as the primary stress index for pressure is 0.5 (Francis et al. [59]).

Strain response in hoop direction at first crown (SG-1) is plotted in Figure 5.7. Peak strain accumulation of 55,490 $\mu\epsilon$ is measured by this gauge, till excitation of 1g ZPA. During this table excitation this gauge got de-bonded. Strain response in hoop direction at the opposite crown location (SG-2) is plotted in Figure 5.8. Peak strain accumulation of 21,985 $\mu\epsilon$ is measured by this gauge, till excitation of 1g ZPA. During this table excitation this gauge also got de-bonded. Strains measured at SG-1 location are relatively higher than that of SG-2. This discrepancy is attributed to the localization of plastic strain and slight thickness variation at two crowns.

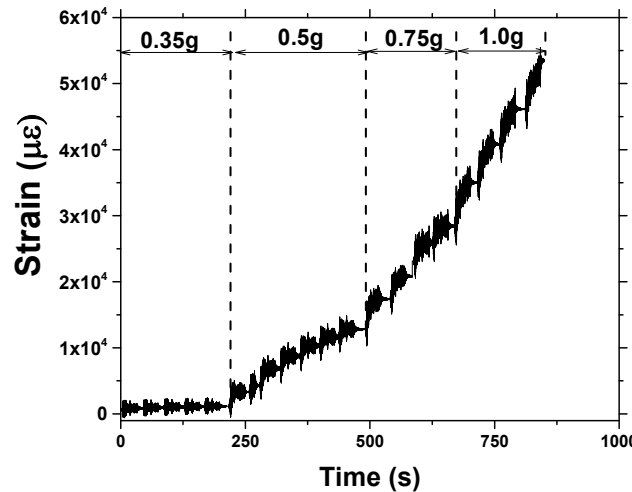


Figure 5.7: Hoop strain time histories at first crown location (SG-1) of elbow-1

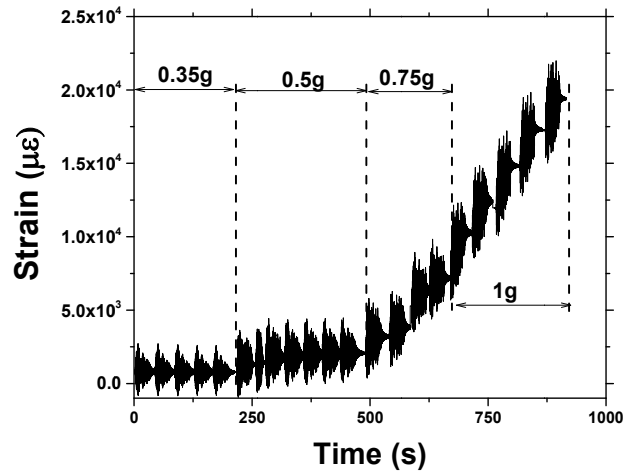


Figure 5.8: Hoop strain time histories at second crown location (SG-2) of elbow-1

When the CSPS-A was subjected to third pass of table excitation of 1.25g ZPA, rupture took place at first crown of elbow-1. The rupture is evident by the jet of water through the crown as shown in Figure 5.9.



Figure 5.9: Photograph of rupture at crown

5.2.1.2 Wavelet analysis for the evaluation of dominant frequency shift for CSPS-A

Evaluation of dominant frequency shift is necessary to understand the influence of in-elasticity on the piping system characteristics. This is also required for the confirmation of whether ratcheting failures are only local manifestation or effects global piping characteristics. Global piping characteristic variation can be inferred from

the shift of its dominant frequency. Wavelets are applied to evaluate this frequency shift, as they give simultaneous time frequency representation (TFR) of any signal. Wavelet analysis is carried out for the strain response at SG-1. TFR for the first 250s of signal is given in Figure 5.10. The dominant peak of the TFR indicates the first natural frequency and is 5.08 Hz. This frequency differs slightly from 5.2 Hz, which is from the sine sweep test. TFR of the last 200s signal is plotted in Figure 5.11. The dominant frequency for this duration is 4.95 Hz.

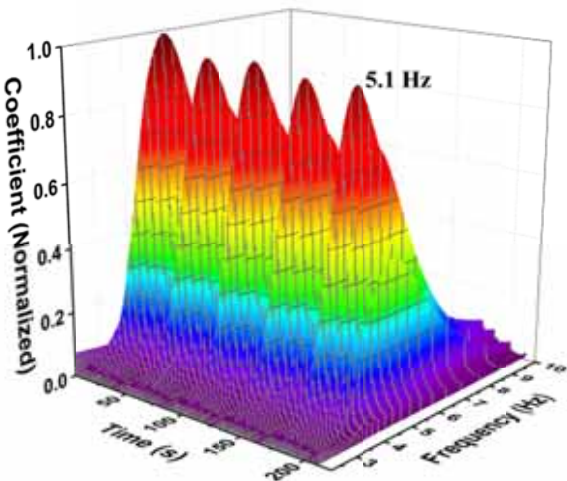


Figure 5.10: TFR of SG-1 strain signal during first 250s duration

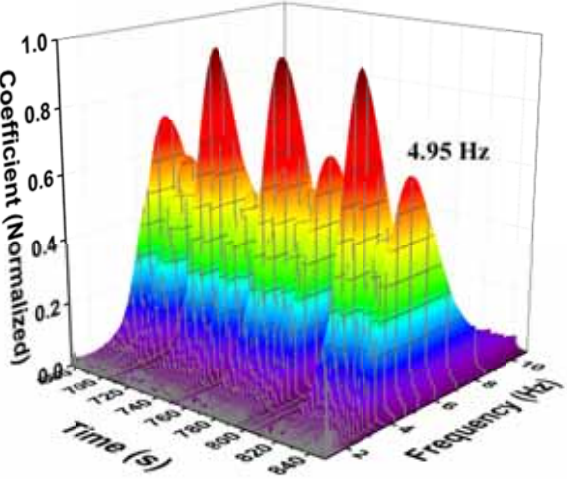


Figure 5.11: TFR of SG-1 strain during the last 200s duration

This infers that the dominant frequency of CSPA-A is reduced by only 2.6% during the test. This frequency reduction is very less when compared to the range of 13-15% of piping components. This is due to load re-distribution and redundancy at system level. Thus, it can be understood that the global stiffness of the piping loop are reduced slightly while local strain accumulation of around 8.32% (extrapolated) occurred before ratcheting failure. In the present study, wavelet analysis is used only to evaluate the dominant frequency and not the damping. Evaluation of accurate damping from the strain signal during random excitation tests necessitates further in-depth study of wavelets.

5.2.1.3 Characterization of ratcheting performance limits

SFA and PRA studies of pressurized piping systems needs identification of ratcheting based Performance Limit States (PLS). In the present work, two PLS are proposed based on the shake table tests and design code guidance. Morishita et. al. [60] and Otani et. al. [61] presented details of recent national benchmark exercises in Japan and proposed JSME code case. In this proposed code case, 1% limit for maximum strain from in-elastic analysis is recommended for earthquake load. This limit of 1% is identified as the first ratcheting based PLS and is denoted by PLS-1.

From the results of piping tests carried out by EPRI, Tagart et. al. [25] proposed a 5% ratcheting limit for Level-D service condition. Also, the same limit was adopted for alternate ratcheting based criterion by 1995 edition of ASME code. NUPEC piping tests [27] also confirmed similar ratcheting failures.

Peak accumulated strains of 5.55% and 2.2% are measured at two crown locations, SG-1 and SG-2 respectively before their failure. Ratcheting at SG-1 crown is higher than that of SG-2 crown. This difference can be due to slightly different

thickness at two crown locations. Also, slight variation in the microstructural elements like dislocations might have resulted in this discrepancy. The location of ratcheting failure of CSPS-A is SG-1 crown and the same is chosen for characterization of ratcheting PLS. The failure has occurred during the table excitation of 1.25g ZPA, while the strain gauge de-bonding occurred much earlier. Hence, the peak ratcheting strain at SG-1 is extrapolated till the failure excitation of 1.25g ZPA, using an exponential fit given by equation 4.1. This gives the extrapolated peak strain of 8.32% corresponding to the failure excitation of 1.25g ZPA. Also, peak ratcheting strain of above 5% was observed in recent test on elbow [38]. Hence, this limit of 5% is identified as the second ratcheting based PLS and is denoted by PLS-2.

5.2.2 Seismic performance assessment of CSPS-B

A shake table facility of CPRI, Bangalore is used to carry out test on CSPS-B. The size of the shake table is 3m x 3m and can take up a pay load of 10 tons. The test is conducted on a Carbon Steel Piping System (CSPS-B) of size 150 DN and schedule 40. The material grade is: SA 333 Gr 6. The loop contains six long radius elbows and one tee joint. The photograph and schematic are shown in Figure 5.12 and Figure 5.13 respectively. Three ends of the system are connected rigidly to the shake table. Two stationary discs of 250 kg each are connected to the system as shown to obtain typical frequencies of industrial piping systems. Strain response at crown locations of two high stressed elbows (Sections X-X and Y-Y) is measured by post yield surface mounted electrical resistance strain gauges. The elbow at section X-X is denoted as elbow-1 and strain gauges on it by SG-1 & SG-2. Other elbow at section Y-Y is denoted as elbow-2 and gauges by SG-4 and SG-5.

Specifications of strain gauges are given below:

- a. Gauge resistance: $120 \pm 0.5 \Omega$
- b. Gauge factor: 2.15 ($\pm 2\%$)
- c. Strain limit: 20% (post yield gauges)
- d. Type of mounting: Surface mounting
- e. Wheatstone bridge circuit arrangement: Quarter-bridge

Accelerometers with measurement range of ± 10 g are used in the shake table tests. In addition, laser displacement sensors with measurement range of ± 75 mm are used in these tests. The CSPS-B is pressurized by water up to its design pressure of 12 MPa. Dominant frequencies of CSPS-B are evaluated from sine sweep test and the first three frequencies of the system are 4.06 Hz, 6.13 Hz and 17.85 Hz.



Figure 5.12: Test setup of CSPS-B

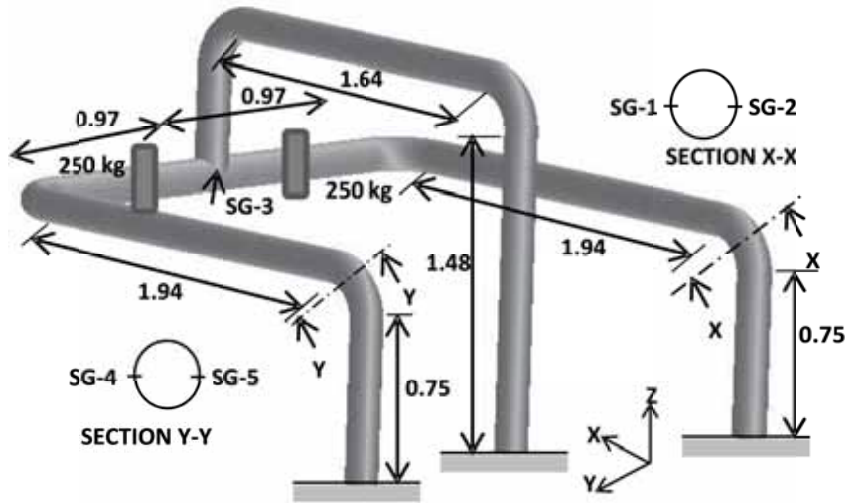


Figure 5.13: Dimensions of C-SPS-B and location of strain gauges

Increasing amplitude tri-axial seismic excitation is applied to the pressurized C-SPS-B to obtain its ratcheting response. Shake table input acceleration time history in X, Y and Z directions are shown in Figure 5.14, Figure 5.15 and Figure 5.16 respectively.

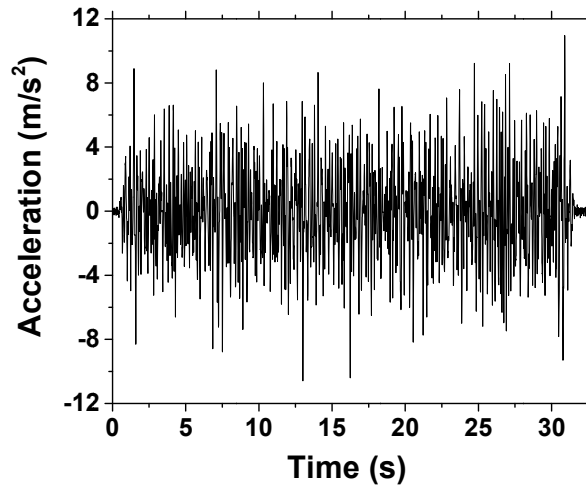


Figure 5.14: Table excitation in horizontal direction (X-axis)

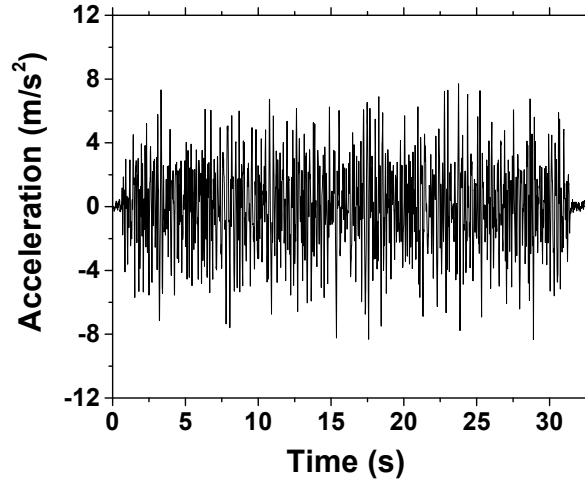


Figure 5.15: Table excitation in horizontal direction (Y-axis)

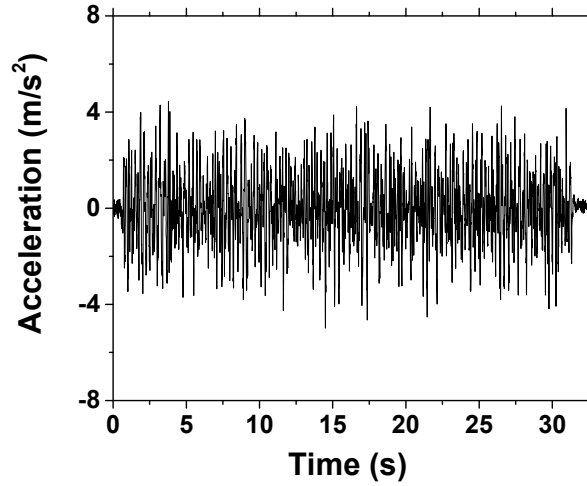


Figure 5.16: Table excitation in vertical direction (Z-axis)

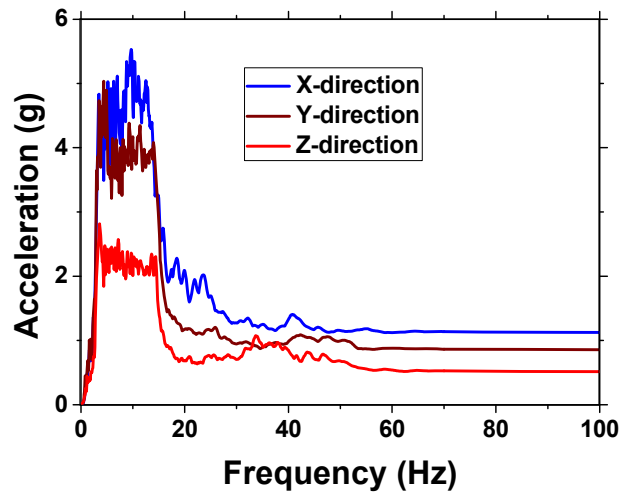


Figure 5.17: Test Response spectra for 2% damping

Corresponding Test Response Spectra (TRS) in three directions for 2% damping are

shown in Figure 5.17. CSPS-B is subjected to this increasing base excitation and the response is measured. Loading details of CSPS-B test are summarized in Table 5.3. The experiment is begun with a pressure of 12 MPa and five passes of table excitation with 1.0g ZPA. Later, the amplitude of table excitation is enhanced to 1.25g and five passes are given. Further high amplitudes of 1.5g to 2.5g are applied with an incremental excitation of 0.25g. The test is continued by raising the pressure to 14 MPa and table excitation of 2.5g ZPA is applied for thirty passes. Finally, the test is done with further higher pressure of 16 MPa with constant table excitation of 2.5g ZPA. The pressure is increased because of the acceleration limit of shake table. Linear stress evaluation has been carried out using ASME code design equation. The resulting stresses in highly stressed elbow (Sec. A-A) for each level of excitation are provided in Table 5.3.

Table 5.3: Loading details for CSPS-B test

ZPA (g)	Internal Pressure (MPa)	No. of base excitation time histories for CSPS-B	Linear stress as per design code ($\times S_m$)
1	12	5	1.77
1.25	12	5	2.21
1.5	12	5	2.65
1.75	12	5	3.10
2	12	5	3.55
2.25	12	5	3.99
2.5	12	5	4.43
2.5	14	30	4.43
2.5	16	14	4.43

For the present elbow: Outside dia. (D_0) is 168 mm, thickness (t) is 7.1 mm, bend radius (R) is 228 mm and the elbow parameter ($h = tR/r_m^2$) is 0.25. For this elbow, B_1 ($-0.1+0.4h$) and B_2' ($0.87/h^{2/3}$) values are 0.0012 and 3.25 respectively. The stresses in elbow-1 corresponding to each table excitation are provided in Table 5.3. The design limit of $3S_m$ ($S_m = 138.3$ MPa for SA 333 Gr 6) is exceeded for table excitation of 1.75g ZPA. It is also observed that the stress in the elbow due to pressures of 12 MPa, 14 MPa

and 16 MPa are 1.23 kPa, 1.44 kPa and 1.64 kPa respectively. Hence, it can be seen that the contribution of pressure to the linear stress as per design code is negligible. However, it was observed that rate of ratcheting increases significantly with an increase in internal pressure. Hence, it can be inferred that an alternate criterion is essential for dealing with protection against ratcheting. Strain response in hoop direction at first crown (SG-1) is plotted in Figure 5.18. Peak strain accumulation of 28,140 $\mu\epsilon$ is measured by this gauge, till excitation of 2.5g ZPA. During this table excitation this gauge got de-bonded. Corresponding strain response in the other symmetric elbow crown (SG-5) is shown in Figure 5.19. This gauge has measured a peak strain of 6,750 $\mu\epsilon$ before its de-bonding. The comparison of hoop strain time histories at these two crown locations is shown in Figure 5.20. It can be seen that the strains measured at symmetric elbow crown locations are slightly different and this discrepancy is attributed to the localization of plastic strain and variation in thickness of elbows. Strain response could not be measured at the opposite crown locations (SG-2 and SG-4) due to their failure. When the CSPS-B was subjected to fourteenth pass of table excitation of 2.5g ZPA at a pressure of 16 MPa, rupture took place at the crown of elbow. The photograph of crack at crown as shown in Figure 5.21.

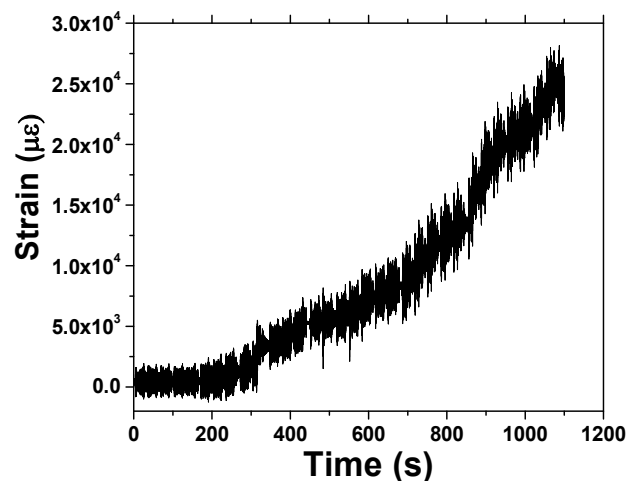


Figure 5.18: Hoop strain time history at crown location (SG-1) of elbow-1

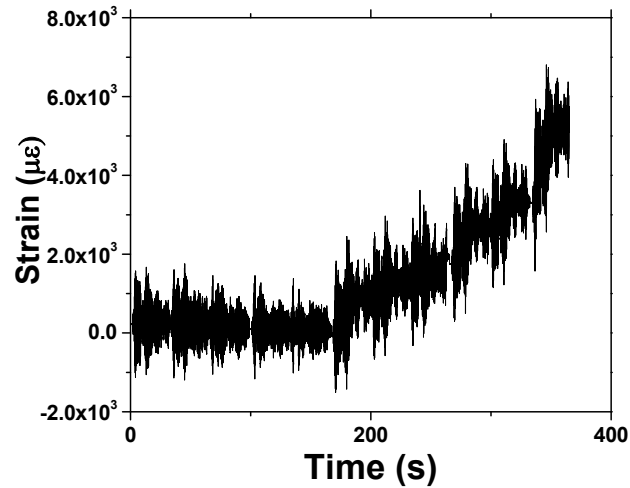


Figure 5.19: Hoop strain time history at crown location (SG-5) of elbow-2

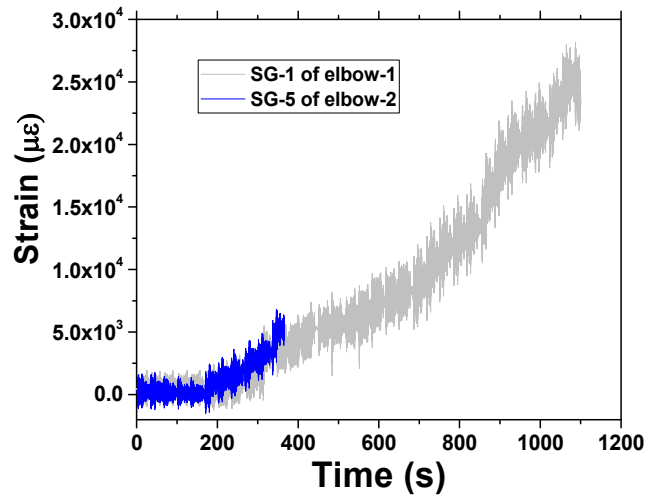


Figure 5.20: Comparison of hoop strain time histories at two crown locations

Hoop strain history at Tee junction (SG-3) is shown in Figure 5.22. A peak strain of 9510 $\mu\epsilon$ is measured at this junction. Initially the strain is accumulated and later the same is saturated. This shows that shake down has occurred at Tee joint. Also, it was observed from Figure 5.22 that rate of ratcheting for pressure of 12 MPa was 13.4 $\mu\epsilon/s$ (slope of strain-time plot, at time of 851 s). At the onset of excitation with pressure of 14 MPa, the rate of ratcheting is increased to 28.8 $\mu\epsilon/s$ (slope of strain-time plot, at time of 1352 s). Hence, it can be observed that rate of ratcheting increases with an increase in internal pressure.



Figure 5.21: Photograph of crack at crown of the elbow

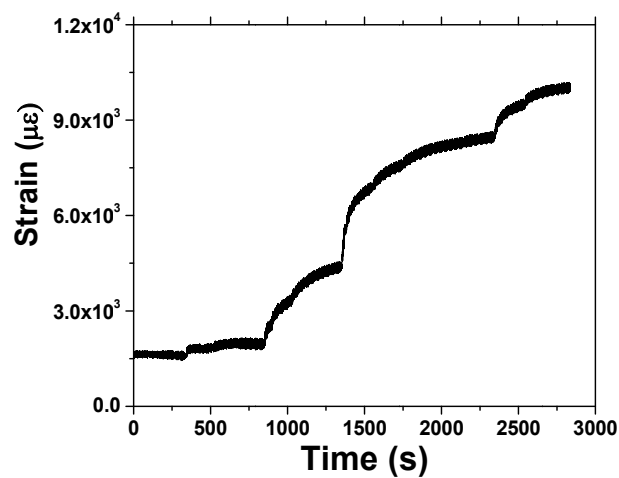


Figure 5.22: Hoop strain time history at Tee junction (SG-3)

5.2.2.1 Wavelet analysis for the evaluation of dominant frequency shift for CSPS-B

Evaluation of dominant frequency shift is necessary to understand the influence of in-elasticity on the piping system characteristics. This is also required for the confirmation of whether ratcheting failures are only local manifestation or effects global piping characteristics. Global piping characteristic variation can be inferred from the shift of its dominant frequency. Wavelets are applied to evaluate this frequency shift, as they give simultaneous time frequency representation (TFR) of any signal. Wavelet analysis is carried out for the strain response at tee junction. TFR for the first

200s of signal is given in Figure 5.23. The dominant peak of the TFR indicates the first natural frequency and is 4 Hz. This frequency differs slightly from 4.08 Hz, which is from the sine sweep test. TFR of the last 160s signal is plotted in Figure 5.24. The dominant frequency for this duration is 3.855 Hz. This infers that the dominant frequency of CSPS-B is reduced by only 3.6% during the test. This frequency reduction is very less when compared to the range of 13-15% of piping components. This is due to load re-distribution and redundancy at system level. Thus, it can be understood that the global stiffness of the piping loop is reduced slightly. In the present study, wavelet analysis is used only to evaluate the dominant frequency and not the damping. Evaluation of accurate damping from the strain signal during random excitation tests necessitates further in-depth study of wavelets. However, damping can be evaluated by carrying out Fast Fourier Transform (FFT) analysis of the signal and subsequent application of half-power bandwidth method. Using this method, it is observed that the damping during the initial stage of the test is 1.65%. The damping during the last phase of the test is obtained as 7.3%. The increase of damping can be attributed to the energy dissipation due to material inelasticity at various locations of the piping system.

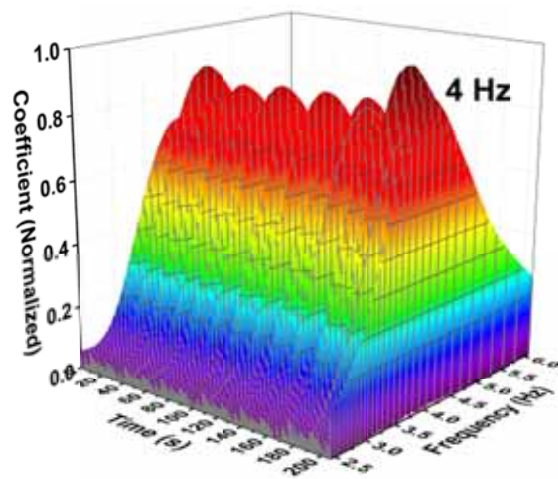


Figure 5.23: TFR of strain at tee joint during the first 200s duration

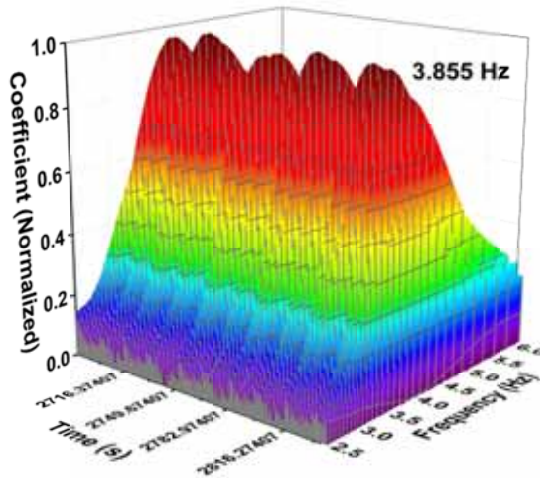


Figure 5.24: TFR of strain at tee joint during the last 160s duration

5.3 Numerical simulation of tested piping systems

Numerical simulation of ratcheting has been carried out for the tested systems, CSPS-A and CSPS-B using IIRS method. First envelope characteristic of elbow are obtained from cyclic plasticity analysis and later response spectrum analysis is carried out iteratively on a line model of piping system such that the moment-rotation values for critical elbow matches with envelope characteristics.

5.3.1 IIRS analysis of CSPS-A

Detailed cyclic plasticity analysis is carried out on shell model of elbow shown in Figure 5.25 to generate cyclic envelope characteristics. Later, iterative response spectrum analysis is carried out on line model of CSPS-A shown in Figure 5.26 to obtain the moment-rotation in critical elbow for incremental seismic excitation.

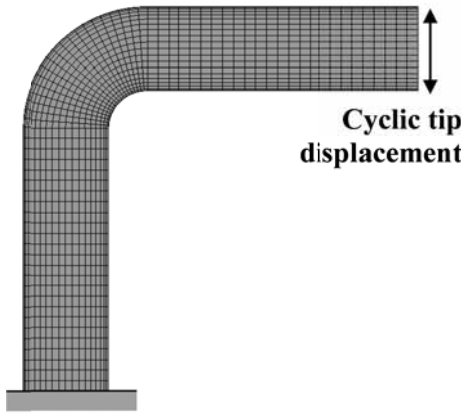


Figure 5.25: Finite element model of elbow

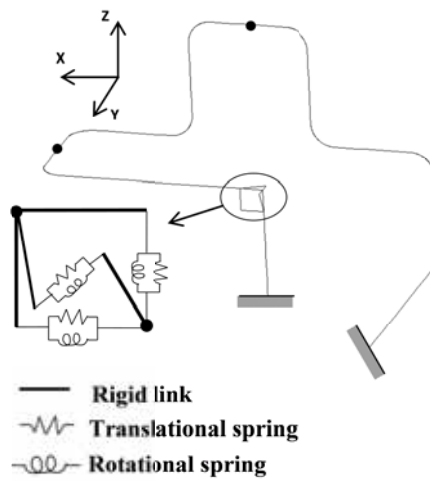


Figure 5.26: Line model of piping system

5.3.1.1 Detailed cyclic plasticity analysis of elbow

Chaboche model is used to obtain ratcheting response in pressurized elbow under cyclic load. Six Chaboche parameters are obtained from stabilized cyclic stress strain loop using procedure given by Chaboche. The Chaboche parameters are (C_1, γ_1) , (C_2, γ_2) and (C_3, γ_3) are (1123000, 280750), (50500, 950) and (5900, 9) respectively. Cyclic yield stress $\sigma_0 = 240$ MPa. The comparison of Chaboche model and uniaxial stabilized hysteresis loop under symmetric strain cycling is given in Figure 5.27.

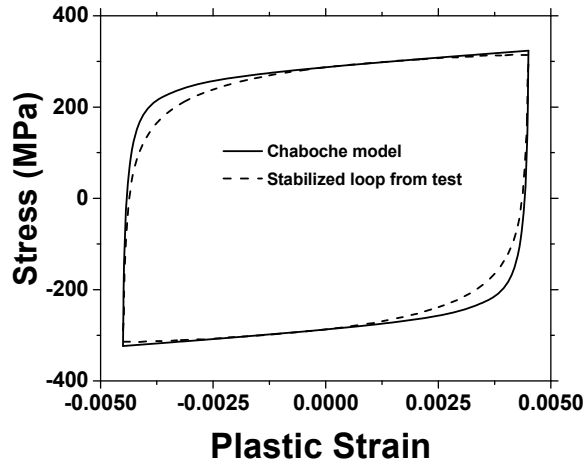


Figure 5.27: Comparison of Chaboche model and uniaxial stabilized hysteresis loop under symmetric strain cycling

Cyclic plasticity analysis is carried out by applying design level internal pressure and incremental cyclic tip displacement. The limit displacement (δ_L) is obtained by double tangent intersection shown in Figure 5.28.

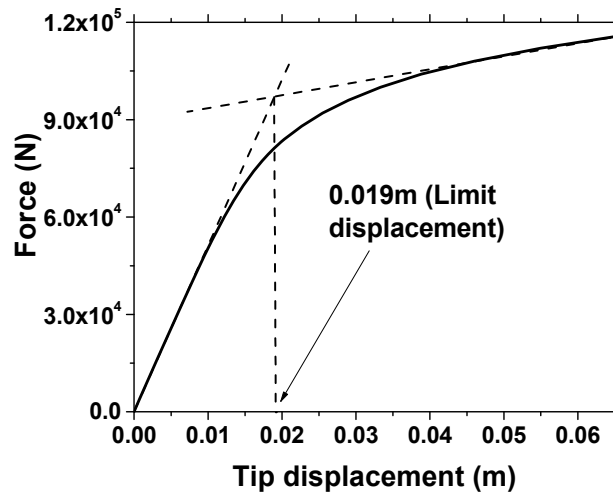


Figure 5.28: Evaluation of elbow tip limiting displacement

Using 10% incremental limit displacement, the cyclic tip displacement given in Figure 5.29 is applied to the elbow and analysis is performed.

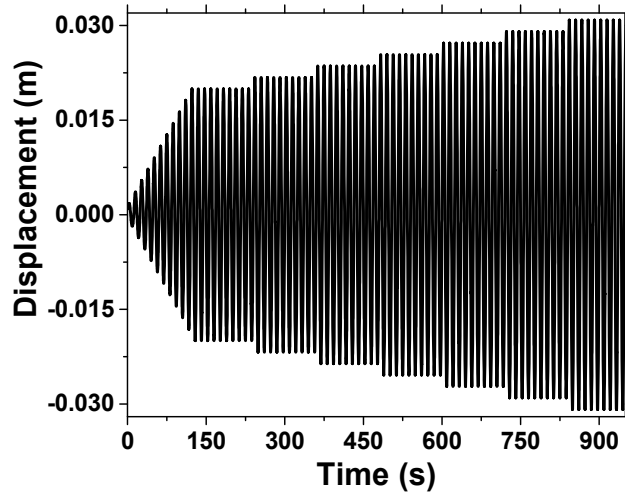


Figure 5.29: Cyclic displacement time history at elbow tip

Cyclic moment-rotation curves of the elbow are given in Figure 5.30.

Corresponding cyclic moment-strain curves are shown in Figure 5.31.

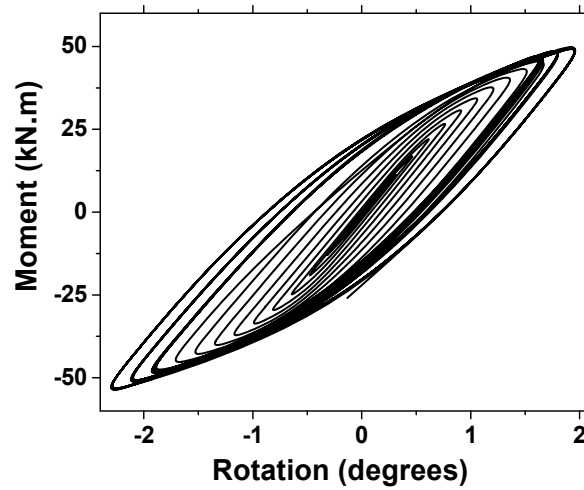


Figure 5.30: Cyclic moment-rotation curves for the C-SPS-A elbow

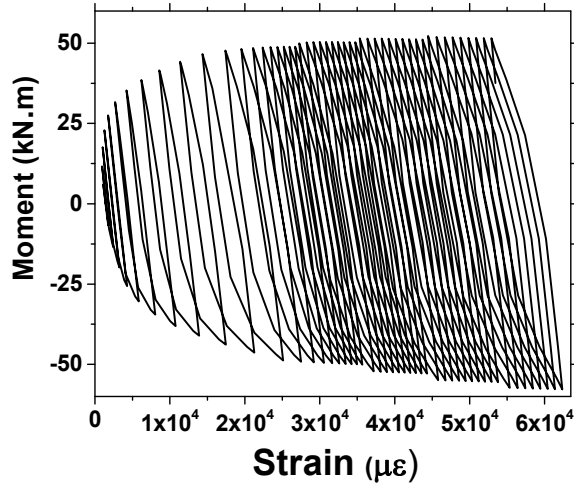


Figure 5.31: Cyclic moment- strain curves for the CSPS-A elbow

Envelope characteristics are obtained by joining the peak values and are shown in Figure 5.32. The envelope moments of CSPS-A elbow for PLS-1 and PLS-2 are 35.8 kN•m and 55.9 kN•m respectively. These limit states are indicated in Figure 5.32.

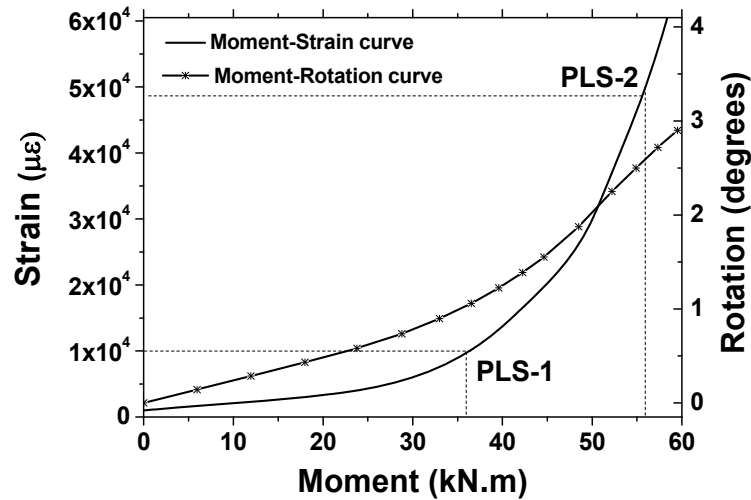


Figure 5.32: Cyclic envelope ε -M- θ characteristic of CSPS- A elbow

5.3.1.2 Iterative analysis of CSPS-A with response spectrum as input

Finite element model of CSPS-A is shown in Figure 5.26. The model comprises of pipe, elbow elements and spring combination for critical elbow. The three frequencies of this model are 5.5 Hz, 8.2 Hz and 14.6 Hz. These values are closer to the frequencies from sine sweep test. Initially the model is subjected to table excitation of

0.35g ZPA and response spectrum analysis is carried out. As per the guidelines of ASCE 4-98 [54], the number of modes for the analysis is based on the cut-off frequency of 100 Hz and missing mass correction is carried out. Equivalent static analysis is carried out by applying force based on missing mass and acceleration corresponding to the cut-off frequency. This response is combined as an extra mode with frequency equals to cut-off frequency [55]. The resulting moment (M) and rotation (θ_e) of high stressed elbow are 25.81 kN•m and 1.08×10^{-2} rad respectively. From Figure 5.32, envelope moment (M_c) corresponding to 1.08×10^{-2} rad is 24.86 kN•m. This gives a difference of 3.82%. To minimize this, the rotational stiffness is revised to 2.302 MN•m/rad and second iteration is carried out. This results in M and θ_e of 25.44 kN•m and 1.10×10^{-2} rad respectively. M_c for 1.10×10^{-2} rad is 25.18 kN•m producing a difference of 1.06%. Next iteration is carried out with a stiffness of 2.278 MN•m/rad. M and θ_e in this iteration are 25.37 kN•m and 1.11×10^{-2} rad respectively. M_c for this rotation is 25.3 kN•m yielding convergence. From Figure 5.32, peak strain corresponds to this moment is 4800 $\mu\epsilon$. The analysis is continued for higher levels of table excitation (0.5g, 0.75g and 1g ZPA). The details of iterations are given in Table 5.4.

Table 5.4: Details of iterations for CSPS-A

Table excitation level, ZPA (g)	Iter. no.	k_{Rz} (MN•m/rad)	M (kN•m)	θ_e ($\times 10^{-2}$ rad)	M_c (kN•m)	Error (%)	ϵ_{elb} ($\mu\epsilon$)
0.35	1	2.390	25.81	1.08	24.86	3.82	4800
	2	2.302	25.44	1.10	25.18	1.03	
	3	2.278	25.37	1.11	25.30	0.28	
0.5	1	2.278	36.24	1.59	32.83	10.39	9650
	2	2.064	35.76	1.73	34.76	2.88	
	3	2.006	35.73	1.78	35.42	0.88	

0.75	1	2.006	53.60	2.67	44.32	20.94	30900
	2	1.658	53.12	3.20	48.17	10.28	
	3	1.504	52.05	3.46	49.67	4.79	
	4	1.435	51.25	3.57	50.26	1.97	
	5	1.407	50.86	3.61	50.49	0.73	
1.0	1	1.407	67.82	4.82	57.71	17.52	71600
	2	1.198	61.86	5.16	60.20	2.76	
	3	1.166	60.58	5.20	60.50	0.13	

The resulting peak strains obtained from analysis are compared with those from ratcheting experiment is shown in Figure 5.33. It can be seen that the peak strains obtained from IIRS analysis matches well with experimental peak strains. Also, table excitation levels for ratcheting based PLS are evaluated from Figure 5.33. The excitation levels from analysis for PLS-1 and PLS-2 are 0.505g and 0.87g respectively. From test results, levels for PLS-1 and PLS-2 are 0.46g and 0.91g respectively. It is observed that IIRS analysis closely predicts the excitation levels for ratcheting based PLS.

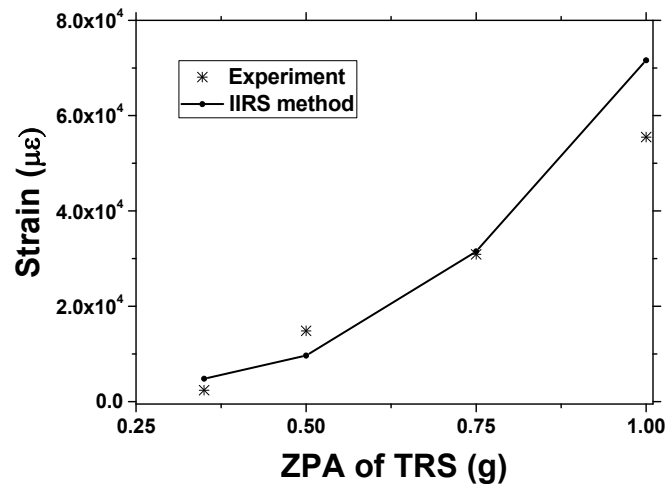


Figure 5.33: Comparison of predicted peak strains with experimental results

5.3.2 IIRS analysis of CSPS-B

Detailed cyclic plasticity analysis is carried out on shell model of elbow shown in Figure 5.34 to generate cyclic envelope characteristics. Later, IRS analysis is carried out on line model of CSPS-B shown in Figure 5.35 to obtain the moment-rotation in critical elbow for incremental seismic excitation.

5.3.2.1 Detailed cyclic plasticity analysis of elbow

Chaboche model is used to obtain ratcheting response in pressurized elbow under cyclic load. Six Chaboche parameters are obtained from stabilized cyclic stress strain loop using procedure given by Chaboche. The Chaboche parameters are (C_1, γ_1) , (C_2, γ_2) and (C_3, γ_3) are (1123000, 280750), (50500, 950) and (5900, 9) respectively. Cyclic yield stress $\sigma_0 = 240$ MPa. The comparison of Chaboche model and uniaxial stabilized hysteresis loop under symmetric strain cycling is given in Figure 5.27. Cyclic plasticity analysis is carried out by applying design level internal pressure and incremental cyclic tip displacement. The limit displacement (δ_L) is obtained by double tangent intersection shown in Figure 5.28. Using 10% incremental limit displacement, the cyclic tip displacement given in Figure 5.29 is applied to the elbow and analysis is performed.

Ratcheting analysis is carried out on 90° long radius elbow of the piping system. Figure 5.34 shows the finite element (FE) model of the elbow which is modeled using shell elements. The ends of the elbow are attached with straight pipes of length more than three times diameter.

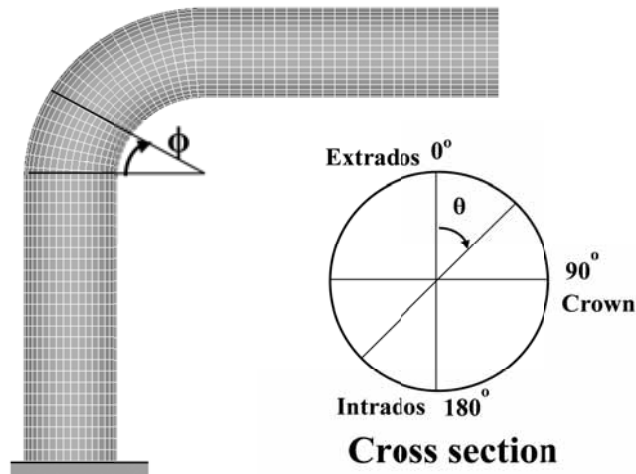


Figure 5.34: FE model of C-SPS-B elbow

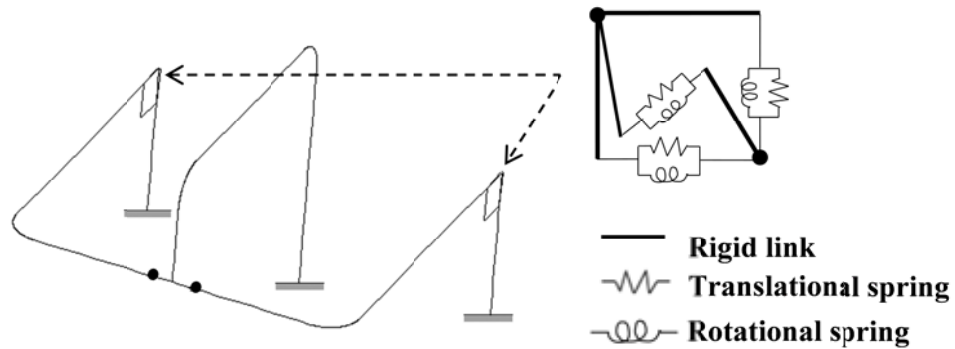


Figure 5.35: Line model of C-SPS-B with combination of springs

A constant internal pressure of 12 MPa is applied to the FE model, which corresponds to the design stress of $1S_m$. Cyclic nonlinear static analysis is carried out to estimate limit displacement by incrementally applying load at the tip of the elbow. The limit displacement (δ_L) for the elbow is 30 mm, which is obtained from the load-displacement characteristics using intersecting tangent method as shown in Figure 5.36. Ratcheting analysis of the elbow is carried out by applying internal pressure and incremental load line displacement (10% increment of δ_L) as shown in Figure 5.37.

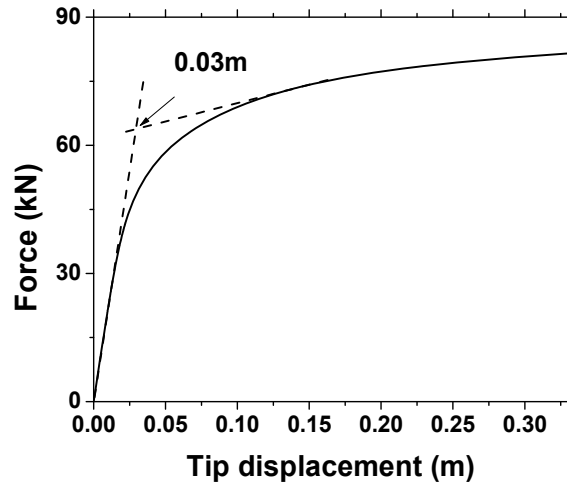


Figure 5.36: Evaluation of limit displacement of CSPS-B elbow

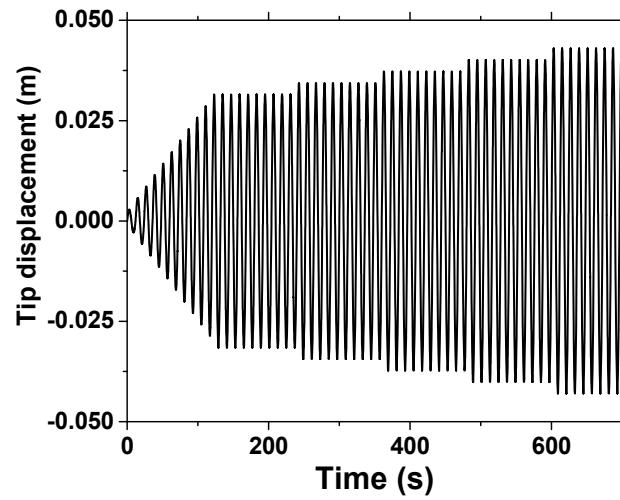


Figure 5.37: Tip displacement time history for ratcheting analysis

Cyclic moment-rotation curves of the elbow are given in Figure 5.38. Cyclic moment-strain curves of the elbow are given in Figure 5.39.

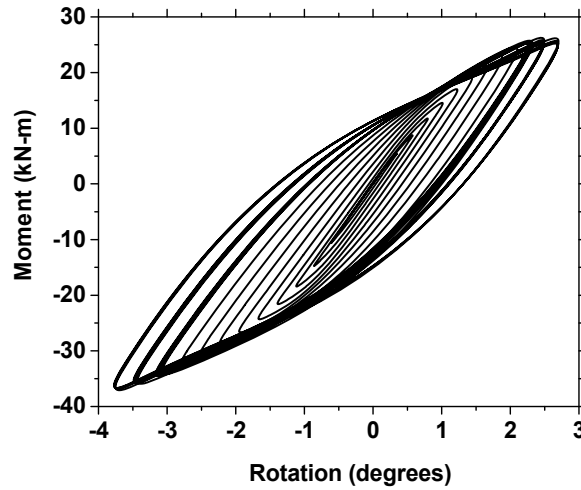


Figure 5.38: Cyclic moment-rotation curves for CSPS-B elbow

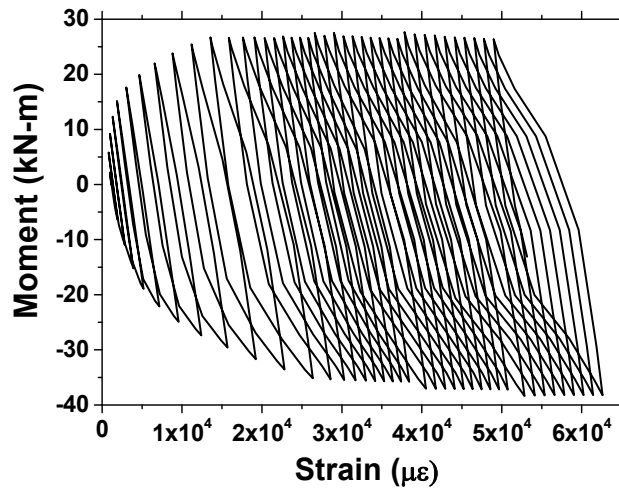


Figure 5.39: Cyclic moment- strain curves for CSPS-B elbow

Envelope characteristics are obtained by joining the peak values and are shown in Figure 5.40. The envelope moments of CSPS-B elbow for PLS-1 and PLS-2 are 25.2 kN•m and 38 kN•m respectively. These limit states are indicated in Figure 5.40.

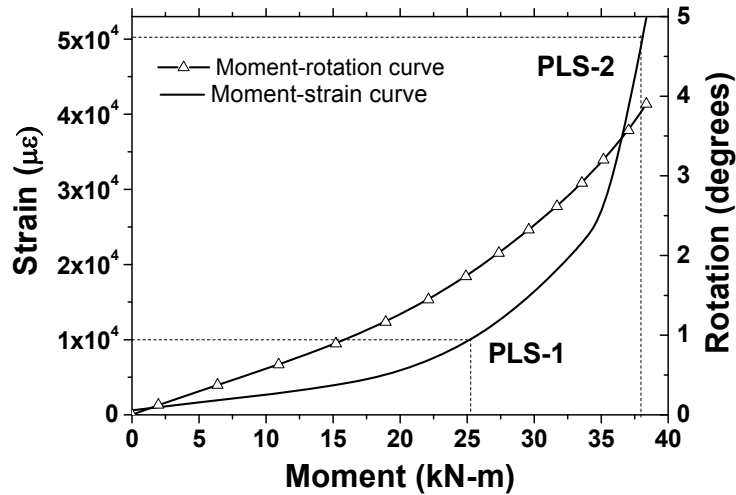


Figure 5.40: Envelope Strain-Moment-Rotation characteristics for CSPS-B elbow

5.3.2.2 Iterative analysis of CSPS-B with response spectrum as input

Line model of CSPS-B is shown in Figure 5.35. The model comprises of pipe, elbow elements and spring combination for critical elbow. The three frequencies of this model are 3.7 Hz, 5.8 Hz and 15.2 Hz. These values are closer to the frequencies from sine sweep test. Initially the model is subjected to table excitation of 1.0g ZPA. The resulting moment (M) and rotation (θ_e) of high stressed elbow are 15.0 kN•m and 1.66×10^{-2} rad respectively. From Figure 5.40, envelope moment (M_c) corresponding to 0.95° is 15.82 kN•m. This gives a difference of 5.19%. To minimize this, the rotational stiffness is revised to 0.907 MN•m/rad and second iteration is carried out. This results in M and θ_e of 15.19 kN•m and 1.59×10^{-2} rad respectively. M_c for 1.59×10^{-2} rad is 15.29 kN•m producing a difference of 0.59%, yielding convergence. From Figure 5.40, peak strain corresponds to this moment is 3800 $\mu\epsilon$. Next iteration is carried out with a stiffness of 0.907 MN•m/rad. M and θ_e in this iteration are 18.99 kN•m and 1.99×10^{-2} rad respectively. M_c for this rotation is 18.32 kN•m giving a difference of 3.69%. The stiffness is revised to 0.875 MN•m/rad and response spectrum analysis is carried out, yielding convergence. Peak strain corresponds to this moment is 4980 $\mu\epsilon$. The analysis

is continued for higher levels of table excitation from 1.5g to 2.5g with an increment of 0.25g. The details of iterations are given in Table 5.5.

Table 5.5: Details of iterations for CSPS-B

Table excitation level, ZPA (g)	Iter. no.	k_{Rz} (MN•m/rad)	M (kN•m)	θ_e ($\times 10^{-2}$ rad)	M_c (kN•m)	Error (%)	ϵ_{clb} ($\mu\epsilon$)
1.0	1	0.860	15.00	1.66	15.82	5.18	3800
	2	0.907	15.19	1.59	15.29	0.65	
1.25	1	0.907	18.99	1.99	18.32	3.66	4980
	2	0.875	18.83	2.04	18.72	0.59	
1.5	1	0.875	22.60	2.46	21.49	5.17	6635
	2	0.832	22.30	2.55	22.11	0.86	
1.75	1	0.832	26.02	2.98	24.61	5.73	9025
	2	0.787	25.58	3.11	25.30	1.11	
	3	0.778	25.48	3.12	25.43	0.20	
2.0	1	0.778	29.12	3.58	27.67	5.24	12350
	2	0.739	28.57	3.70	28.24	1.17	
	3	0.731	28.43	3.72	28.36	0.25	
2.25	1	0.731	31.99	4.19	30.34	5.44	16200
	2	0.693	31.22	4.31	30.82	1.30	
	3	0.684	31.02	4.35	30.93	0.29	
2.5	1	0.684	34.47	4.82	32.68	5.48	20615
	2	0.649	33.47	4.94	33.05	1.27	
	3	0.640	33.21	4.96	33.12	0.27	

Comparison of peak strains with experimental results for CSPS-B is shown in Figure 5.41. It is observed that predicted strains are higher than experimental results for excitation with 1g ZPA. The predicted peak strain is closer to the experimental strain for excitation with 1.25g ZPA. The experimental strains are slightly higher for

excitations with 1.5g ZPA and 1.75g ZPA. For further excitation, the predicted strains are less than the experimental peak strains. This discrepancy is due to the use of cyclic parameters obtained from specimens not from the piping loop. Also, the strains measured at symmetric elbows are different and this discrepancy is attributed to different thickness distribution of elbows. The predicted strain accumulation by IIRS method is same for both symmetric elbows, due to consideration of same thickness. Consideration of thickness variation in numerical simulation can cover such uncertainties.

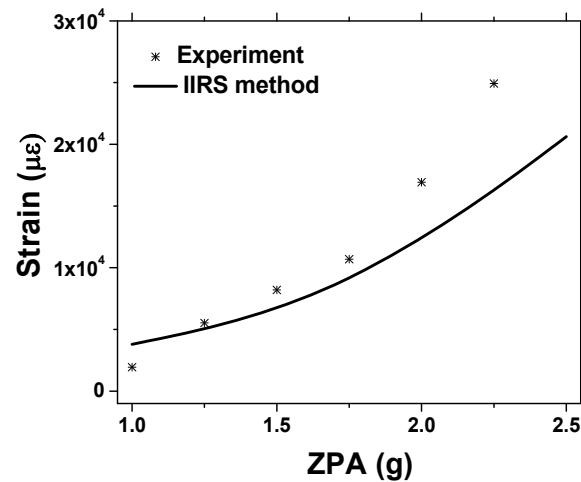


Figure 5.41: Comparison of predicted strain accumulation at crown with test results (CSPS-B)

5.4 Outcome and discussion

This chapter presents the experimental and numerical studies on pressurized piping systems under seismic load. The research carried out has highlighted the following salient aspects:

From the shake table tests, it is observed that strain has been accumulated significantly at crown of a critical elbow before the formation of a through wall crack. Thus it is concluded that fatigue-ratcheting has caused the failure of the piping system.

From the wavelet analysis, it is found that the dominant frequency of the piping systems before ratcheting failure is only 2-4% less than the initial value; whereas for piping components, the reduction is in the range of 13-15%. Thus the frequency reduction at piping system level is much less than that of component level. This is due to the load re-distribution and redundancy at system level.

After strain accumulation of above 5%, ratcheting failure of elbow of CSPS-A is observed. The extrapolated peak ratcheting strain corresponding to failure excitation level of the piping loop is 8.32%. In earlier tests on an elbow, peak strain accumulation of above 5% was measured at crown location before failure. Hence, the ratcheting strain limit of 5% is considered as a performance limit.

It is also observed that strain accumulation at two identical crown locations of elbow is not similar. This discrepancy can be attributed to plastic strain localization, thickness variation and different microstructural features such as dislocations at both crown locations.

The piping systems are analyzed using IIRS method to evaluate ratcheting. It is observed that this method has reasonably predicted the strain accumulation for different excitation levels for CSPS-A. For CSPS-B, this method has predicted slightly different peak strains compared to the test results. This discrepancy is due to the use of cyclic parameters obtained from specimens not from the piping system.

CHAPTER 6 SEISMIC FRAGILITY ANALYSIS OF PRESSURIZED PIPING SYSTEMS CONSIDERING RATCHETING

6.1. Introduction:

Probabilistic Risk Assessment (PRA) is usually carried out to ensure the safety of nuclear piping systems, as it account for inherent randomness in piping properties and earthquake events. PRA consists of two steps; evaluation of probability of exceedance from hazard analysis and the next step is evaluation of capacity in the form of seismic fragility. Seismic fragility curves provide the conditional exceedance probability of a Performance Limit State (PLS) at a given level of seismic excitation. These curves are generated by Seismic Fragility Analysis (SFA) which is an important requisite for PRA. SFA studies on piping system available in the literature are based on the failure mode of plastic collapse. This was the assumed failure mode for seismic load by earlier edition of ASME code (before 1995).

Hence, SFA of pressurized piping systems based on ratcheting, which is the predominant failure mode is necessary. In the present study, a frame work has been provided for SFA of pressurized piping systems. The methodology has been demonstrated for typical pressurized piping systems, considered for an international benchmark exercise, known as Metallic Component Margins (MECOS) exercise. The details of this benchmark exercise are given in Labbe et. al. [62]. This benchmark was organized by Organization for Economic Co-operation and Development—Nuclear Energy Agency (OECD-NEA) to evaluate the seismic margins with respect to existing design practices. This exercise utilized the shake table test results of Carbon Steel

Piping System (CSPS) and Stainless Steel Piping System (SSPS) of same configuration and loading. These piping systems are considered at a typical equipment location of Reactor Building (RB) [63]. Uncertainty in floor motion at this elevation is considered from the analysis of RB under available earthquake records. Usually, uncertainty other than ground motion variability is not considered in SFA of piping systems (Kennedy and Ravindra [4], Ju and Gupta [5] and Firoozabad et. al. [6]).

Piping response under seismic load depends up on corresponding spectral acceleration (S_a) of the piping systems. S_a primarily depends up on damping value (ξ) and fundamental natural frequencies (f) of the piping systems in addition to randomness of seismic events. Hence, the uncertainty in damping value and dominant frequency of piping system are considered along with the variation in floor motion. The spectral acceleration also depends on the concrete properties and soil conditions. Characterization of uncertainties of concrete and soil conditions requires lot of in-situ information. As such information is not available, these uncertainties are not considered. SFA methodology is provided in the next section.

6.2. Details of fragility assessment methodology

Uncertainty in damping is obtained from the results of statistical analysis for damping of earlier tested piping components and systems. Floor Response Spectra (FRS) are generated at a typical equipment elevation by the time history analysis of a typical Reactor Building (RB) under twenty intra plate earthquake records. Two ratcheting based Performance Limit States (PLS) and design stress limit are considered. A validated IIRS method is used to evaluate ratcheting strains in the piping system. Response surface technique in conjunction with Monte Carlo simulations is used for SFA. Methodology for SFA of pressurized piping systems is provided in the flow chart of Figure 6.1. Steps to be followed for this methodology are given below:

- a. Obtain variation in damping (ξ) and natural frequency (f)
- b. Identify the efficient set of DOE cases corresponding to sampling points (ξ_i, f_i)
- c. Obtain an ensemble of piping models corresponding to (ξ_i, f_i)
- d. Get the set of earthquake records and obtain the set of FRS from the linear transient analyses of primary structure
- e. Carry out IIRS analysis of the ensemble of piping models under set of FRS using envelope cyclic characteristics of elbow (obtained from ratcheting analysis)
- f. Evaluate excitation levels for different PLS
- g. Evaluate response surface models for each PLS
- i. Carry out Monte-Carlo simulations to obtain seismic fragility curves

6.2.1. Details of floor motion variability

Floor motion variation is obtained by the time history analysis of RB under twenty earthquake records obtained from intra-plate rock sites considered for seismic hazard analysis of a typical PI site [64]. The details of these records are provided in Table 6.1. Peninsular Indian (PI) region, which is an intra-plate region, contains many nuclear facilities.

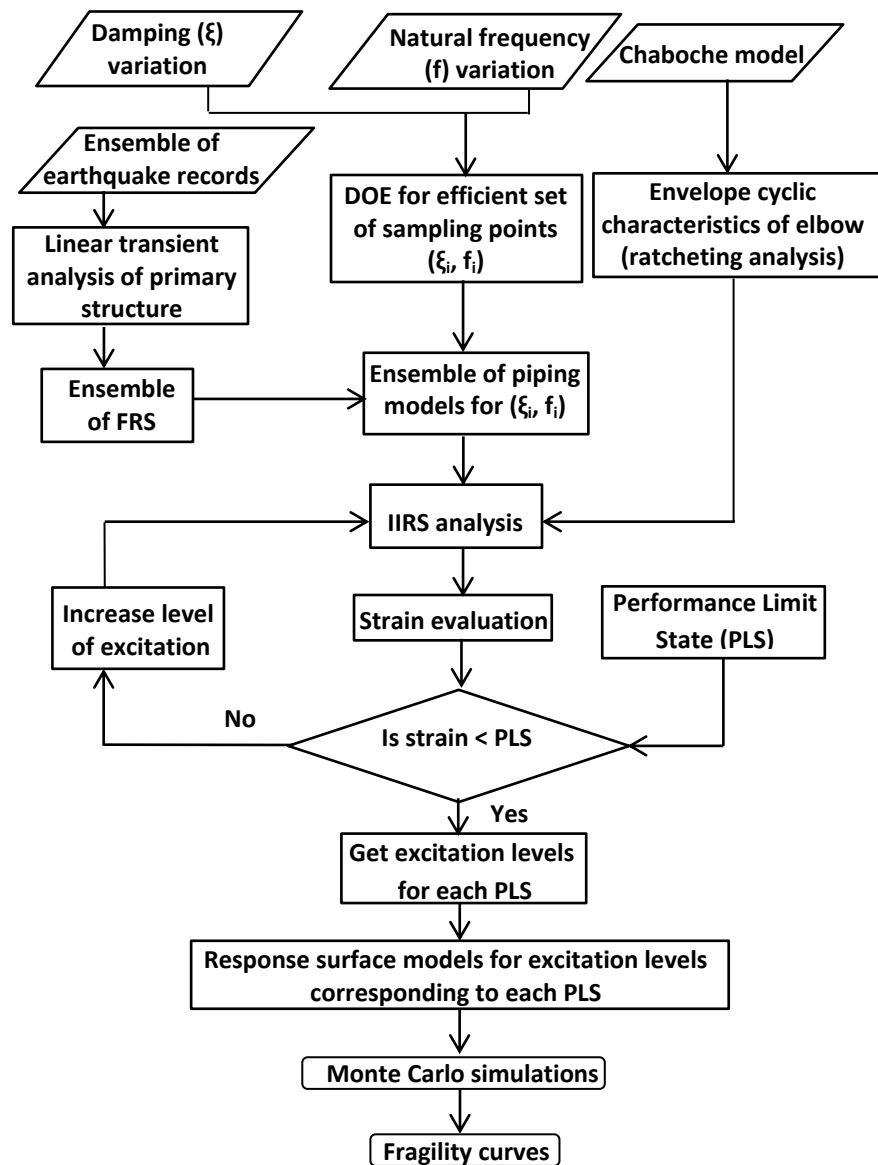


Figure 6.1: Flow chart showing fragility assessment methodology

Number of peak-peak load cycles in an earthquake depends on earthquake duration, which in turn depends on its magnitude. In the seismic hazard analysis of a typical PI site [64], 6.2 was the maximum magnitude (M_{\max}) considered. As the present SFA is aimed for a typical PI site, earthquake records on intra-plate hard rock sites with magnitudes (5.8 to 6.5), which closer to typical M_{\max} are considered.

Table 6.1: Details of intra plate earthquake records

S. No.	Name of earthquake	R_{epi} (km)	Station name	Component	PGA (g)
1	EQ-1	45.1	Chicoutimi-Nord	Transverse	0.131
2	EQ-1	45.1	Chicoutimi-Nord	Radial	0.106
3	EQ-1	91.85	St-Andre-du-Lac-St-Jean	Transverse	0.091
4	EQ-1	91.85	St-Andre-du-Lac-St-Jean	Radial	0.099
5	EQ-1	112.9	Les	Transverse	0.102
6	EQ-1	112.9	Les	Radial	0.125
7	EQ-1	147.6	Quebec	Transverse	0.05
8	EQ-1	147.6	Quebec	Radial	0.05
9	EQ-1	165	St.-Pascal	Transverse	0.046
10	EQ-1	165	St.-Pascal	Radial	0.055
11	EQ-2	45.3	Site 3	Transverse	0.194
12	EQ-2	45.3	Site 3	Radial	0.186
13	EQ-3	53.5	Charlottesville	Transverse	0.1
14	EQ-3	53.5	Charlottesville	Radial	0.122
15	EQ-3	124.1	Reston Fire Station	Transverse	0.04
16	EQ-3	124.1	Reston Fire Station	Radial	0.09
17	EQ-3	256.4	Charlottesville	Transverse	0.0017
18	EQ-3	256.4	Charlottesville	Radial	0.002
19	EQ-4	12.7	Koyna	Transverse	0.38
20	EQ-4	12.7	Koyna	Radial	0.48

Notes:

1. EQ-1 refers to Saguenay earthquake (25.11.1988) of Magnitude 5.9
2. EQ-2 refers to Nahanni earthquake (23.12.1985) of Magnitude 6.9
3. EQ-3 refers to Mineral Virginia earthquake (23.8.2011) of Magnitude 5.8
4. EQ-4 refers to Koyna earthquake (10.12.1967) of Magnitude 6.5.

Time history analysis of the RB is carried out under these twenty intra-plate records. Floor Response Spectra (FRS) at a typical equipment elevation are obtained from the acceleration time histories at this location. These twenty FRS satisfies the minimum requirement of number of records for SFA, suggested by Cimellaro et. al. [65]. The finite element model of typical RB of an Indian PHWR is shown in Figure 6.2, and is modeled with beam elements. The properties of equivalent beam model were evaluated by Reddy et. al. [63] and the same are used in the present work. It comprises of Inner Containment Wall (ICW), Outer Containment Wall (OCW) and an internal structure (IS) resting on a massive circular raft.

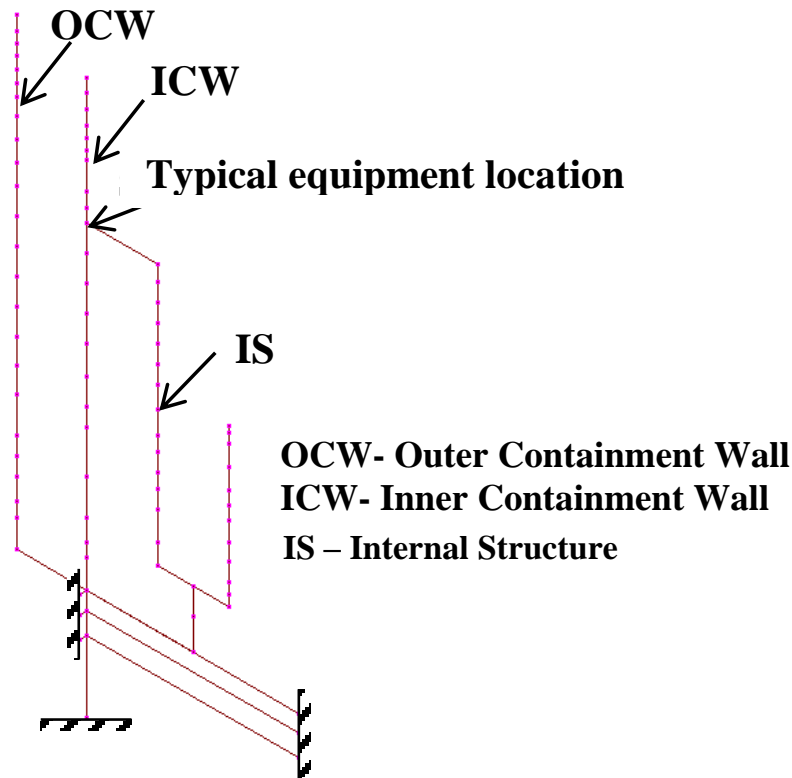


Figure 6.2: FE model of typical Indian PHWR reactor building

Acceleration time histories at typical equipment elevation are evaluated from the linear transient analysis of RB under twenty records. FRS for required damping are evaluated from these time histories.

6.2.2. Evaluation of variation in damping

Variability in damping values is obtained from the results of statistical analysis of damping of the present as well as earlier tested piping components and systems (Muthumani et. al. [38], Ravi Kiran et. al. [39], Gopalakrishnan et. al. [66] and RSD internal report [67]). The details of the tested components and systems are provided in Table 6.2.

Table 6.2: Details of tested piping components and systems

S. No.	Description	Pipe size DN (mm)	Wall thickness, (mm)	Material	Internal pressure (MPa)	Base excitation type
1.	Elbow (Large radius)	80	5.5	SS	18	Harmonic
2.	Elbow (Short radius)	80	5.5	CS	21.3	Seismic
3.	Tee joint	80	5.5	CS	21.3	Seismic
4.	Piping system	150	7.1	CS	12	Seismic
5.	Piping system	150	7.1	SS	12	Seismic
6.	Piping system	80	5.5	CS	21.3	Seismic
7.	Piping system	100	8.6	CS	20.6	Seismic
8.	Piping system with damper	100	8.6	CS	-	Sine sweep

(Note: Stainless steel is denoted by SS and Carbon steel with CS)

At component level, Muthumani et. al. [38] tested a pressurized large radius stainless steel elbow of size 3-inch Nominal Bore (NB). Also, a pressurized 3 inch NB carbon steel elbow and tee have been tested under incremental earthquake load. At system level, 6 inch NB carbon steel and stainless steel piping systems (Ravi Kiran et.

al. [40]) of same configuration have been tested under same internal pressure and incremental seismic load. A pressurized 3 inch NB carbon steel piping system (Ravi Kiran et. al. [39]) was tested under incremental earthquake load. Another pressurized 4 inch NB carbon steel piping system was tested under multi-support excitation by Gopalakrishnan et. al [66]. In addition, effectiveness of dampers on piping system was studied on a 4 inch NB carbon steel piping system [67]. Damping values evaluated from all these tests are compiled and statistical analysis has been carried out. Damping values are plotted with respect to frequency of the tested component or piping system in Figure 6.3. The histogram of these damping values is given in Figure 6.4.

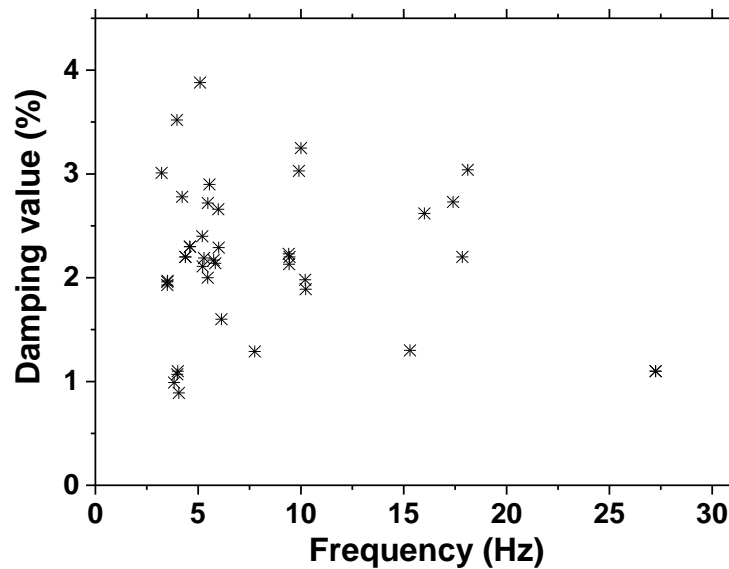


Figure 6.3: Damping values of tested components and piping systems with frequency

The data follows an approximate normal distribution with mean value of 2.2% and standard deviation of 0.714%. These statistics are based on the data of shake table tests of laboratories. Hence, for actual industrial applications, damping of piping systems from in-situ measurements is to be used.

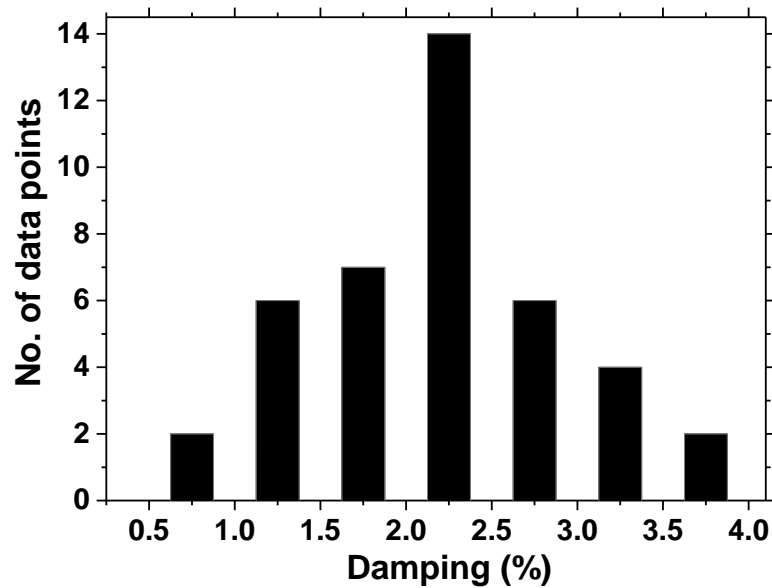


Figure 6.4: Histogram of damping values from shake table tests

6.2.3. Numerical tool used for evaluation of ratcheting

In the literature, Incremental Dynamic Analysis (IDA) was widely used for SFA of steel and RC structures. For the present SFA of piping systems, IIRS method which is similar to IDA is considered for evaluation of ratcheting strains. As this method utilizes response spectrum as input, several simulations can be carried out, which is required for SFA.

6.2.4. Ratcheting based Performance Limit States (PLS) for piping systems

SFA of pressurized piping systems needs identification of ratcheting based Performance Limit States (PLS). In the present work, two PLS are proposed based on the shake table tests and design code guidance. Morishita et. al. [60] and Otani et. al. [61] presented details of recent national benchmark exercises in Japan and proposed JSME code case. In this proposed code case, 1% limit for maximum strain from in-elastic analysis is recommended for earthquake load. This limit of 1% is identified as the first ratcheting based PLS and is denoted by PLS-1. From the results of piping tests carried out by EPRI, Tagart et. al. [25] proposed a 5% ratcheting limit for Level-D

service condition. Also, the same limit was adopted for alternate ratcheting based criterion by 1995 edition of ASME code. NUPEC piping tests [27] also confirmed similar ratcheting failures.

Peak ratcheting strain of above 5% was observed in recent test on elbow [38]. In the shake table test on CSPA-A also, similar ratcheting failure has occurred after a peak ratcheting strain of around 8.32%. This limit of 5% is identified as the second ratcheting based PLS and is denoted by PLS-2. The design code [9] stress limit of $3S_m$ is chosen as the third PLS and is denoted by PLS-3.

6.2.5. Evaluation of fragility

In the present work, Response Surface Method (RSM) is applied for fragility evaluation. The RSM uses Design of Experiments (DOE) techniques to identify efficient set of simulations and then use regression analysis to create a polynomial approximation of analysis results over variable space (Towashiraporn [11]). DOE techniques suggest an efficient set of sampling points (Montgomery [12]) at which the structural/ piping response is to be computed. For this purpose, many different types of DOE can be used and Full Factorial Design (FFD) is the simplest and commonly used (Montgomery [12]). In FFD, each variable is normalized and equally spaced to obtain the normalized values of -1, 0 and +1. In this DOE method, the total number of variable combinations (design points) is 3^p , where 'p' is number of variables. Corresponds to each set of sampling points, IIRS method is applied to obtain ratcheting in piping system, under different FRS. Using polynomial representation of response surfaces, several Monte Carlo simulations are carried out to evaluate seismic fragility of piping system.

6.3. Case study: Fragility assessment for Carbon Steel Piping System (CSPS) and Stainless Steel Piping System (SSPS)

As a case study, the above mentioned methodology is applied to generate seismic fragility curves for a carbon steel and stainless steel piping systems shown in Figure 5.13, which were considered for an international benchmark exercise called ‘Metallic Component Margins under High Seismic Loads’ (MECOS) benchmark conducted by OECD-NEA. The details of this benchmark exercise are given in Labbe et. al. [62]. The objective of the benchmark exercise was to quantify seismic margins in piping systems with respect to existing design practices. Results of shake table tests conducted on the piping system to study ratcheting were utilized for this exercise. The schematic of the piping system is shown in Figure 5.13. The size of the piping system is DN 150 mm and schedule 40 and was anchored to the shake table at three places.

6.3.1. Fragility assessment for a Carbon Steel Piping System (CSPS)

Fragility curves corresponding to three PLS are generated for CSPS.

6.3.1.1. Selection of set of simulations

Optimized set of simulations are obtained using Design of Experiments (DOE). Full factorial design of DOE is used. As two parameters, damping and dominant frequency are used in the present study the total number of simulations are nine (3^p where $p=2$). Normal distribution parameters for the damping are obtained from the statistical analysis of test data. A 10% variation in the dominant frequency is considered by appropriately choosing the mass dispersion. This is similar to the variation considered by Descelier et. al. [68]. These two parameters are normalized in the range of -1 to +1 and the set of parameters for simulations are provided in Table 6.3. Mean along with three sigma limits are used for damping while mean and 10% variation is considered for dominant frequency.

Floor Response Spectra (FRS) at typical equipment elevation are obtained from the response acceleration time histories of linear transient analysis of RB under twenty records. In the shake table test of CSPS, a wideband broadened response spectrum was used to subject the piping system to peak spectral acceleration. In the present analysis also the dominant frequency is chosen as 3.3 Hz, corresponding to the first spectral peak of FRS. IIRS analyses are conducted for all nine set of parameters under twenty FRS corresponding to respective damping value. Hence, a total 180 IIRS simulations are carried out.

Table 6.3: Different cases of Design of Experiments (DOE)

Damping		Dominant frequency		Simulation set no.
Physical variable, ξ (%)	Normalized parameter, x_1	Physical variable, f (Hz)	x_2	
0.058	-1	2.98	-1	1
0.058	-1	3.3	0	2
0.058	-1	3.63	1	3
2.2	0	2.98	-1	4
2.2	0	3.3	0	5
2.2	0	3.63	1	6
4.342	1	2.98	-1	7
4.342	1	3.3	0	8
4.342	1	3.63	1	9

6.3.1.2. IIRS simulations of CSPS

In IIRS simulations, response spectrum analysis is carried out iteratively until convergence of elbow response from system analysis with component level envelope characteristics shown in Figure 5.38, generated in Section 5.3.2.1 of Chapter 5. The simulations are performed for nine sets given in Table 6.3. FRS corresponding to the required damping are obtained from the acceleration response from transient analysis of RB beam model. The normalized FRS of twenty intra-plate records for 0.058%, 2.2% and 4.342% damping values are shown in Figure 6.5, Figure 6.6 and Figure 6.7 respectively.

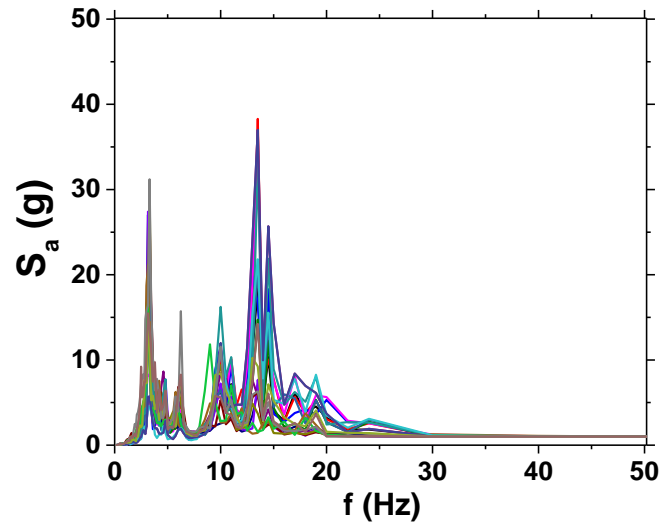


Figure 6.5: FRS of twenty records for 0.058% damping

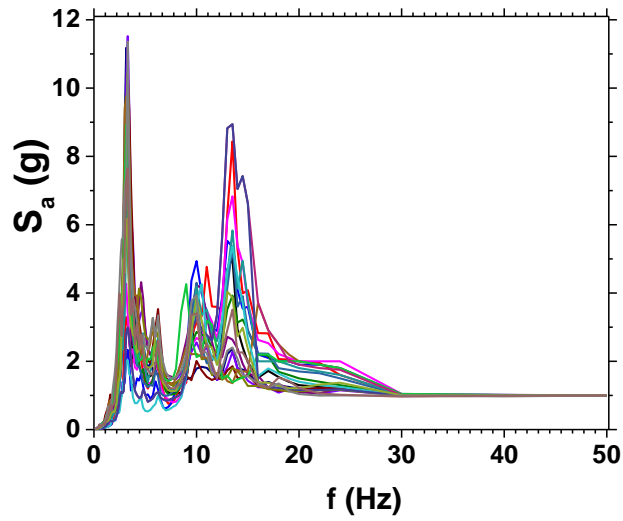


Figure 6.6: FRS of twenty records for 2.2% damping

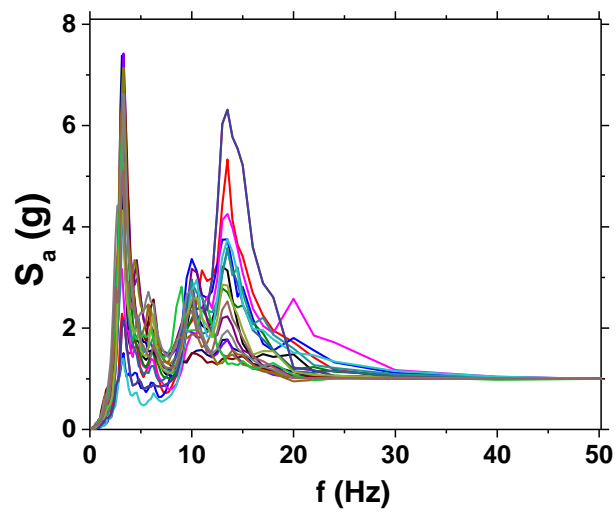


Figure 6.7: FRS of twenty records for 4.342% damping

This results in a total of 180 analyses of CSPS. For each analysis, an excitation with 0.1g ZPA is applied to the FE model of CSPS and IIRS analysis is carried out. Resulting rotation and moment in high stressed elbow are obtained and compared with envelope elbow characteristics. In-plane rotational stiffness of the elbow is modified iteratively till convergence. The ratcheting strain of elbow corresponds to this converged moment is obtained from envelope results and is shown in Figure 5.38. The input level of base excitation is repeated until 5% ratcheting (PLS-2) is reached. Predicted peak ratcheting at crown of elbow-1 for CSPS under all 20 FRS corresponding to fifth simulation set (mean damping and mean frequency) is shown in Figure 6.8. Excitation levels in terms of ZPA for PLS-1 and PLS-2 are evaluated. It is to be noted that PLS-1 is for 1% ratcheting limit, while PLS-2 is for 5% ratcheting limit.

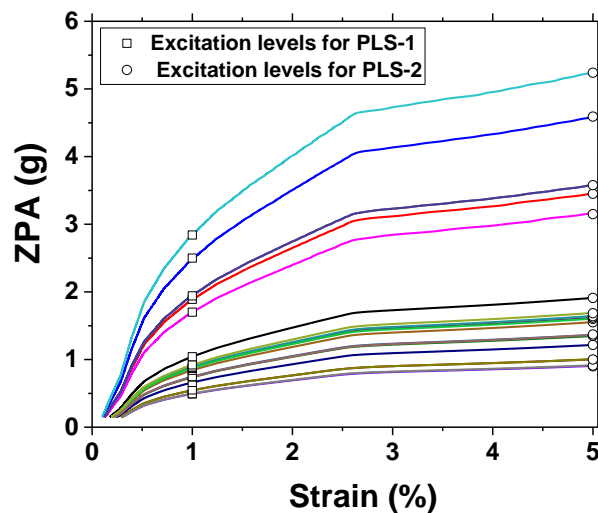


Figure 6.8: Maximum ratcheting strain in elbow-1 of CSPS for fifth DOE case of mean damping and mean frequency under 20 FRS

The levels of floor excitation in terms of ZPA for PLS-1 are shown in Figure 6.9. It can be noticed that the lowest level of 0.181g corresponding to DOE set-4 (lowest damping and mean dominant frequency) and the highest level is 6.96g, corresponding to DOE set-9 (highest damping and highest dominant frequency).

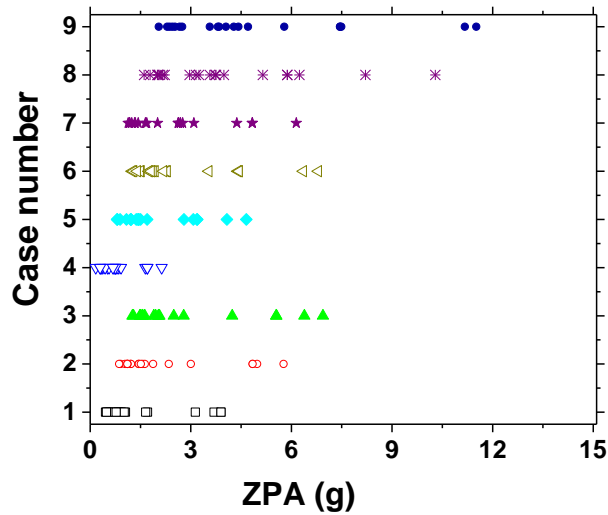


Figure 6.9: The floor excitation levels (ZPA of FRS) for PLS-1 in all nine DOE cases

The levels of floor excitation in terms of ZPA for PLS-2 are plotted in Figure 6.10. It can be seen that the smallest value is 0.33g, which again correspond to fourth DOE set (lowest damping and mean dominant frequency) and the highest value is 13g, which corresponds to ninth DOE set (highest damping and highest dominant frequency).

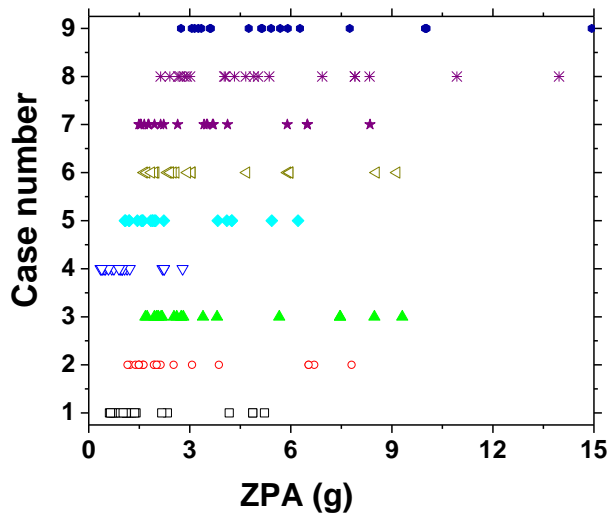


Figure 6.10: The floor excitation levels (ZPA of FRS) for PLS-2

The floor excitation levels for PLS-3 are obtained by using equation (2.3). Similarly IIRS simulations are carried out for the remaining eight DOE sets, and floor excitation levels corresponds to three PLS are obtained. The floor excitation levels for all sets correspond to PLS-3 are given in Figure 6.11.

Where, \hat{a} is the floor excitation level from response surface. Polynomial coefficients are obtained from least-square regression. The closeness of the data to the fitted response surface is checked by coefficient of determination (R^2) [11]:

$$R^2 = \frac{\text{Error sum of squares (E)}}{\text{Total sum of squares (T)}} \quad (6.2)$$

where ,

$E = b^1 X'Y - \frac{(1'Y)^2}{N}$, $T = Y'Y - \frac{(1'Y)^2}{N}$ and $1'$ a 1x N vector of ones. The polynomial coefficients for all PLS along with coefficients of determination are provided in Table 6.4. It can be seen that these values are greater than 0.99. This check ensures that second degree polynomial approximation for response surface is adequate.

Table 6.4: Polynomial coefficients for all PLS

Limit state		p ₁	p ₂	p ₃	p ₄	p ₅	p ₆	R-square value
PLS-1	LB	0.487	0.228	0.274	0.019	0.275	-0.011	0.999
	MEAN	1.187	0.502	0.561	0.140	0.686	-0.101	0.999
	UB	2.998	1.118	1.320	0.360	1.728	-0.372	0.991
PLS-2	LB	0.894	0.417	0.503	0.038	0.509	-0.020	0.999
	MEAN	2.187	0.932	1.037	0.260	1.274	-0.186	0.998
	UB	5.563	2.134	2.469	0.663	3.263	-0.737	0.991
PLS-3	LB	0.438	0.204	0.244	0.017	0.246	-0.010	0.999
	MEAN	1.052	0.422	0.495	0.120	0.581	-0.090	0.998
	UB	2.620	0.876	1.137	0.292	1.366	-0.312	0.991

6.3.1.4. Generation of fragility curves for CSPS

Ten thousand sampling points for the two variables, damping and dominant frequency are selected using Monte Carlo method. Floor excitation levels for each sampling point are evaluated from the response surfaces correspond to each PLS.

Probability of each PLS for a given floor excitation level, \hat{a} , is obtained from the fraction of sampling points for which each occurs at a level lower than \hat{a} . Numerical fragility curves for each PLS are obtained by plotting these probability values with respect to floor excitation level (Baker [15]).

Kennedy and M. K. Ravindra [4], Zentner [7] and Baker [15] obtained fragility parameters with an assumption of log-normal distribution. In this log-normal assumption, the fragility function is given by:

$$P_f = \Phi \left(\frac{\ln(\hat{a}/A_m)}{\beta} \right) \quad (6.3)$$

Where, P_f is the conditional exceedance probability of PLS at a particular floor excitation level, \hat{a} , Φ is the cumulative distribution function of standard normal distribution, A_m is the median and β is the standard deviation of $\ln \hat{a}$. The parameters for log-normal fragility function (A_m and β) are evaluated from logarithm of each floor excitation level corresponding to each PLS using the following equations [15]:

$$\ln(A_m) = \frac{1}{N} \sum_{i=1}^N \ln \hat{a}_i \quad (6.4)$$

$$\beta = \sqrt{\frac{1}{N-1} \sum_{i=1}^N \left(\ln \left(\frac{\hat{a}_i}{A_m} \right) \right)^2} \quad (6.5)$$

Where, N is the total no. of sampling points. The parameters for log-normal fragility function for each PLS are listed in Table 6.5. The first parameter, A_m (median of \hat{a}) equals to the mean of $\ln \hat{a}$ for the case of log-normal distribution of \hat{a} .

Table 6.5: The parameters for log-normal fragility function for three PLS of CSPPS

Performance limit state	Lower Bound confidence level		Median confidence level		Upper Bound confidence level	
	$A_m(g)$	β	$A_m(g)$	β	$A_m(g)$	β
PLS-1	0.47	0.42	0.87	0.33	2.86	0.31
PLS-2	0.86	0.38	1.57	0.33	5.3	0.31
PLS-3	0.4	0.37	0.76	0.32	2.5	0.29

Numerical fragility curves are obtained from the conditional exceedance probability at a particular floor excitation level for each PLS. Then, parameters for log-normal fragility function are evaluated and corresponding log-normal fragility function is obtained. Both numerical fragility curve and corresponding log-normal fragility function fit for PLS-1 are shown in Figure 6.12. Lower bound fragility curves correspond to 95% confidence level is denoted by LB. Upper bound fragility curves correspond to 5% confidence level is denoted by UB and the median fragility curves by 'M'. The experimental excitation level of PLS-1 for CSPPS is 1.38g and it is noticed that this excitation level is in the range (0.49g to 2.87g) of upper and lower bounds of fragility curves with mean probability of exceedance.

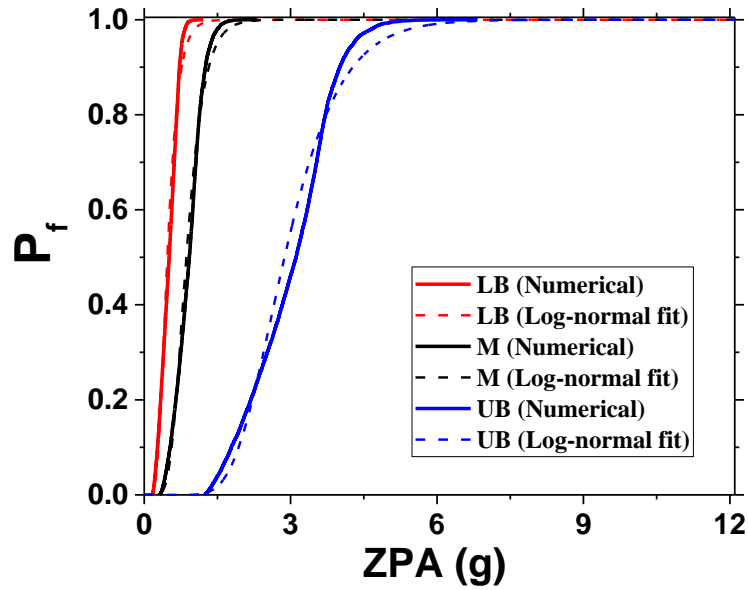


Figure 6.12: Fragility curves for first limit state, PLS-1 (1% strain limit)

The fragility curves for, PLS-2 are shown in Figure 6.13. The experimental excitation level corresponds to PLS-2 is 2.67g ZPA and is observed to be in the range (0.87g to 5.34g) of fragility curves with mean probability of exceedance for 95% and 5% confidence levels.

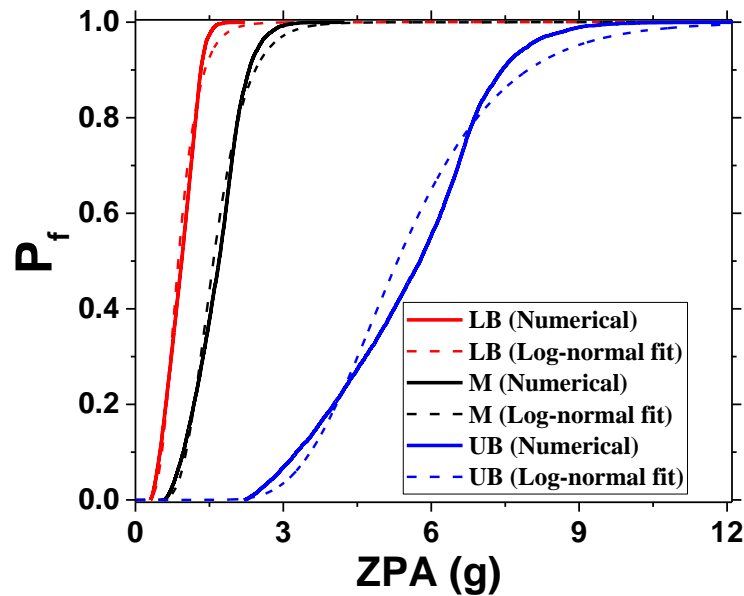


Figure 6.13: Fragility curves for second limit state, PLS-2 (5% strain limit)

Fragility curves for PLS-3 are shown in Figure 6.14. The experimental excitation level corresponds to PLS-3 is 1.75g ZPA and is observed to be in the range (0.41g to

2.51g) of fragility curves with mean probability of exceedance for 95% and 5% confidence levels.

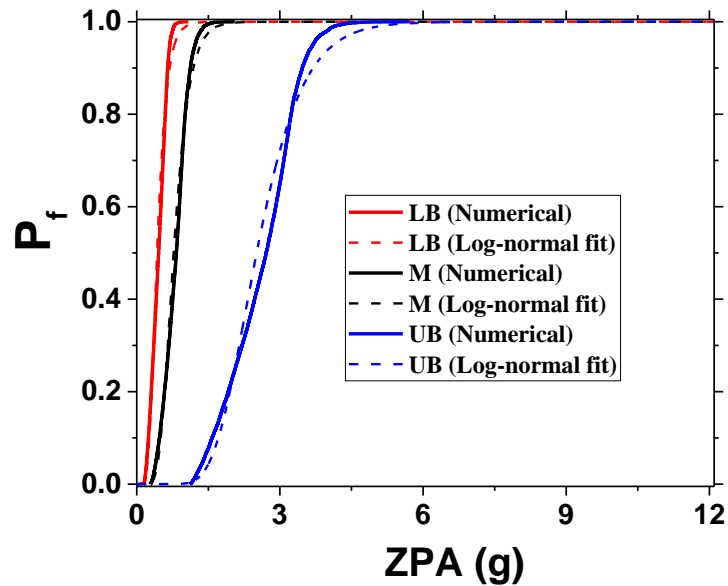


Figure 6.14: Fragility curves for third limit state, PLS-3 (codal stress limit)

6.3.2. Case study: Fragility assessment for a Stainless Steel Piping System (SSPS)

Fragility curves corresponding to three PLS are generated for SSPS. The material is stainless steel of grade SS316L.

6.3.2.1. Selection of set of simulations

Optimized set of simulations are obtained using Design of Experiments (DOE) and the same set of parameters of CSPS are considered for SSPS also and are provided in Table 6.3. A total 180 IIRS simulations are carried out.

6.3.2.2. IIRS simulations of SSPS

In the first phase of IIRS method, cyclic envelope characteristics are generated from the ratcheting analysis of elbow using Chaboche model. The six Chaboche parameters are: $C_1=1085000$, $C_2=43000$, $C_3=4100$, $\gamma_1=271250$, $\gamma_2=800$, $\gamma_3=9$ for stainless steel [43] and the comparison with uniaxial stabilized hysteresis loop for stainless steel is shown in Figure 6.15. The shell model of the elbow, shown in Figure 5.38 is subjected to internal pressure of 12 MPa and cyclic displacement shown in

Figure 6.16. Envelope cyclic strain-moment-rotation curves are obtained by joining the peak values of strain-moment and moment-rotation curves. The resulting characteristics are shown in Figure 6.17. For validation, IIRS analysis is carried out on the line model shown in Figure 5.33, under incremental tri-axial excitation shown in Figure 5.17. The comparison of predicted peak strain with test results [40] is shown in Figure 6.18. It can be seen that predicted strains compares well with test results.

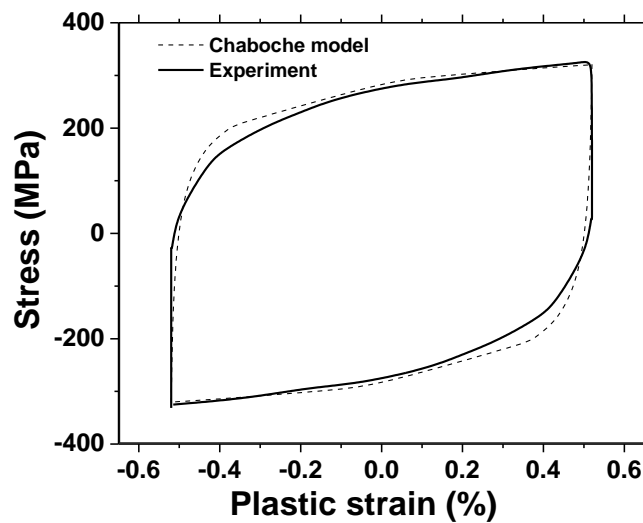


Figure 6.15: Comparison of Chaboche model with results from uniaxial cyclic tests

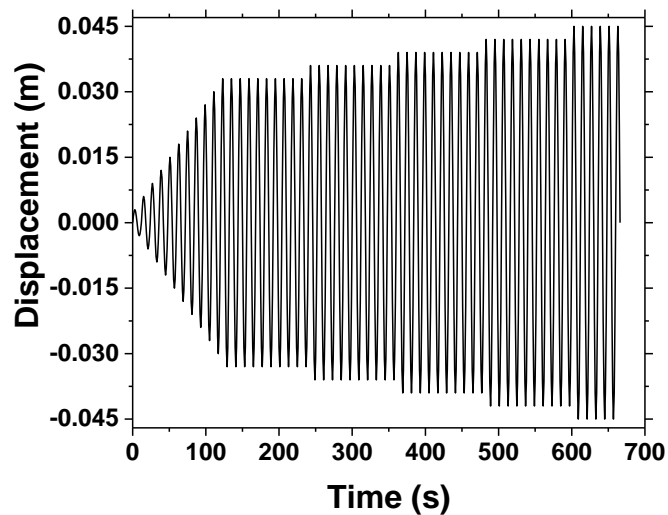


Figure 6.16: Applied displacement at elbow tip

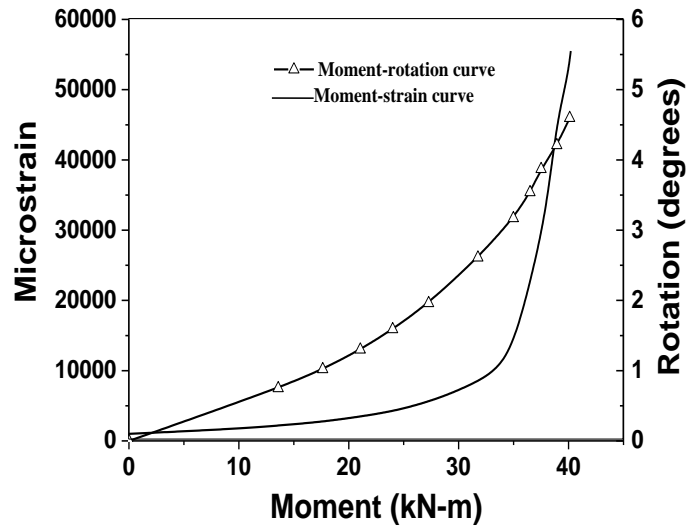


Figure 6.17: Cyclic strain-moment-rotation curves for elbow

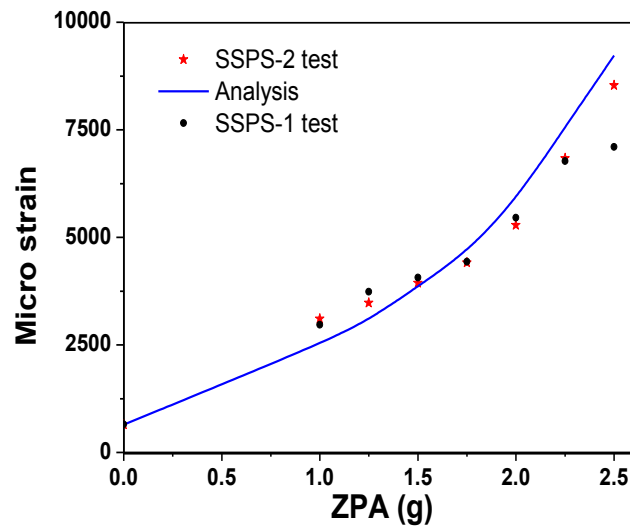


Figure 6.18: Comparison of predicted peak strain with test results

Excitation levels for three PLS at design pressure are evaluated from the strain gauge measurements of elbow crown of two ratcheting tests on stainless steel piping systems (SSPS-1 and SSPS-2) [40]. The tests were conducted at design pressure of 12 MPa until shake table capacity of 2.5g ZPA and later at constant excitation of 2.5g ZPA and higher pressures. To obtain excitation levels for design pressure, the strains are extrapolated using an exponential fit given in equation (4.1). The excitation levels in terms of ZPA for SSPS-1 are 3.1g and 5.45g for PLS-1 and PLS-2 respectively. The levels for SSPS-2 are 2.9g and 4.75g for PLS-1 and PLS-2 respectively. The level for both SSPS for PLS-3 is 1.74g ZPA.

Later, IIRS simulations are performed for nine sets given in Table 6.3 corresponding to FRS for twenty intra-plate records. This results in a total of 180 analyses of SSPS. For each analysis, an excitation with 0.1g ZPA is applied to the FE model of SSPS and IIRS analysis is carried out. Resulting rotation and moment in high stressed elbow are obtained and compared with envelope elbow characteristics.

In-plane rotational stiffness of the elbow is modified iteratively till convergence. The ratcheting strain of elbow corresponds to this converged moment is obtained from envelope results. The input level of base excitation is repeated until 5% ratcheting (PLS-2) is reached. Predicted peak ratcheting at crown of elbow-1 for SSPS under all 20 FRS corresponding to fifth simulation set (mean damping and mean frequency) is shown in Figure 6.19. Excitation levels in terms of ZPA for PLS-1 and PLS-2 are evaluated.

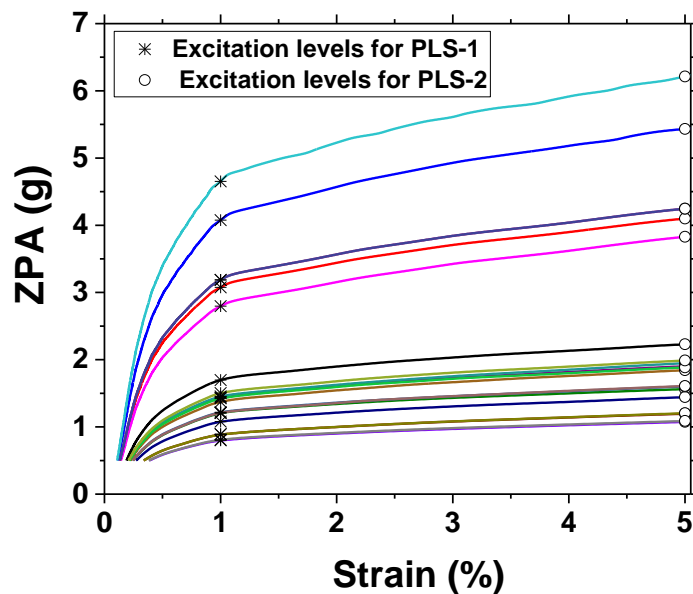


Figure 6.19: Maximum ratcheting strain in elbow-1 of SSPS for DOE case with mean values of damping and frequency under 20 records

The levels of floor excitation in terms of ZPA for PLS-1 are shown in Figure 6.20. It can be noticed that the lowest level of 0.351g corresponding to DOE set-4

(lowest damping and mean dominant frequency) and the highest level is 11.51g, corresponding to DOE set-9 (highest damping and highest dominant frequency).

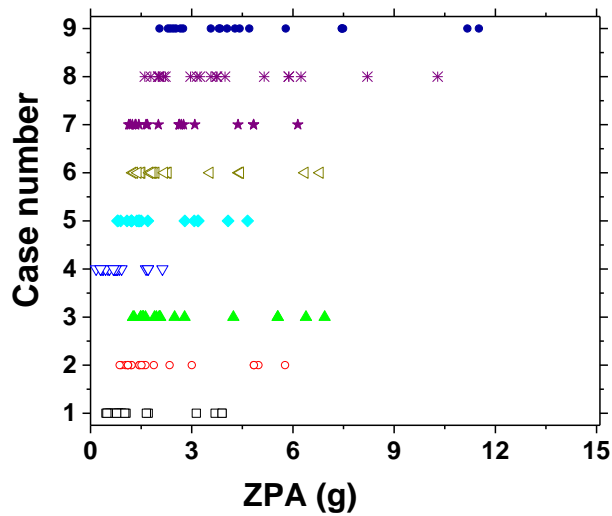


Figure 6.20: The floor excitation levels (ZPA of FRS) for PLS-1 in all nine DOE cases

The levels of floor excitation in terms of ZPA for PLS-2 are plotted in Figure 6.21. It can be seen that the smallest value is 0.56g, which again correspond to fourth DOE set (lowest damping and mean dominant frequency) and the highest value is 15.66g, which corresponds to ninth DOE set (highest damping and highest dominant frequency).

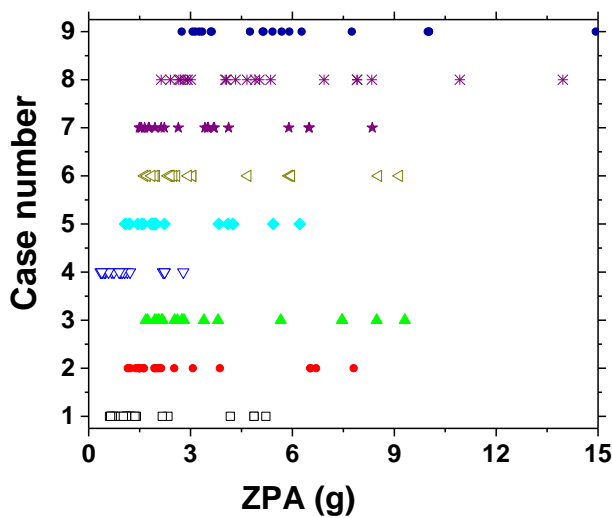


Figure 6.21: The excitation levels (ZPA of FRS) for PLS-2 (5% ratcheting) in all nine DOE cases

Fragility curves for PLS-3 are shown in Figure 6.22. It can be seen that the smallest value is 0.166g, which again correspond to fourth DOE set (lowest damping and mean dominant frequency) and the highest value is 7.36g, which corresponds to ninth DOE set (highest damping and highest dominant frequency).

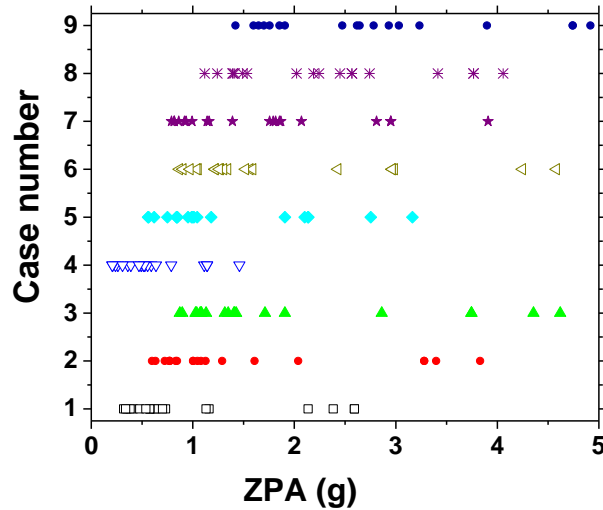


Figure 6.22: The excitation levels (ZPA of FRS) for performance level based on codal stress limit (PLS-3) in all nine DOE cases

Response surfaces are generated by polynomial regression using equation (1) and the polynomial coefficients are given in Table 6.6.

Table 6.6: Polynomial coefficients for response surfaces of different PLS

Limit state		P ₁	P ₂	P ₃	P ₄	P ₅	P ₆
PLS-1	LB	0.768	0.371	0.467	0.030	0.491	-0.039
	MEDIAN	1.450	0.887	0.655	0.127	0.984	-0.146
	UB	4.926	1.870	2.183	0.602	2.880	-0.633
PLS-2	LB	1.048	0.490	0.603	0.048	0.618	-0.035
	MEDIAN	1.920	1.162	0.890	0.184	1.308	-0.181
	UB	6.599	2.579	2.964	0.824	3.971	-0.875
PLS-3	LB	0.554	0.258	0.309	0.021	0.311	-0.013
	MEDIAN	1.014	0.604	0.453	0.091	0.662	-0.105
	UB	3.313	1.107	1.437	0.369	1.727	-0.394

6.3.3. Details of fragility evaluation of SSPS

The parameters for log-normal fragility function for each PLS are listed in Table 6.7.

Table 6.7: Log-normal fragility function parameters for three performance levels

Performance limit state	Lower Bound confidence level		Median confidence level		Upper Bound confidence level	
	$A_m(g)$	β	$A_m(g)$	β	$A_m(g)$	β
PLS-1	0.72	0.42	1.39	0.33	4.67	0.31
PLS-2	1.00	0.39	1.84	0.34	6.24	0.32
PLS-3	0.53	0.37	0.97	0.33	3.15	0.3

Numerical fragility curves are obtained from the conditional exceedance probability at a particular floor excitation level for each PLS. Then, parameters for log-normal fragility function are evaluated and corresponding log-normal fragility function is obtained. Both numerical fragility curve and corresponding log-normal fragility function fit for PLS-1 are shown in Figure 6.23. The experimental excitation levels of PLS-1 for SSPS-1 and SSPS-2 are 3.1g and 2.9g respectively and it is noticed that these excitation levels is in the range of fragility curves with mean probability of exceedance for 95% and 5% confidence levels.

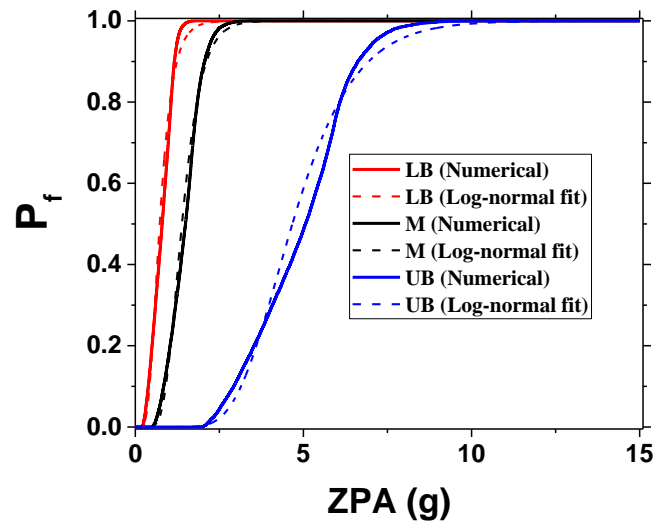


Figure 6.23: Fragility curves for 1% strain performance level (PLS-1)

Numerical and log-normal fragility curves for PLS-2 are shown in Figure 6.24. The experimental excitation levels of PLS-1 for SSPS-1 and SSPS-2 are 5.45g and 4.75g respectively and it is noticed that these excitation levels is in the range of fragility curves with mean probability of exceedance for 95% and 5% confidence levels.

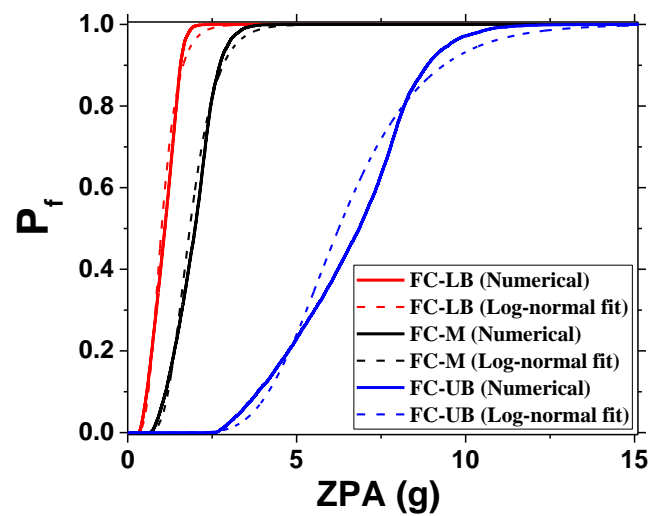


Figure 6.24: Fragility curves for 5% strain performance level (PLS-2)

Numerical and log-normal fragility curves for PLS-3 are shown in Figure 6.25. The experimental excitation level corresponds to PLS-3 for SSPS is 1.74g ZPA and is observed to be in the range of fragility curves with mean probability of exceedance for 95% and 5% confidence levels.

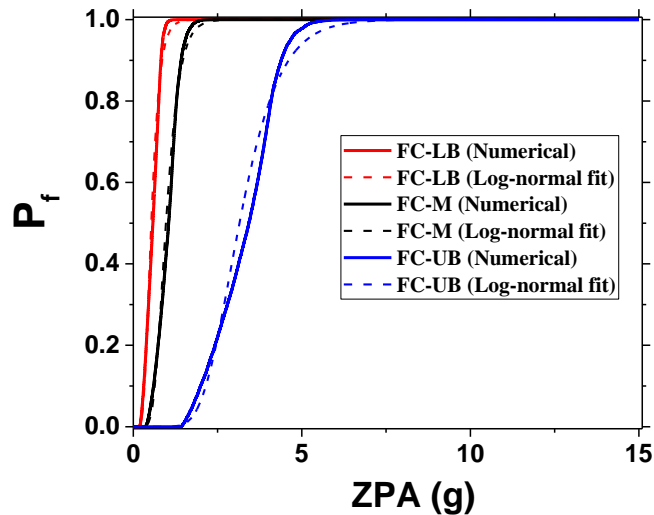


Figure 6.25: Fragility curves for performance level based on codal stress limit (PLS-3)

6.4. Outcome and discussion

This chapter presents the methodology for generation of fragility curves for pressurized piping systems considering ratcheting. The methodology has been illustrated for carbon steel and stainless steel piping systems of same configuration. The research carried out has highlighted the following salient aspects:

It is concluded that Incremental Iterative Response Spectrum (IIRS) method, which is validated with experimental results in the previous chapters can be used for simulation of ratcheting in pressurized piping systems under seismic load. This method is also found to be suitable for evaluation of seismic fragility considering ratcheting.

From the case study of SFA, it is observed that experimental excitation levels of different PLS for both carbon steel and stainless steel piping systems are within the range of upper and lower bounds of fragility curves with median probability of exceedance.

In the case study of SFA, it is found that excitation levels corresponding to 5% ratcheting limit for stainless steel piping system are 13-15% higher than those for carbon steel piping system. Hence, it is concluded that stainless piping systems requires

relatively higher levels of excitation to attain a ratcheting performance limit state than carbon steel piping systems. This is attributed to cyclic hardening in stainless steels, which reduces rate of ratcheting.

It can be concluded that the methodology presented in this work can be used for evaluation of seismic fragility of pressurized piping systems.

CHAPTER 7 RISK-BASED SEISMIC PERFORMANCE ASSESSMENT OF PRESSURIZED PIPING SYSTEMS CONSIDERING RATCHETING

7.1 Introduction

Once Seismic fragility curves are generated, the next step is to obtain the site specific seismic hazard to carry out risk-based seismic performance assessment. Site specific seismic hazard is generated using Probabilistic Seismic Hazard Analysis (PSHA). In the present study, hazard information for a typical Peninsular Indian (PI) site is used for risk assessment. The frame work for the risk assessment is described first and later, the details of its application to carbon and stainless steel piping systems are provided.

7.2 Methodology for risk assessment

As shown in Figure 7.1, seismic risk is obtained by the convolution of hazard curves with fragility information [69]. Usually seismic risk is measured in terms of Annual Exceedance Probability (AEP) and is evaluated by risk integral [3] given in equation (1.1).

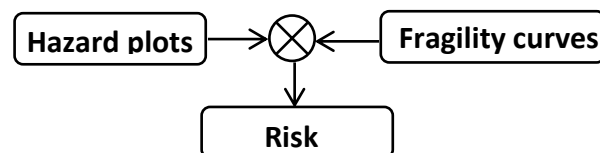


Figure 7.1: Frame work for risk assessment of piping systems

7.3 Site specific seismic hazard

Site specific seismic hazard plot of a Peninsular Indian (PI) site [64] for spectral acceleration is shown in Figure 7.2. This plot gives information of annual exceedance frequency with respect to spectral acceleration.

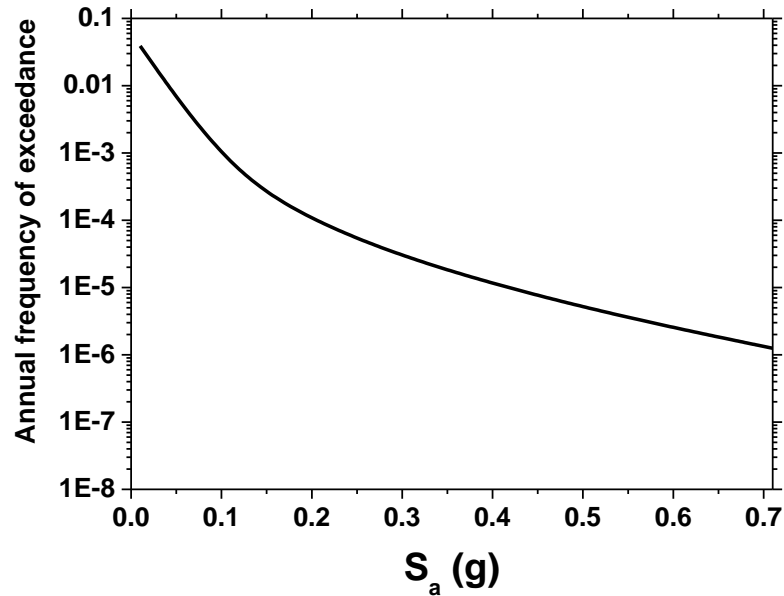


Figure 7.2: Seismic hazard plot of a Peninsular Indian (PI) site

7.4 Seismic risk evaluation

Usually seismic hazard plots are given in terms of a power law [3] as follows:

$$H(\lambda) = k_0 \lambda^{-k} \quad (7.1)$$

Where, k_0 is constant

and k gives the slope of the curve in log-log scale, which represents the steepness.

k_0 and k values for the given seismic hazard curve are 11.1×10^{-7} and 2.4 respectively.

The seismic risk is obtained by convoluting this hazard curve with fragility curves of three PLS.

The hazard curve is convoluted with mean fragility curves of different PLS using numerical integration of risk integral of equation (7.1). The fragility curves of PLS-1,

PLS-2 and PLS-3 for CSPS and SSPS generated in Chapter 5 are used for this purpose.

The resulting AEP for three PLS of CSPS is shown in Figure 7.3.

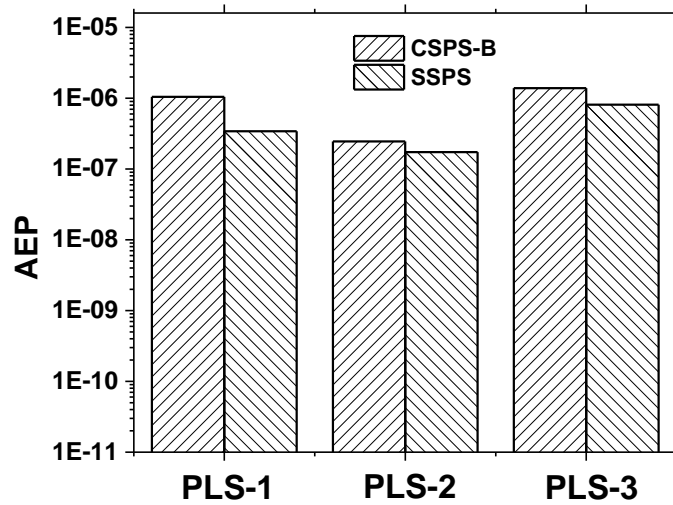


Figure 7.3: AEP of SSPS and CSPA-B for the three PLS

The resulting AEP values of CSPA for PLS-1, PLS-2 and PLS-3 are 1.046×10^{-6} , 2.46×10^{-7} and 1.39×10^{-6} respectively. The AEP values of SSPS for PLS-1, PLS-2 and PLS-3 are 0.34×10^{-6} , 1.73×10^{-7} and 0.81×10^{-6} respectively.

It is observed that the seismic risk of SSPS for PLS-1, PLS-2 and PLS-3 are 33%, 71% and 58% of risk for CSPA respectively. Hence, it is concluded that seismic risk for stainless steel piping systems is relatively lower than that of carbon steel piping systems. It is also observed that the risk in terms of AEP without considering ratcheting is higher than AEP considering ratcheting for the present case study. Hence, it is concluded that consideration of ratcheting significantly influence the seismic risk assessment of piping systems.

7.5 Outcome and discussion

This chapter presents the methodology for seismic risk assessment of pressurized piping systems considering ratcheting. The methodology has been illustrated for carbon

steel and stainless steel piping systems of same configuration. The research carried out has highlighted the following salient aspects:

Seismic risk is quantified in terms of Annual Exceedance Probability (AEP), which is obtained by convolution of fragility curves with site specific hazard curves. From the case study on risk assessment of carbon steel and stainless steel piping systems, it is observed that the AEP values are lower than the recommended target value for Structures, Systems and Components (SSC) of nuclear facilities.

From the case study, it is also found that AEP values of stainless steel piping system for PLS-1, PLS-2 and PLS-3 are 33%, 71% and 58% of those for carbon steel piping system respectively. Hence, it is concluded that seismic risk for stainless steel piping systems is relatively lower than that of carbon steel piping systems.

Seismic risk for stainless steel and carbon steel piping systems of the case study, considering 5% ratcheting limit is 18% and 21% of that of design stress limit respectively. Hence, it is concluded that consideration of ratcheting reduces conservatism in seismic risk assessment of piping systems.

Finally it is concluded that the methodology demonstrated for evaluation of seismic risk of pressurized piping systems considering ratcheting can be applied to any general piping system if site specific hazard information is known.

References

- [1] ASCE, “Seismic Design Criteria for Structures, Systems and Components in Nuclear Facilities”. American Society of Civil Engineers, ASCE Standard 43-05, 2005.
- [2] Regulatory Guide 1.208, “A Performance-Based Approach to define the Site-Specific Earthquake Ground Motion”, U.S. Nuclear Regulatory Commission (USNRC), Washington, DC, 2007.
- [3] R. P. Kennedy, “Performance-goal based (risk informed) approach for establishing the SSE site specific response spectrum for future nuclear power plants”, *Nuclear Engineering and Design*, 241, pp. 648–656, 2011.
- [4] R. P. Kennedy and M. K. Ravindra, “Seismic Fragilities for Nuclear Power Plant Risk Studies”, *Nuclear Engineering and Design* 79, pp. 47-68, 1984.
- [5] B. S. Ju and A. Gupta, “Seismic fragility of threaded Tee-joint connections in piping systems”, *International Journal of Pressure Vessels and Piping* 132-133, pp. 106-118, 2015.
- [6] E. S. Firoozabad, B. G. Jeon, H. S. Choi and N. S. Kim, “Seismic fragility analysis of seismically isolated nuclear power plants piping system”, *Nuclear Engineering and Design*, 284, pp. 264–279, 2015.
- [7] I. Zentner, “Numerical computation of fragility curves for NPP equipment”, *Nuclear Engineering and Design* 240, pp. 1614–1621, 2010.
- [8] G. I. Schueller, N. C. Hampl and H. J. Pradlwarter, “Fragility of primary piping of nuclear power plants”, *Nuclear Engineering and Design* 110, pp. 221-227, 1988.
- [9] ASME, ASME Boiler and Pressure Vessel Code, Section III, Division 1, The American Society of Mechanical Engineers, New York, 2010.

- [10] EPRI, “Piping and Fitting Dynamic Reliability Program”, Vol. 1—Project summary, EPRI TR-102792-V1, Project 1543-15, 1994.
- [11] P. Towashiraporn, “Building seismic fragilities using response surface metamodels”, Ph.D. dissertation, Georgia Institute of Technology, 2004.
- [12] D. C. Montgomery, “Design and Analysis of Experiments”, John Wiley & Sons, Inc, 1997.
- [13] D. Vamvatsikos and C. A. Cornell, “Incremental dynamic analysis.” *Earthquake Engineering & Structural Dynamics* 31(3), pp. 491–514, 2002.
- [14] C. C. Mitropoulou, M. Papadrakakis, “Developing fragility curves based on neural network IDA predictions”. *Engineering Structures* 33(12), pp. 3409–21, 2011.
- [15] J. W. Baker, “Efficient Analytical Fragility Function Fitting Using Dynamic Structural Analysis”, *Earthquake Spectra* 31 (1), DOI: 10.1193/021113EQS025M, 2013.
- [16] F. Jalayer, “Direct Probabilistic Seismic Analysis: Implementing Non-Linear Dynamic Assessments”, Ph.D. dissertation, Dept. of Civil and Environmental Engineering, Stanford University, Stanford, CA, 2003.
- [17] E. M. Beaney, “Response of Tubes to Seismic Loading”, CEGB Report, TPRD/B/0605/N85, Berkeley Nuclear Laboratories, R&D Department, Berkeley, UK, 1985.
- [18] E. M. Beaney, “Response of Pressurized Straight Pipes to Seismic Excitation”, CEGB Report, TPRD/B/0826/R86, Berkeley Nuclear Laboratories, R&D Department, Berkeley, UK, 1986.

- [19] E. M. Beaney, "The Behaviour of Discrete Components in Pipework subjected to Seismic Loading", CEGB Report, RD/B/6225/R89, Berkeley Nuclear Laboratories, R&D Department, Berkeley, UK, 1989.
- [20] E. M. Beaney, "Failure of Elbows under Seismic Loading", Nuclear Electric Report, TD/SID/REP/0134, Technology Division, Nuclear Electric Plc, UK, 1991.
- [21] EPRI, "Piping and Fitting Dynamic Reliability Program", Vol. 2—Component Tests Report, EPRI TR-102792-V2, Project 1543-15, 1994.
- [22] EPRI, "Piping and Fitting Dynamic Reliability Program," Vol. 3—System Tests Report, EPRI TR-102792-V3, Project 1543-15, 1994.
- [23] EPRI, "Piping and Fitting Dynamic Reliability Program", Vol. 4— Fatigue-Ratchet Tests, EPRI TR-102792-V4, Project 1543-15, 1994.
- [24] EPRI, "Piping and Fitting Dynamic Reliability Program", Vol. 5— Piping Design Rules Revisions, EPRI TR-102792-V5, Project 1543-15, 1994.
- [25] S. W. Tagart Jr, Y. K. Tang, D. J. Guzy, and S. Ranganath, "Piping dynamic reliability and code rule change recommendations", Nuclear Engineering and Design, 123, pp. 373-385, 1990.
- [26] C. A. Kot, M. G. Srinivasan, B. J. Hsieh, L. Malcher, D. Schrammel, H. Steinhilber and J. F. Costello "SHAM: High-level seismic tests of piping at the HDR", Nuclear Engineering and Design 118, pp. 305-318, 1990.
- [27] G. DeGrassi and C. Hofmayer, "Seismic Analysis of Simplified Piping systems for the NUPEC Ultimate Strength Piping Test Program", NUREG/CR-6889, BNL-NUREG-74978-2005, U.S. Nuclear Regulatory Commission, 2005.

- [28] F. Touboul, "Piping Seismic Design Criteria: Fatigue-Ratchetting Behaviour Under High Cyclic Loadings", Transactions of 13th International conference on Structural Mechanics in Reactor Technology (SMIRT 13), 1995.
- [29] F. Touboul, N. Blay, and M. H. Lacire, "Experimental, Analytical, and Regulatory Evaluation of Seismic Behavior of Piping Systems" ASME Journal of Pressure Vessel Technology, 121(4), pp. 388–392, 1999.
- [30] RCC-MR code, "Design and Construction Rules for Mechanical Components of FBR Nuclear Islands," Section I, Subsection B: Class 1 Components, 1994.
- [31] K. Yahiaoui, D. G. Moffat, and D. N. Moreton, "Response and cyclic strain accumulation of pressurized piping elbows under dynamic in-plane bending", The Journal of Strain Analysis for Engineering Design, 31(2), pp. 135–151, 1996.
- [32] K. Yahiaoui, D. G. Moffat, and D. N. Moreton, "Response and cyclic strain accumulation of pressurized piping elbows under dynamic out-of-plane bending", The Journal of Strain Analysis for Engineering Design, 31(2), pp. 153–166, 1996.
- [33] D.N. Moreton, K. Yahiaoui and D. G. Moffat, "Onset of Ratchetting in Pressurized Piping Elbows Subjected to In-Plane Bending Moments", International Journal of Pressure Vessel and Piping 68, pp. 73-79, 1996.
- [34] X. Chen, B. Gao and G. Chen, "Ratcheting Study of Pressurized Elbows Subjected to Reversed In-Plane Bending", ASME Journal of Pressure Vessel Technology, 128, pp. 525-532, 2006.
- [35] S. Vishnuvardhan, G. Raghava, P. Gandhi, M. Saravanan, S. Goyal, P. Arora, S.K. Gupta and V. Bhasin, "Ratcheting failure of pressurised straight pipes and elbows under reversed bending", Int. J. Press. Vessels Pip, 105–106, pp. 79–89, 2013.

- [36] D. Boussaa, K. Dang Van, P. Labbe and H.T. Tang, “Fatigue-Seismic Ratcheting Interactions in Pressurized Elbows”, *Journal of Pressure Vessel Technology*, 116, pp. 396-402, 1994.
- [37] G. Slagis, “Evaluation of Seismic Response Data for Piping”, WRC Bulletin 423, Welding Research Council, New York, 1997.
- [38] K. Muthumani, N. Lakshmanan, N. Gopalakrishnan, K. Satish Kumar, S.Avinash, L. R. Seshi Reddy, “Report on Shake table studies on a pipe elbow with steady internal pressure”, Project No. CNP 054941, SERC, Chennai, 2002.
- [39] A. Ravi Kiran, M.K. Agrawal, G.R. Reddy, R. K. Singh, K.K. Vaze, A.K. Ghosh and H.S. Kushwaha, “Fatigue-Ratcheting Study of Pressurized Piping System under Seismic Load”, *Transactions, SMiRT 19*, Toronto, Paper No. K12/4, 2007.
- [40] A. Ravi Kiran, P. N. Dubey, M. K. Agrawal, and G. R. Reddy, “Experimental and Numerical Studies of Ratcheting in Pressurized Stainless Steel Piping Systems Under Seismic Load,” Bhabha Atomic Research Centre, Mumbai, India, BARC External Report No. SIRD/BARC/2015/E/018, 2015.
- [41] T. Hassan, Y. Zhu and V. Matzen, “Improved ratchetting analysis of piping components”, *International Journal of Pressure Vessels and Piping*, 75, pp. 643–52, 1998.
- [42] P. J. Armstrong and C. O. Frederick, “A mathematical representation of the multiaxial Baushinger effects”, CEGB Report, RD/b/N/731, Berkeley Nuclear Laboratories, R&D Department, Berkeley, UK, 1966.
- [43] S. C. Kulkarni, Y. M. Desai, T. Kant, G. R. Reddy, P. Prasad, K. K. Vaze and C. Gupta, “Uniaxial and biaxial ratchetting in piping materials—experiments and analysis”, *International Journal of Pressure Vessels and Piping*, 81, pp. 609–617, 2004.

- [44] J. L. Chaboche, "Time-Independent Constitutive Theories for Cyclic Plasticity", *International Journal of Plasticity*, 2, pp. 149-188, 1986.
- [45] A. Ravi Kiran, M. K. Agrawal, G. R. Reddy, K. K. Vaze, A. K., Ghosh and H. S. Kushwaha, "Ratcheting Study in Pressurized Piping Components under Cyclic Loading at Room Temperature", BARC External Report No. SIRD/BARC/2006/E1013, 2006.
- [46] G. DeGrassi, C. Hofmayer, A. Murphy, K. Suzuki and Y. Namita, "BNL Nonlinear Pre-Test Seismic Analyses for NUPEC Ultimate Strength Piping Program", *Transactions, SMiRT 17*, Prague, Czech Republic, Paper No. K15/1, 2003.
- [47] K. R. Jaquay, J. E. Larson and H. T. Tang, "A simplified method for inelastic piping system seismic Response prediction", *Nuclear Engineering & Design*, 107, pp. 169-181, 1988.
- [48] A. Ravi Kiran, M.K. Agrawal, G.R. Reddy, R. Ramesh Babu, R. K. Singh, K.K. Vaze, A.K. Ghosh and H.S. Kushwaha, "Analysis of a piping System under Seismic load using Incremental Hinge Technique", *ICONE 16-48224*, May 11-15, Florida, USA, 2008.
- [49] G.S. Hanspal, "Development of incremental hinge technique to predict the behaviour of piping system subjected to internal pressure and seismic loading", M. Tech thesis, HBNI, 2011.
- [50] F. Touboul, N. Blay, P. Sollogoub and S. Chapuliot, "Enhanced seismic criteria for piping" *Nuclear Engineering and Design* 236, pp. 1-9, 2006.
- [51] E. S. Firoozabad, B. G. Jeon, H. S. Choi and N. S. Kim, "Failure criterion for steel pipe elbows under cyclic loading", *Engineering Failure Analysis*, 66, pp. 515-525, 2016.

- [52] G. E. Varelis, S. A. Karamanos and A. M. Gresnigt, “Pipe elbows under strong cyclic loading”, *ASME Journal of Pressure Vessel Technology*, 135 (1), pp. 011207:1-9, 2013.
- [53] J. Morlet, G. Arens, E. Fourgeau and D. Glard, “Wave propagation and sampling theory Part I: Complex signal and scattering in multilayered media”, *Geophysics*, 47 (2), pp. 203-221, 1982.
- [54] ASCE, “Seismic Analysis of Safety-Related Nuclear Structures and Commentary”, American Society of Civil Engineers, ASCE Standard 4-98, 2000.
- [55] G. R. Reddy, M. H. Prasad and A. Verma, “Textbook of Seismic Design Structures, Piping Systems, and Components: Structures, Piping Systems, and Components”, Springer, doi: 10.1007/978-981-13-3176-3, 2019.
- [56] Y. Urabe, K. Takahashi, K. Sato and K. Ando K, “Low Cycle Fatigue Behavior and Seismic Assessment for Elbow Pipe Having Local Wall Thinning”, *ASME Journal of Pressure Vessel Technology*, 135, pp. 041802:1-8, 2013.
- [57] S. Asada and T. Nakamura, “Simplified Elastic-Plastic Analysis Methods in the JSME Rules on Design and Construction”, *Journal of Environment and Engineering*, 6 (4), pp. 753-764, 2011.
- [58] RCC-M Code, “Design and Construction Rules for Mechanical Components of PWR Nuclear Islands, Sections B & C 3600, Class 1 & 2 Components, Piping Design”, AFCEN, Paris, 2000.
- [59] L. Francis and P. Cecile, “Stress Analysis Criteria for Piping. RCC-M 2002 Rules and Validation”, *Transactions of 20th International Conference on Structural Mechanics in Reactor Technology (SMiRT 20)*, 2009.
- [60] M. Morishita, A. Otani, T. Watakabe, I. Nakamura, T. Shibutani and M. Shiratori, “Seismic qualification of piping systems by detailed inelastic Response analysis

- Part 1- a code case for piping seismic evaluation based on detailed Inelastic response analysis”, Proceedings of the ASME 2017 Pressure Vessels and Piping Conference, Paper No. PVP2017-65166, pp. V008T08A001: 7, doi:10.1115/PVP2017-65166, 2017.
- [61] A. Otani, T. Shibutani, M. Morishita, I. Nakamura, T. Watakabe and M. Shiratori, “Seismic qualification of piping systems by detailed inelastic Response analysis Part 2- A guideline for piping seismic inelastic response analysis”, Proceedings of the ASME 2017 Pressure Vessels and Piping Conference, Paper No. Paper No. PVP2017-65190, pp. V008T08A002: 10, doi:10.1115/PVP2017-65190, 2017.
- [62] P. B. Labbe, G. R. Reddy, C. Mathon, F. Moreau, and S. A. Karamanos, “The OECD-NEA Programme on Metallic Component Margins Under High Seismic Loads (MECOS)”, Proceedings of the ASME Pressure Vessels and Piping Conference, ASME Paper No. PVP2016-63119, Volume 8: Seismic Engineering, doi: 10.1115/PVP2016-63119, 2016.
- [63] G. R. Reddy, H. S. Kushwaha, S. C. Mahajan, S. P. Kelkar, and G. V. Karandikar, “Development of 3-D beam model for seismic analysis of 500 MWe reactor building”, Technical Report no. BARC/1996/I/004, Bhabha Atomic Research Centre, Mumbai, India, 1996.
- [64] “Design Basis Seismic Ground Motion for BARC–Vizag site based on PSHA”, RSD report, Ref. No: GRR/SSES/RSD/110769/2015 dated 18.8.2015, Bhabha Atomic Research Centre, Mumbai, India, 2015.
- [65] G. P. Cimellaro, A. M. Reinhorn, A. D’Ambrisi, M. De Stefano, “Fragility analysis and seismic record selection”, Journal of Structural Engineering, 137 (3), pp. 379–390, 2009.

- [66] N. Gopalakrishnan, K. Satish Kumar, C. K. Madheswaran, R. Sreekala, G. V. Rama Rao, C. Bharathi Priya, S. Harish Kumaran, J. Prakashvel, P. Vasudevan and G Lakshmikanth, “Multi-Support Excitation Test on Piping System”, CSIR-SERC report, Project no. SSP 16241, 2015.
- [67] “Evaluation of Damping of Pipe Supported on Seismic Supports”, RSD internal report, Bhabha Atomic Research Centre, Mumbai, India, 2015.
- [68] C. Descelier, C. Soize, and S. Cambier, “Nonparametric-parametric model for random uncertainties in nonlinear structural dynamics – application to earthquake engineering”, *Earthquake Engineering & Structural Dynamics*, 33, pp. 315–327, 2003.
- [69] M. Hari Prasad, P. N. Dubey, G. R. Reddy R. K. Saraf and A. K. Ghosh, “Seismic PSA of Nuclear Power Plants A Case Study”, Technical Report no. BARC/2006/E/015, Bhabha Atomic Research Centre, Mumbai, India, 2006.

Thesis Highlight

Name of the Student: **RAVI KIRAN AKELLA**

Name of the CI/OCC: **BARC, Mumbai**

Enrolment No.: **ENGG01201504016**

Thesis Title: **RISK-BASED SEISMIC PERFORMANCE ASSESSMENT OF PRESSURIZED PIPING SYSTEMS CONSIDERING RATCHETING**

Discipline: **Engineering Sciences**

Sub-Area of Discipline: **Earthquake Engineering**

Date of viva voce: **18.02.2020**

Seismic performance assessment of pressurized piping systems is a vital requirement to ensure the safety of nuclear facilities. Risk-based seismic performance assessment of pressurized piping systems is an evolving area to achieve predictable and desirable performance under different levels of earthquakes with a targeted risk. Such an assessment necessitates site specific hazard and fragility information of performance limit states based on actual failure mode. As the predominant failure mode of pressurized piping systems under seismic load is ratcheting, it is required to generate seismic fragility curves of piping systems considering ratcheting. In the literature on Seismic Fragility Analysis (SFA) of piping systems, failure criterion used was plastic collapse, which was the assumed failure mode by earlier version of design code. No studies have reported for seismic fragility analysis of piping systems considering ratcheting, which is actual failure mode. Also, the ASME nuclear piping design code has provided ratcheting based design criterion which was later discontinued due to insufficient experimental data and lack of validated numerical tools.

Hence, the first objective of the present work is to evaluate ratcheting based performance levels of piping systems, which requires validated numerical tools. This objective is met by carrying out experimental and numerical studies on pressurized piping components and systems. Initially, ratcheting behaviour in a carbon steel elbow and tee joint under incremental seismic excitation is studied. Later ratcheting response of pressurized piping systems under incremental excitation is investigated.

The second objective is to develop a methodology for ratcheting based SFA of pressurized piping systems. In the present work, a methodology is developed for SFA of pressurized piping systems considering ratcheting and the flow chart is shown in Figure 1. In this procedure, Response Surface Method (RSM) along with Monte Carlo simulations are used for fragility evaluation. The methodology has been illustrated for

SFA of carbon steel and stainless steel piping systems, which were considered for an international benchmark exercise on seismic margin assessment. Subsequently, the fragility curves of the piping systems are convoluted with hazard curves for a typical Peninsular Indian site to obtain seismic risk in terms of annual exceedance probability of ratcheting based performance limits. Recommendations for carrying out seismic performance, fragility and risk assessments of pressurized piping systems considering ratcheting have been provided.

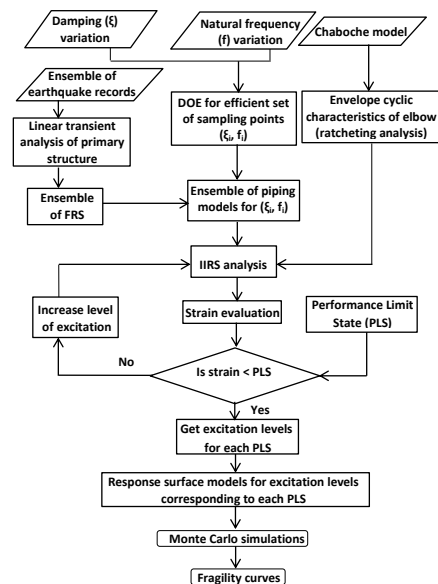


Figure 1. Flow chart showing fragility assessment methodology